RADIATIVE HEAT TRANSFER IN FIBRE INSULATIONS

By

NEIL LLEWELLYN McKAY, B.Sc., M.Sc.

A Thesis

Submitted to the School of Graduate Studies

in Partial Fulfilment of the Requirements

for the Degree

Doctor of Philosophy

McMaster University

© December 1984

RADIATIVE HEAT TRANSFER IN FIBRE INSULATIONS

DOCTOR OF PHILOSOPHY (1985) McMASTER UNIVERSITY
(Physics) Hamilton, Ontario

TITLE: Radiative Heat Transfer in Fibre Insulation.

AUTHOR: Neil Llewellyn McKay, B.Sc. (Queen's University)
M.Sc. (McMaster University)

SUPERVISOR: Professor T. Timusk

NUMBER OF PAGES: ix , 162

ABSTRACT

A first principles method of calculating combined radiative and conductive heat flow in fibrous insulation is presented. Using the measured complex refractive index for the bulk material, the scattering and absorption cross-sections are calculated for an isolated cylinder from expressions analogous to those of Mie theory for spheres. An average over fibre angles gives the cross-sections for the insulation material. Results for extinction and absorption compare well with direct measurements on polyester insulation materials. The scattering is found to be highly anisotropic. A properly-weighted average over scattering angles, combined with the calculated absorption cross-section, gives the parameters needed for a diffusion model of radiative heat transport.

The equations describing combined radiative and conductive heat flow are solved by an approximate method, and the results are compared with measurements of thermal resistance on several samples of commercial polyester-fibre insulation. The excellent agreement, with no adjustable parameters in the theory, indicates that the diffusion model adequately describes radiative heat transport in such materials. The method is used to predict the effect of possible alterations to the fibres.

ACKNOWLEDGEMENTS

I would like to express my thanks to those who have helped me in this work. Dr. Brian Farnworth of DREO provided the original impetus for the project and provided the thermal measurements used in this thesis. Carlos Zarate worked on this project originally, and left me a large collection of reference material and journal articles. My supervisor, Dr. Timusk, always provided useful suggestions and encouragement when the work became stuck. I particularly thank the tag-team duo of Erie Long and Helen Kennelly for their quick and accurate typing of this thesis.

TABLE OF CONTENTS

LIST OF FIGURES

LIST OF TABLES

CHAPTER 1

INTRODUCTION

Heat is transferred through fibre insulation materials by conduction through the fibres and surrounding air, by convective motion of the air, and by infrared radiation propagating from fibre to fibre. Radiation has long been recognized as an important mechanism of heat transfer in low-density glass-fibre insulation (Verschoor and Greebler, 1952; Larkin and Churchill 1959; Bankvall , 1973). Until recently, thermal radiation in polyester and other textile fibre insulation materials was ignored, and the heat transfer was assumed to result from conduction and convection. Differences in performance among various materials were ascribed to varying amounts of convection.

While investigating the performance of sleeping bag insulation materials for the Canadian Army, Dr. Brian Farnworth of the Defence Research Establishment, Ottawa was able to show that convection in these materials is completely absent, and the overall thermal conductivity could be explained by a combination of conduction through the air and fibres and thermal radiation (Farnworth, 1983; Farnworth et al. 1979). They used a 2-flux model with a single absorption parameter fitted to the thermal measurements. At McMaster we investigated whether we could determine this parameter

from purely optical measurements on the insulation materials. In the course of this we were obliged to consider in more detail the behaviour of thermal radiation in polyester sleeping-bag insulation and in fibrous insulation in general.

We first discovered that in these materials the scattering cross-sections were at least as large as the absorption, and the pure-absorption model had to be abandoned. Similarly a simple model based on isotropic scattering which used measured extinction (absorption plus total scattering) cross-sections gave thermal conductivities much lower than those observed experimentally. The problem was that the scattering was strongly peaked in the forward direction, and the anisotropy in the scattering had to be included in the model. This was possible because of the very simple geometrical structure of the material. The fibres were of uniform diameter, were reasonably well separated from each other, and were fairly random in orientation. We were able to calculate all the optical parameters in detail as functions of scattering angle and radiation frequency, and predict accurately the heat flow, which had not previously been done for any commercial fibrous insulation.

The problem of radiative transfer is in general difficult, involving an integrodifferential equation (the equation of transfer) with three or more variables -- the radiation frequency, one or two angular variables, and at least one

space variable. In the case of heat transfer in insulation materials used at ordinary temperatures, it is possible to simplify the problem considerably, because the radiation is everywhere close to thermodynamic equilibrium. Chandrasekhar (1960) and Pomraning (1973) both describe numerical procedures which can provide arbitrary accuracy in the general problem, as well as simpler procedures for approximate solutions. Viskanta (1965) has published accurate numerical solutions for heat flow in grey (frequency-independent optical properties) absorbing, scattering, and conducting media for various values of the parameters. Yuen and Tien (1980) and Yuen and Wong (1980) have investigated methods of solving the heat-transfer problem and obtaining accurate temperature profiles in the case of linear-anisotropic scattering. Modest and Azad (1980) have also published accurate numerical results for theoretical materials, and found that simplified models could be reasonably successful. These results are discussed further in Chapter 2.

In the case of heat transfer in reasonably thick insulation materials at ordinary temperatures it is possible to obtain sufficient accuracy with a simplified model. Chapter 2 describes a diffusion model which includes the scattering anisotropy in a natural way. Essentially the model removes the angular variable from the problem by assuming that the intensity of the radiation varies smoothly with direction,

and may be represented by the zeroth and first-degree Legendre polynomials in cos θ. For this reason it is called the P-1 model by Pomraning (1973). No assumptions about the form of the scattering function are required; the scattering in the polyester materials we investigated varies strongly and unpredictably with angle. Explicit expressions for the optical parameters in terms of the differential scattering and absorption cross-sections are derived in Chapter 2 for an isotropic material (eg. randomly-oriented fibres); these have been given elsewhere. We also derive such expressions in the case of an axially-symmetric material (eg. fibres randomly-oriented in the plane of the batt) and show that the model and its method of solution are not essentially changed, although the calculation of the optical parameters is somewhat more complicated. The relation between this diffusion model and the commonly-used two-flux model is also described here. A modified form of the two-flux model which is occasionally used (eg. Berquam and Seban, 1971) is shown to be exactly equivalent to the diffusion model used here.

The frequency variable is also removed from the problem by averaging over frequency with appropriate thermal weight functions, to give an approximate description in terms of frequency-independent "grey" optical parameters. We are left with a pair of coupled nonlinear differential equations for the total radiative flux and energy density, and the

temperature T(x). A third equation is added by requiring that the total heat flux, the sum of the radiative and conductive contributions, be constant. Grey Lambertian boundaries are added to give a complete description of the problem. It is solved by an approximate method which linearised the differential equations, rather than by an exact numerical quadrature. This method leads to a better intuitive understanding of the relation between the heat flow and the optical parameters of the material and the boundary walls. Terms due to conduction, radiation, boundary surfaces, and the interaction between radiative and conductive heat transport can be related qualitatively to typical length scales of the insulation slab.

A careful investigation of the approximations at the end of Chapter 2 indicate that the solution ought to be accurate if the optical parameters can be determined with sufficient precision.

Several methods have been used to obtain the optical parameters of fibrous materials. The simplest is simply to fit one or more parameters of a single radiative-transfer model to the thermal measurements. Then the dependence of thermal resistance on temperature, density, thickness, etc. may be tested against the model. Battacharyya (1980) fits a backscattering parameter to a two-flux model which assumes zero absorption and finds good agreement with the measurements of Hollingsworth (1980) on glass-fibre materials.

Farnworth et al. (1979) fit a fibre emissivity (essentially an absorption parameter) to thermal measurements on Polarguard and Hollofil (two polyster sleeping-bag insulation materials, made by Celanese and Dupont, respectively) and also find the model agrees well with experiment. Davis and Birkebak similarly fit an "emissivity" parameter in their investigation of heat transport in animal fur. Such single-parameter fits do not generally indicate the type of process (absorption or scattering) involved. As discussed in Chapter 2, it is only the (usually small) boundary effects which change when an absorbing material is exchanged for one which scatters isotropically. To distinguish between the two types requires measurements with widely varying boundary emissivities on thin samples. Indeed, our calculations (Chapter 4) indicate that the assumptions mentioned above are not correct. Polyester fibres are found to scatter about as much radiation as they absorb, and glass fibres are strongly absorbing in the thermal infrared region.

Direct optical measurements on insulation materials have been of two types - optically thin samples or optically thick samples. The former employs samples thin enough that multiple scattering is presumed not to be a factor in the measurement. The simplest experiment measures the transmission as a function of wavelength, which yields the extinction coefficient (absorption plus total scattering). In general this is not closely related to the heat transfer unless the

scattering is isotropic. Schuetz (1982) measured the transmission of thin samples of foam and of glass-fibre batting, and found the results underestimated the radiative conductivity by 10% and 60% respectively. Verschoor and Greebler (1952) obtained good agreement (better than 10%) with heat-transfer measurements on glass-fibre felts. The fibre diameters were very small (1.5 - 2.6 μm), and the scattering would be more nearly isotropic than for glass building insulation (fibre diameter typically ∿ 12 μm) or the 25-μm polyester insulations.

Larkin and Churchill (1959) and Cabannes et al. (1979) have measured transmission through thick samples and fitted the results to a simple radiative-transfer model which describes both the diffusion of nonthermal radiation and the heat transport in the same material. These fitted parameters can therefore be used to predict the thermal resistance. In both cases the agreement was reasonably good. This procedure is similar to that of fitting the parameters directly to thermal measurements, and no analysis has been given to demonstrate that the method can in practice distinguish accurately between absorption and scattering in the medium.

In general the theory indicates that the absorption, the scattering, and the angular variation of the scattering are all needed to describe the radiation. Schuetz (1982) has measured the scattering as a function of angle for glass-

fibre and foam materials, but used a laser to obtain a sufficiently strong signal. As a result the measurement was made only at a single wavelength (10 μm), and had to be combined with other measurements and approximations to give frequency-averaged parameters.

Our approach was to measure the properties of the bulk material, and then calculate the absorption and scattering from electromagnetic theory. The fibres were treated as uniform infinite cylinders randomly oriented in space. One material (Hollofil) had a hole in the centre of the fibre, but this was ignored for the purposes of the scattering calculations. We used the solution of Wait (1955) for scattering from infinite dielectric cylinders at oblique incidence, and averaged the results over incident (fibre) angles.

We describe the method and present results for various refractive indices in Chapter 3. It is shown from simple geometrical arguments that the differential scattering cross-section (and therefore the phase function) for randomly-oriented cylinders diverges in the forward direction. This explains the very slow convergence of expansions of this function in Legendre polynomials. But the total scattering and absorption cross-sections are shown to be qualitatively similar to published results for aligned fibres at perpendicular incidence (Kerker, 1969; Van de Hulst, 1957). Expressions for the scattering and absorption parameters of

the heat-transfer model are written in a form suitable for rapid computation.

Chapter 4 presents the results of the calculations and the experimental measurements. The complex refractive index n-ik for polyester is obtained from measurements on Mylar sheet. This is used together with the measured fibre radius and the bulk density of polyester to calculate all the optical properties of the insulation materials. A check on the procedure is provided by direct measurements of extinction and absorption cross-sections of the insulation materials. Agreement is reasonably good. Discrepancies in the measured and calculated extinction for Hollofil are qualitatively explained by the effect of the hole in the fibres.

Predictions of the thermal resistance of both polyester materials were compared with direct measurements performed by Dr. Farnworth at DREO (Farnworth et al. 1979; McKay et al. 1984). The agreement is excellent, generally within the 5% accuracy of the measurements for a range of batting densities and mean temperatures. Our calculation used no adjustable parameters and no measurements on the insulation materials themselves except the fibre radius; the other input parameters were the bulk properties of the material from which the fibres were made.

Such realistic first-principles calculations had not been performed prior to our reporting these results (McKay et al.

1983). A similar procedure was developed independently by Caps et al. (1983) and applied to micron-sized glass fibre materials, with similar success. The demonstrated accuracy of the method for these materials allows us to make quantitative predictions of the effect of varying the size and composition of the fibres. In the last section of Chapter 4 we present results of the radiative conductivity parameter as a function of fibre radius for a constant refractive index approximating that of polyester , for metallic fibres, and for glass fibres and discuss the results. It is shown that there is an optimum fibre size for dielectric materials (if we do not consider the mechanical properties). The variations as the fibre material is changed are significant but not as dramatic as those brought about by varying the fibre radius.

Finally in Chapter 5 we summarize the major results presented here and indicate how the calculations may be refined in the future.

CHAPTER 2

HEAT TRANSPORT

2.1 Introduction

The thermal measurements which are used in Chapter 4 for comparison with predicted values of thermal resistance were performed on low-density polyester-fibre materials designed for insulation in clothing and sleeping bags. Both the small-scale structure of the material and the geometry used for the thermal measurements have a simplicity which facilitates the construction of an accurate model. In this Chapter we shall discuss the various modes of heat transport in fibrous insulation and show how they can be calculated from the properties of the bulk material from which the fibres are made.

Throughout this work the temperature will be assumed to vary in one direction only. The thermal measurements, performed by B. Farnworth at the Defence Research Establishment, Ottawa, were arranged to have this one-dimensional behaviour in order to simplify the analysis. The samples used were large slabs 60 cm × 60 cm in area and no more than 5 cm in thickness. Effects due to heat loss at the edges of the batt were eliminated by the design of the experiments (Farnworth et al., 1979; Farnworth, 1983; McKay et al., 1984a).

The materials themselves consist of cylindrical fibres with a very uniform diameter of about 25 μm. Under normal conditions of use or measurement, the filling factor f (volume fraction occupied by the fibres) is small, at most a few percent, and less than 1% for the uncompressed batt. We will repeatedly take advantage of this dilute nature of the material, by assuming that the properties of a single isolated fibre may be used to calculate the optical properties of the material as a whole and the fibre contribution to the conductive heat losses.

The material 'Polarguard', made by Celanese, consists of very long (∿ 1 m or more) solid polyester fibres. During manufacture they are given a roughly helical or zig-zag structure with a segment or coil size of 1 or 2 mm. On a very large scale the fibres run approximately parallel to the surface of the batt, but on a scale of a millimeter or so the material is very disorganised, consisting of nearly straight segments with spatial orientations which appear random on casual inspection. It will be treated as a collection of long straight cylinders whose orientations are randomly distributed in three dimensions. Ultimately the only firm justification for these approximations will be the success of the model in reproducing the thermal measurements.

The second material, 'Hollofil', is made by Dupont. It consists of short (∿ 10 cm) fibres that are not solid,

but have a central hole 8 μm in diameter, so that about 10% of the material is removed. There is no apparent large-scale organisation to the fibres, and the approximation of random orientation ought to be very accurate. The hole in the fibre is a complication which will be considered only by applying first-order corrections to calculations for solid cylinders. In the case of heat conduction through the fibres, this should be completely adequate. The contribution of the hole should be roughly proportional to its volume, and is thus only a small correction to the fibre conduction, which in turn is a small part of the total heat transfer. Its contribution to the scattering, however, may be much larger, being approximately proportional to the surface area of the hole, which is about 30% of the fibre area. This error will be discussed further in subsequent chapters.

The function of the fibres in an insulation material is to inhibit radiative transfer and to immobilise the air, preventing heat loss by convection. Farnworth (1983) showed that convection is completely negligible in these materials. Heat transfer takes place by conduction through the air, by conduction through the fibres, and by propagation of thermal radiation from fibre to fibre. Each of these processes must be included in a calculation of the total heat loss.

Conduction is considered first. The idea is to replace the heterogeneous mixture of air and fibres by a homogeneous material characterised by a single thermal

conductivity, which is taken to be the conductivity for the mixture in the absence of radiative transport. To calculate this parameter, we solve Laplace's equation for a single isolated long fibre in air with the temperature gradient uniform at large distances from the fibre. The extra heat flow as compared to the case with no fibre present is obtained as a function of fibre angle (with respect to the applied temperature gradient). Averaging over angles and multiplying by the number of fibres per unit volume gives an approximation to the conductivity K of the mixture which is valid in the limit of small filling factor f.

For the case of hollow fibres, an approximate correction for the hole is obtained by treating the hole as a cylinder embedded in a medium (the fibre) in the same way. The correction is valid if the volume of the hole is small compared to the fibre volume. Since the fibre correction itself is a small part of the total conductivity, this procedure is more than adequate.

In Section 2.3 a model for the radiative part of the heat transport is developed. Several methods exist which allow the numerical solution of the radiative equation of transfer to arbitrary accuracy (for example, see Chandrasekhar, 1960; Viskanta, 1967; Yuen and Wong, 1980). But for the problem of heat transfer in insulation materials, in which temperature gradients are modest and the materials are reasonably thick (at least 5 optical depths), sufficient

accuracy can be obtained using very simple models chosen to include the effects of radiative boundary conditions, of anisotropy in the scattering, and of interaction between the conduction and radiation fluxes. We develop a diffusion model (also called the P-1 model by Pomraning, 1973) which includes these effects and is summarised in a pair of first-order differential equations, together with a pair of algebraic boundary conditions. This model specifies a procedure for weighting the scattering according to angle to account for the greater effectiveness of large-angle scattering compared with scattering in the forward direction. The equations arewritten for a single group of frequencies, with appropriately averaged scattering and absorption parameters.

The diffusion-model equations are also developed for a material which is not isotropic, in the sense that the scattering and absorption depend on the incident direction and not just on the angle between the incident and scattered rays. Normally the model is developed only for isotropic media. Although the randomly-oriented fibres we consider do not require this more general model, it is clearly of interest for some types of fibre insulation (for example, glass-fibre materials) in which the fibres are aligned preferentially in the plane of the batt.

Finally in this Section, two other differential approximations to the radiative transfer problem are

described briefly and related to the diffusion model, as both are frequently used in modelling heat transfer. The usual two-flux model is shown to give somewhat different results, while the other model, derived from the use of a 2-point Gaussian quadrature to integrate the radiative intensity over angle, is exactly equivalent to the diffusion model.

Section 2.4 presents an approximate analytic solution of the differential equations similar to that of Larkin and Churchill (1959) and of Farnworth (1983). It is based on linearising the equations in the temperature, and has the advantage of providing a more intuitive understanding of the relationship between the heat flux and the material parameters than a purely numerical solution would allow. Parameters are defined which characterise the "radiative thermal conductivity", the interaction between conduction and radiation fluxes, and the apparent radiative thermal resistance of the boundary surfaces.

In the last Section of this Chapter, the accuracy of the various approximations is considered. For the particular conditions relevant to thermal measurements on insulation, the errors introduced are small, and probably add up to less than 1%.

Two sources of error, the assumption that the fibres are randomly oriented and the use of "grey" (or frequency-independent) equations with frequency-averaged parameters, are difficult to evaluate quantitatively, and may contribute

1 or 2% each. The comparison of calculated and measured thermal resistances must be used to evaluate these two approximations.

2.2 Heat Transport by Conduction

In the absence of convection, the total heat flux H may be written

$$H = F - K \frac{dT}{dx} \qquad (2\text{-}1)$$

for a uniform slab perpendicular to the x-direction, which approximates the conditions of the thermal measurements. The radiative flux is F, and T is the temperature, assumed to vary only in the x-direction. There are no sources or sinks of energy in the medium, so that under steady-state conditions, H is a constant independent of x. The heterogeneous mixture of fibres and air is represented by a single thermal conductivity K whose value can be calculated from the conductivities of the two separate media.

Consider the contribution to the heat conduction of a single long straight fibre isolated from its neighbours. Assuming temporarily that the radiative flux is zero, the divergence of the heat flux $-K\underline{\nabla}T$ must vanish. If the weak temperature dependence of K is ignored, then T must obey Laplace's equation except at the surface of the fibre. In cylindrical coordinates,

$$\frac{\partial^2 T}{\partial r^2} + \frac{1}{r}\frac{\partial T}{\partial r} + \frac{1}{r^2}\frac{\partial^2 T}{\partial \phi^2} + \frac{\partial^2 T}{\partial z^2} = 0 \; . \qquad (2\text{-}2)$$

Suppose the fibre occupies the region r<a, and that the applied temperature gradient (at large distance from the fibre) makes an angle θ_f to the fibre axis. We can express this by applying a boundary condition on a cylindrical surface r=R, with the intention of letting R become very large compared to the fibre radius a:

$$T(r=R) = T_0 + T_1(z \cos \theta_f + R \sin \theta_f \cos \phi) \quad . \qquad (2\text{-}3)$$

The solution to Laplace's equation (2-2) which has the appropriate symmetry has the form

$$T = \sum_{n=-\infty}^{\infty} A_n r^n \cos n\phi + Bz \qquad (2\text{-}4)$$

where the coefficients A_n and B are chosen separately for r>a (outside the fibre) and for r<a. A term in log r has been omitted because it would imply a heat source or sink in the fibre. Matching terms in (2-4) and (2-3) gives, in the region a<r<R,

$$T = T_0 + T_1 \cos \theta_f \cdot z + (A_{-1}r^{-1} + A_1 r)\cos \phi \qquad (2\text{-}5)$$

where

$$A_{-1}R^{-1} + A_1 R = T_1 \sin \theta_f R \quad . \qquad (2\text{-}6)$$

Matching (2-5) with (2-4) at r=a, and requiring that T is finite at r=0 gives, for r<a,

$$T = T_0 + T_1 \cos \theta_f \cdot z + A_1' r \cos \phi \qquad (2\text{-}7)$$

with

$$A_1' a = A_{-1} a^{-1} + A_1 a \ . \qquad (2\text{-}8)$$

We further require that the heat flux $-K\nabla T$ be continuous across the boundary, so that

$$K_{air}(-A_{-1} a^{-2} + A_1) = K_f A_1' \qquad (2\text{-}9)$$

where K_{air} and K_f are the thermal conductivities of air and of the fibre material (polyester), respectively. Then (2-9), (2-8), and (2-6) are solved to give

$$A_1' = \frac{2T_1 \sin \theta_f}{(1 - \frac{a^2}{R^2})\frac{K_f}{K_{air}} + 1 + \frac{a^2}{R^2}} \qquad (2\text{-}10)$$

$$A_1 = \frac{(1 + \frac{K_f}{K_{air}})T_1 \sin \theta_f}{1 + \frac{a^2}{R^2} + (1 - \frac{a^2}{R^2})\frac{K_f}{K_{air}}} \qquad (2\text{-}11)$$

$$A_{-1} = \frac{(\frac{K_f}{K_{air}} - 1)a^2 T_1 \sin \theta_f}{1 + \frac{a^2}{R^2} + (1 - \frac{a^2}{R^2})\frac{K_f}{K_{air}}} \ . \qquad (2\text{-}12)$$

The fibre contribution to the heat flux is calculated by integrating $K(r)\hat{n} \cdot \nabla T$ over a surface perpendicular to the

average temperature gradient, and subtracting the value obtained if there is no fibre and the temperature gradient is constant. The unit vector $\hat{n}$ is given by

$$\hat{n} = \hat{z} \cos \theta_f + (\hat{r} \cos \phi + \hat{\phi} \sin \phi) \sin \theta_f$$

where $\hat{\phi}$, $\hat{r}$, and $\hat{z}$ are the coordinate vectors, and the surface element normal to $\hat{n}$ may be written as $ds = (r/\cos \theta_f) d\phi dr$. Since ∇T is independent of z the integral is easily performed. For $r<a$, we have

$$\hat{n} \cdot \nabla T = T_1 \cos^2 \theta_f + A_1' \sin \theta_f$$

and for $r>a$,

$$\hat{n} \cdot \nabla T = T_1 \cos^2 \theta_f + A_1 \sin \theta_f - A_{-1} r^{-2} \cos 2\phi \ .$$

The term in $\cos 2\phi$ vanishes on integration. In the absence of the fibre, the total integrated heat flux would be just $K_{air} \cdot T_1 \cdot \pi R^2 / \cos \theta_f$, and with the fibre present it is

$$\int H \cdot ds = \frac{\pi}{\cos \theta_f} \{\cos^2 \theta_f [a^2 (K_f - K_{air}) + R^2 K_{air}] \cdot T_1$$

$$+ \sin \theta_f [a^2 (A_1' K_f - A_1 K_{air}) r R^2 A_1 K_{air}]\} \ . \qquad (2\text{-}13)$$

The difference is the contribution of the fibre, and using

(2-10), (2-11), and (2-13) it may be written

$$\int \Delta H \cdot ds = \frac{\pi a^2 T_1}{\cos \theta_f} (K_f - K_{air}) \{\cos^2 \theta_f + \frac{2 \sin^2 \theta_f}{1 + \frac{a^2}{R^2} + (1 - \frac{a^2}{R^2}) \frac{K_f}{K_{air}}}\}$$

or, as $R \to \infty$,

$$\int \Delta H \cdot ds \approx \frac{\pi a^2 T_1}{\cos \theta_f} (K_f - K_{air}) \{\cos^2 \theta_f + \frac{2 \sin^2 \theta_f}{1 + \frac{K_f}{K_{air}}}\} \quad (2\text{-}14)$$

As might be expected, this expression is proportional to the average temperature gradient T_1, so it is easily converted to a thermal conductivity. For a collection of parallel fibres, the number of fibres crossing unit area (where the area element is perpendicular to the temperature gradient) is $f \cos \theta_f / \pi a^2$, where f is again the volume fraction occupied by the fibres. So the thermal conductivity of the mixture of air and aligned fibres is

$$K(\theta_f) = K_{air} + f(K_f - K_{air}) (\cos^2 \theta_f + \frac{2 \sin^2 \theta_f}{1 + \frac{K_f}{K_{air}}}) \quad (2\text{-}15)$$

For randomly-oriented fibres, (2-15) is integrated over angles to obtain

$$K = K_{air} + f(K_f - K_{air}) \cdot \frac{K_f + 5K_{air}}{3K_f + 3K_{air}} . \quad (2\text{-}16)$$

Bhattacharyya (1980) obtained an expression which reduces to (2-16) for small volume fractions f by considering a fibre as the limiting case of a prolate spheroid.

For polyester, the fibre thermal conductivity is about 5 times that of air, so the fractional correction to K_{air} is about 2f, which will be in the range 2% to at most 10%. In the case of hollow fibres, we can correct further for the presence of the hole, but it is clear that such corrections will be small and need not be calculated with great precision. The simplest procedure is simply to replace the filling factor f in (2-15) and (2-16) with $(f-f_h)$, where f_h is the fraction of the total insulation volume occupied by the holes in the fibres. This estimate can be improved with little extra work by noting that the temperature inside the solid fibre considered above has a constant gradient, although the direction differs from that of the average temperature gradient in the medium (see equations (2-7) and (2-10)). If the hole diameter is sufficiently small compared to the fibre diameter, the same analysis may be used for the hole as was used for the solid fibre. Then, in place of (2-15), we have for aligned fibres

$$K = K_{air} + (K_f - K_{air})\{(f-f_h)\cos^2\theta_f + \left(f - \frac{2f_h}{1 + \frac{K_{air}}{K_f}}\right)\frac{2\sin^2\theta_f}{1 + \frac{K_f}{K_{air}}}\} \qquad (2\text{-}17)$$

which may be averaged over angles to give

$$K = K_{air} + (K_f - K_{air})\left[(f-f_h)\,\frac{K_f + 5K_{air}}{3K_f + 3K_{air}} - f_h \cdot \frac{2}{3}\,\frac{K_f/K_{air}-1}{(K_f/K_{air}+1)^2}\right] \qquad (2\text{-}18)$$

for a randomly-oriented collection of hollow fibres. Terms of higher order in the ratio of hole cross-section to fibre cross-section (the ratio f_h/f) have been discarded. For the Hollofil fibres we are dealing with, this ratio is about 10%, meaning that in (2-18) the hole correction itself will be accurate to about 10%, and in any case will be less than 2% of the total conductivity K. Ignoring the hole entirely would introduce a barely discernable error in the final heat transport calculation.

In deriving the expression (2-16) for the conductivity, we discarded terms in a^2/R^2, the ratio of the squared radius of the fibre to that of the boundary cylinder. Since R can be increased to about half the separation between fibres before the assumptions used in the calculation are violated, this ratio a^2/R^2 is approximately the filling factor f. Therefore the correction for the fibres in (2-16) ignores terms of order f^2, leading to errors in the conductivity K of about 1% or less at large batting compressions (f~5-10%) and much smaller errors at normal densities (f≈1%).

2.3 The Diffusion Model of Radiative Transfer

The second major component of the heat transfer in low-density insulation materials is the radiative flux F. In contrast to the conduction transfer discussed in the previous section, the behaviour of the radiation is entirely determined by the properties of the fibres. In this section we develop a description of the radiative part of the heat flow for a homogeneous material whose infrared optical properties are obtained in Chapter 3 by averaging the properties of a single fibre over angle.

A complete description of the radiation involves specifying the radiative intensity $I(x,\nu,\theta)$ as a function of frequency ν, position x, and angle θ (measured from the x-axis). The medium is assumed to be either isotropic, or at least symmetric with respect to rotations about the x-axis, so that I is independent of the azimuthal angle ϕ. It is also assumed that the radiation is unpolarised. From the definition of the intensity as radiative power per unit area per unit solid angle and per unit frequency interval, we see that the radiative flux of equation (2-1) is

$$F(x) = \int_0^\infty d\nu \cdot 2\pi \int_{-1}^{1} I(x,\nu,\mu) \cdot \mu d\mu \qquad (2\text{-}19)$$

where as usual $\mu = \cos\theta$. Therefore the variations of I with angle and frequency, which greatly complicate the radiative

transfer problem, are not needed in detail in heat transport calculations. In the model developed below, approximations to the angle and frequency dependence of the intensity are introduced in order to remove these variables from the problem. The result is a pair of approximate differential equations which, together with (2-1), may be solved for the temperature T and the radiative flux F.

For unpolarised radiation in a slab, the equation of transfer is (e.g., Chandrasekhar, 1960)

$$\mu \frac{dI}{dx} = A\{B(\nu,T) - I\} + \int_{4\pi} [I(\Omega')S(\Omega',\Omega) - I(\Omega)S(\Omega,\Omega')]d\Omega' \qquad (2\text{-}20)$$

where Ω represents the direction (θ,ϕ) and the solid angle element is $d\Omega = \sin\theta d\theta d\phi$. The absorption cross-section per unit volume is represented by A, and $S(\Omega,\Omega')$ is the cross-section per unit solid angle $d\Omega'$ for scattering from the direction Ω to the direction Ω'. The Planck blackbody intensity is $B(\nu,T) = 2h\nu^3/c^2(e^{h\nu/kT}-1)^{-1}$, where h is Planck's constant, k is Boltzmann's constant, and c is the speed of light. The frequency dependence has been suppressed, as has the direction Ω of the radiation (except in the integral). The equation expresses the change in $I(x,\nu,\mu)$ with x as a sum of thermal emission into the beam, absorption from the beam, scattering into the beam, and scattering out

of the beam. For an isotropic material, A is independent of angle. The scattering S is symmetric in its angular arguments, and for an isotropic material, such as the randomly-oriented fibres we are considering, it is a function only of the angle θ_s between the incident and scattered directions.

The diffusion model takes advantage of the fact that in heat transfer problems involving thick media and small temperature gradients, the intensity $I(\nu,\theta)$ must approach the isotropic blackbody intensity regardless of the particular properties of the insulating medium. We define angular moments of the intensity

$$I_n = 2\pi \int I(\mu)\mu^n d\mu \ . \qquad (2\text{-}21)$$

Then multiplying the equation of transfer (2-20) by unity and μ in turn and integrating over all angles Ω yields a pair of differential equations for these moments:

$$\frac{dI_1}{dx} = A(4\pi B(T) - I_0) \qquad (2\text{-}22)$$

$$\frac{dI_2}{dx} = -(A+S_0)I_1 + \int_{4\pi} d\Omega \int_{4\pi} d\Omega' S(\theta_s) I(\mu')\cdot\mu \qquad (2\text{-}23)$$

where the total scattering cross-section is

$$S_0 = 2\pi \int_{-1}^{1} S(\mu)\, d\mu \ . \qquad (2\text{-}24)$$

The argument θ_S of the scattering function in (2-23) depends on both integration variables. It is convenient to change the integration over scattered directions Ω to an integral over scattering angle θ_S, that is, over angles relative to the direction Ω'. We write

$$\cos\theta = \mu = \cos\theta_S \cos\theta' + \sin\theta_S \sin\theta' \cos\phi_S \tag{2-25}$$

where ϕ_S describes the azimuthal rotation of the scattered (Ω') direction about the incident direction. This relation is the first-order case of the addition theorem for spherical harmonics.

Using (2-25) to substitute for μ in the integral in (2-23) allows us to write this integral as

$$2\pi \int_{-1}^{1} d\mu' \int_{-1}^{1} d\mu_S \int_{0}^{2\pi} d\phi_S \; S(\mu_S) I(\mu') \times (\mu_S \mu' + \sin\theta_S \sin\theta' \cos\phi_S) \; .$$

The term in $\cos\phi_S$ conveniently vanishes on integration over ϕ_S, leaving a product of two independent integrals. Defining

$$S_1 = 2\pi \int_{-1}^{1} \mu S(\mu) d\mu \tag{2-26}$$

we may rewrite (2-23) as

$$\frac{dI_2}{dx} = -(A + S_0 - S_1)I_1 . \qquad (2\text{-}27)$$

To close the system of equations (2-27) and (2-23) we set

$$I_2 \approx \frac{1}{3} I_0 \qquad (2\text{-}28)$$

which is equivalent to demanding that the second Legendre moment of $I(\theta)$ vanish. Generally we shall assume the slightly stronger condition that I is a linear function of $\cos\theta$, that is that all Legendre moments higher than first order vanish. This is necessary in formulating boundary conditions. Because the Legendre expansion is truncated after n=1, this description is also called the P-1 model (Pomraning, 1973), and higher-order approximations can be generated by proceeding to higher moments (and more differential equations) before truncating the expansion.

It is important to note that no approximations to the scattering function were required, except that the medium be isotropic. The diffusion model takes account of anisotropy in the scattering by weighting the scattering at large angles more than scattering in the forward direction. The scattering enters in (2-27) only as a difference S_0-S_1, which can be thought of as a single scattering parameter defined using a weight function of $(1 - \cos\theta_s)$:

$$S_0 - S_1 = 2\pi \int_{-1}^{1} S(\mu)(1-\mu)\,d\mu \ . \qquad (2\text{-}29)$$

Scattering at 180° receives twice the weight of scattering at right angles, and forward ($\theta_S=0$) scattering has zero weight.

So far the frequency variable has been ignored in the derivations. Both the absorption and scattering coefficients are strongly frequency-dependent, but again, these variations are largely washed out in the intensity $I(\theta,\nu)$ if the system is close to thermodynamic equilibrium. Equations (2-22) and (2-27) are integrated over frequency to give the approximate "grey" equations

$$\frac{dF}{dx} = \rho\kappa_A(4\sigma T^4 - U) \qquad (2\text{-}30)$$

$$\frac{dU}{dx} = - 3\rho\kappa_T F \qquad (2\text{-}31)$$

with (2-28) substituted into (2-27) before integrating. Here U and F are the frequency integrals of I_0 and I_1, respectively, so that U is proportional to the energy density, and F is the radiative flux defined previously. The Stefan-Boltzmann constant is denoted by σ, and the density of the batting is ρ. We have introduced the frequency-averaged cross-sections per unit mass defined by

$$\frac{1}{\rho\kappa_T} = \frac{1}{N}\int_0^\infty \frac{1}{A(\nu) + S_0(\nu) - S_1(\nu)} \frac{dB(\nu,T)}{dT}\, d\nu \qquad (2\text{-}32)$$

$$\kappa_A = \frac{1}{N}\int_0^\infty A(\nu)\, \frac{dB(\nu,T)}{dT}\, d\nu \qquad (2\text{-}33)$$

where

$$N = \int_0^\infty \frac{dB(\nu,T)}{dT}\, d\nu$$

The averaging formula used for the 'transport opacity' κ_T is the usual Rosseland prescription and arises because $I_0(x,\nu) \approx B(T(x),\nu)$ in (2-28) and thus in (2-27) if the medium is close to thermodynamic equilibrium, as is the case if the insulation is optically thick and the temperature gradient is small. Similarly the formula (2-33) for the mean absorption is obtained by assuming in equation (2-22) that the difference between I_0 and $4\pi B(T)$ is to first order equivalent to a difference in temperature between the radiation and the material at a given position x. Other averaging prescriptions have been suggested but are less suitable for this particular problem (Pomraning, 1973).

Boundary surfaces of temperature T_H and T_C are placed at x=0 and x=L, respectively, assuming grey walls obeying Lambert's law with emissivities ε_H and ε_C. The incoming radiation at each surface is considered to have an angular distribution linear in cos θ, and the net flux at the wall is matched to that in the material to give a boundary condition for the radiation.

At x=0, the incoming intensity is

$$I(\mu) = \frac{1}{4\pi} (I_0 + 3I_1 \cdot \mu) \quad , \quad \mu<0$$

and so the incoming flux is

$$2\pi \int_0^\infty d\nu \int_{-1}^{\infty} I(\mu)\mu d\mu = -\frac{1}{4} U + \frac{1}{2} F$$

where U and F refer to the radiation in the medium.

A fraction ε_H of this incoming flux is absorbed at the wall, and the remainder is reflected diffusely, so that it adds to the outgoing flux $\varepsilon_H \sigma T_H^4$ emitted by the wall. Therefore the net power/unit area radiated by the wall is the difference of the emitted and absorbed fluxes, given by

$$F_W = \varepsilon_H(\sigma T_H^4 + \frac{1}{4} U - \frac{1}{2} F) \quad . \qquad (2\text{-}35)$$

In this equation, F really represents the coefficient of the cos θ term in the incoming radiation (within a factor $3/4\pi$) and not necessarily the total flux. Deep in the medium the radiative intensity is linear in cos θ over all solid angles, but at the wall we are assuming the intensity is uniform in the outgoing hemisphere, and has the form (2-34) in the incoming hemisphere, with a discontinuity at μ=0. The usual boundary condition results from setting F_W=F in (2-35), effectively matching the flux in the medium away from the

wall with the flux at the boundary. This yields

$$F(0) = \frac{\varepsilon_H}{2-\varepsilon_H} \left(2\sigma T_H^4 - \frac{1}{2} U(0)\right) \qquad (2-36)$$

$$F(L) = -\frac{\varepsilon_C}{2-\varepsilon_C} \left(2\sigma T_C^4 - \frac{1}{2} U(L)\right) . \qquad (2-37)$$

A discussion of other methods of generating boundary conditions for differential approximations to the radiative transfer problem may be found in the book by Pomraning (1973) and in Shokair and Pomraning (1981).

Equations (2-1), (2-30), and (2-31), along with the definitions (2-32) and (2-33) form a system of coupled non-linear differential equations in T(x), F(x), and U(x). Together with the boundary conditions (2-36) and (2-37) and the specified values of the temperature at the walls, these equations constitute an approximate description of combined radiative and conductive heat transport in a slab of insulation.

Although the equations of the diffusion model are usually developped only for the case of an isotropic medium (in which absorption and scattering properties do not depend on the incident direction) the model is readily extended to more general materials. For fibrous insulations, these would include in particular materials in which the fibres are not randomly distributed in space, but are aligned to some degree parallel or perpendicular to the heat flow

direction. Then in the equation of transfer (2-20) the absorption constant will be a function of direction Ω, and we will not be able to make the simplifying assumption that the scattering function depends only on the scattering angle. We restrict ourselves to materials whose properties depend on θ but not on the azimuthal angle about the direction of heat flow, as would be the case for a fibrous material in which the fibres tend to lie in the plane of the slab, but are not aligned with respect to the long edges of the batt. We also require that the batt look the same from both sides, that is, the properties are identical in the μ and $-\mu$ directions. Then, writing explicitly $I(\mu) = \frac{1}{4\pi}(I_0+3I_1\mu)$ and proceeding as before to multiply the equation of transfer by 1 or by μ and integrating over all angles gives

$$\frac{dI_1}{dx} = A_0(4\pi B(T) - I_0). \tag{2-38}$$

$$\frac{1}{3}\frac{dI_0}{dx} = -(A_2 + S_{2,0} - S_{1,1})I_1 \tag{2-39}$$

where

$$A_n = \frac{n+1}{4}\int_{4\pi} A(\mu)\mu^n d\Omega \tag{2-40}$$

$$S_{n,m} = \frac{(n+1)(m+1)}{4\pi}\int_{4\pi}\int_{4\pi} S(\Omega,\Omega')\mu^n\mu^m d\Omega d\Omega' \quad . \tag{2-41}$$

The normalisation on the optical parameters A_n and $S_{n,m}$ has been chosen to make the correspondence between (2-38), (2-39) and (2-22), (2-27) simple. The only difference in the case

of an oriented material is in the definition of the absorption and scattering parameters.

Throughout this chapter we have dealt with cross-sections per unit volume for the frequency-dependent optical parameters. It is common in theoretical discussions to use dimensionless parameters for the angular part of the scattering (phase function), for the ratio of scattering to total extinction cross-section (albedo for single scattering) and for the first angular moment of the scattering (anisotropy parameter). To facilitate comparisons between this work and others, Table 2-1 lists several optical parameters found in the literature with definitions in terms of the notation used in this chapter. For our purposes, the total scattering cross-section is an awkward parameter to use for normalisation. As we shall see in the next chapter, the scattering is strongly peaked in the forward direction. Direct measurements of the scattering cross-section as a function of angle will generally yield a phase function (for instance) which is larger than the calculated values because of the difficulty of measuring the scattering very close to the incident beam (Shuetz, 1983) and which causes the total cross-section to be underestimated. Similarly, for opaque objects large compared to the wavelength, the total extinction cross-section calculated from geometrical optics is just half that calculated from wave optics (Van de Hulst, 1957). The difference is just the diffracted radiation which fills the

TABLE 2-1

Definitions of Radiation Parameters

Parameter	Typical Symbol	Corresponding Parameter in Present Work
Scattering Cross-Section per Unit Volume	σ	S_0
Extinction Coefficient	β	$S_0 + A$
Single-Scattering Albedo	ω_0	$\frac{S_0}{S_0 + A}$
Phase Function	$P(\Omega,\Omega')$	$\frac{S(\Omega,\Omega')}{S_0}$
Anisotropy Parameter	$\left\{\begin{matrix}\langle\cos\ \theta_s\rangle \\ \omega_1/\omega_0\end{matrix}\right\}$	$\frac{S_1}{S_0}$
Effective or Modified Extinction Coefficient	K_E^*	$A + S_0 - S_1$

All the above parameters are in general functions of the radiation frequency ν.

geometrical shadow of the scatterer. It is scattered at very small angles, and has no significant effect on the radiative transfer. Some authors (Modest and Azad, 1980a, 1980b; Shuetz, 1983) introduce a modified total scattering cross-section with part or all of this forward-scattering peak excluded, and a corresponding modified phase function. The missing scattering is reintroduced into the problem as a delta function, and eventually contributes nothing to the heat transport. Note that the scattering enters into the diffusion model only through the difference S_0-S_1, to which the scattering at zero degrees contributes nothing (equation (2-29)). We may therefore calculate this parameter by geometrical or wave methods as appropriate, without the necessity for simultaneously keeping an eye on the total cross-section S_0.

At this point we should mention other commonly-used differential approximations for radiative transfer and discuss their relationship with the diffusion model. Models based on the assumption of isotropic scattering or pure absorption are essentially special cases of the diffusion model, and can be obtained by setting $S_1=0$ (for isotropic scattering) or $S_0=S_1=0$ (for pure absorption) in equation (2-32), which defines κ_T. For the polyester fibre insulations we are considering, both assumptions are inadequate and lead to very inaccurate predictions for radiative heat transfer.

The two-flux model is widely used to characterise radiative transfer in insulation materials (Larkin and Churchill, 1959; Farnworth, 1983; Berquam and Seban, 1971). Here the radiation is divided into two hemispheres and the left and right fluxes F_L and F_R are treated separately. Differential equations are developed by considering the change in F_R and F_L in passing through a thin slab of insulation of thickness dx. Calculating the various contributions in terms of the basic absorption and scattering cross-sections requires an assumption about the angular variation of the intensity. Generally the radiation is assumed to be isotropic in each hemisphere separately, with a discontinuity at 90°. Neglecting the frequency dependence of the optical parameters, we have

$$\frac{dF_R}{dx} = - 2A(\sigma T^4 - F_R) - 2bS_0(F_R - F_L) \qquad (2\text{-}42)$$

$$- \frac{dF_L}{dx} = - 2A(\sigma T^4 - F_L) + 2bS_0(F_R - F_L) \; . \qquad (2\text{-}43)$$

The backscattering fraction b is calculated by considering the fraction of an incident ray in the left hemisphere which is scattered into the right hemisphere, and integrating over incident angles. For isotropic scattering, $b = \frac{1}{2}$. The other parameters A and S_0 are the same absorption and total scattering cross-sections used above, but here they are assumed frequency-independent for simplicity. The

relationship between the two-flux and the diffusion model is clearly seen if we take the sum and difference of the two-flux equations, giving

$$\frac{d}{dx}(F_R - F_L) = A[4\sigma T^4 - 2(F_R + F_L)] \qquad (2\text{-}44)$$

$$2\,\frac{d}{dx}(F_R + F_L) = -\,4(A + 2bS_0)(F_R - F_L)\ . \qquad (2\text{-}45)$$

To compare with the diffusion model we note that the net flux F is $F_R - F_L$, and the energy density U corresponds to $2(F_R + F_L)$. Then, (2-44), (2-45) are identical to the diffusion-model equations (2-30), (2-31) except that the factor 3 in (2-31) is replaced by 4 in (2-45), and $S_0 - S_1$ in the definition of κ_T has been replaced by $2bS_0$. For isotropic scattering, $b = \frac{1}{2}$, and the two scattering parameters are identical. Therefore the factor 4/3 indicates a real difference between the models. For a thick batt, the two-flux model predicts only 3/4 of the radiative flux given by the diffusion model. Direct comparisons (Berquam and Seban, 1971; McKay et al., 1983) confirm the superior accuracy of the diffusion approximation. The two-flux model is sometimes modified by adding a factor $\sqrt{3}/2$ in front of F_L and F_R on the right hand side of (2-42) and (2-43) (Berquam and Seban, 1971). This will make the prediction for the heat flux identical to that of the diffusion model. This strange-looking factor arises from a very different approximate

solution of the equation of transfer in which the angular moments of the intensity are evaluated by a low-order Gaussian quadrature (e.g., Pomraning, 1973). Consider equations (2-22) and (2-27), which were derived as intermediate steps in the diffusion model and involve no approximations to the equation of transfer. Instead of setting $I_2 = \frac{1}{3} I_0$ in (2-27), as in the diffusion model, we evaluate the moments I_0, I_1, and I_2 by a 2-point Gauss-Legendre quadrature. Recall that this means setting

$$\int_{-1}^{1} f(\mu)d\mu \approx f(\mu^+) + f(\mu^-) \tag{2-46}$$

where $\mu^{\pm} = \pm 1/\sqrt{3}$ are the zeros of the Legendre polynomial $P_2(\mu)$. Then

$$I_0 \approx I^+ + I^- \tag{2-47}$$

$$I_1 \approx \frac{1}{\sqrt{3}} (I^+ - I^-) \tag{2-48}$$

$$I_2 \approx \frac{1}{3} (I^+ + I^-) \tag{2-49}$$

where $I^{\pm} = I(\mu^{\pm})$. Substituting in (2-22) and (2-27) gives a pair of differential equations for I^+ and I^- which may be rearranged into the form of the two-flux equations (2-42), (2-43) if desired. Note that (2-47) and (2-49) guarantee that $I_2 = \frac{1}{3} I_0$, so the resulting equations must be identical

to those of the diffusion model. In the present case, the crucial approximation is generated by assuming that the angular variation of $I(\mu)$ is sufficiently smooth that a two-point Gaussian quadrature is adequate, whereas in the diffusion model we use the similar requirement that the second Legendre moment of $I(\mu)$ be small compared to I_0.

This two-point or two-beam model keeps track of the intensity only at two particular angles, one in each hemisphere, and in this is similar to the usual 2-flux model. But the two flux model assumes a particular shape for the angular radiation in each hemisphere, with a different overall constant for left and right-going radiation and an unphysical discontinuity at 90°. In the other case, it does not matter how the angular part of the radiation behaves as long as it remains smooth enough that the Gaussian quadrature is accurate. In this it better represents radiative transport of heat under near-equilibrium conditions.

2.4 Approximate Solution of the Model Equations

The equations (2-1), (2-30) and (2-31) are nonlinear, and must be solved numerically. However, an important advantage of a differential formulation of the heat-transfer problem lies in the intuitive understanding of the process which results from an approximate analytic solution. For our purposes, the approximation can also be reasonably accurate. For the modest temperature differences across the batt (10-20 K at a temperature of about 300 K) used in the thermal measurements, the equations are "nearly" linear.

The nonlinearity arises primarily because of the T^4 term in (2-30). The thermal conductivity of air is approximately proportional to $T^{1/2}$, a much slower variation. The optical parameters κ_T and κ_A also depend on temperature since they are thermally-weighted averages over frequency, but as we shall see in Chapter 3, this variation is small. Therefore, we ignore the temperature dependence of K, κ_T and κ_A, evaluating them all at the mean temperature $T_m = (T_H + T_C)/2$. The temperature is written as $T(x) = T_m + t(x)$ and, therefore,

$$T^4 \approx T_m^4 + 4T_m^3 t \ . \qquad (2\text{-}50)$$

The first neglected term, as a fraction of T_m^4, is $6t^2/T_m^2$. For $T_m = 300$ K and $t \leq 10$ K, equation (2-50) is accurate to

better than 1%. Under the same conditions, K is constant to about 1.5% if we assume $K \propto T^{\frac{1}{2}}$, as is the case for a dilute gas of hard spheres. The calculations of the next chapter show that κ_A and κ_T for the polyester materials are also constant within 1 or 2% over the same temperature range.

The method of linearising the differential equations has been used by Larkin and Churchill (1959) and more recently by Farnworth (1983) to solve a two-flux model of combined radiative and conductive heat transport, which leads to differential equations with essentially the same structure as the diffusion model. The solution will be outlined here, and formulae presented for the simpler case of identical boundary walls, $\varepsilon_H = \varepsilon_C$. A FORTRAN program which calculates the heat flux for any set of parameters is listed in Appendix I.

To begin with, we use (2-31) to substitute for F in (2-1), giving

$$H = \frac{-1}{3\rho\kappa_T}\frac{dU}{dx} - K\frac{dt}{dx} \qquad (2\text{-}51)$$

which is integrated from the left boundary (x=0) to give, after some rearrangement,

$$U(x) = U(0) - 3\rho\kappa_T[Hx + K(t(x)-t(0))] \; . \qquad (2\text{-}52)$$

Since K is assumed constant, and H is constant, (2-1) may be

differentiated to give

$$\frac{d^2t}{dx^2} = \frac{1}{K}\frac{dF}{dx} \qquad (2\text{-}53)$$

Finally we use (2-52) to substitute for U(x) in (2-30), and combine this with (2-53) to obtain a second-order differential equation in the temperature alone,

$$\frac{d^2t}{dx^2} = -p^2C_0 - p^2C_1x + p^2t \qquad (2\text{-}54)$$

where

$$p = [(3\rho\kappa_T)(\rho\kappa_A)(\frac{K_R}{K} + 1)]^{\frac{1}{2}} \qquad (2\text{-}55)$$

$$K_R = \frac{16\sigma T_m^3}{3\rho\kappa_T} \qquad (2\text{-}56)$$

$$p^2C_0 = -\rho\kappa_A[K(4\sigma T_m^4 - U(0)) - 3\rho\kappa_T t(0)] \qquad (2\text{-}57)$$

$$C_1 = -\frac{H}{K_R+K} \qquad (2\text{-}58)$$

The solution to (2-54) has the form

$$t(x) = C_0 + C_1x + C_2e^{-px} + C_3e^{+p(x-L)} \qquad (2\text{-}59)$$

We see immediately that C_1 represents the temperature gradient at positions sufficiently far from the boundaries that the exponentials are small. Thus K_R is interpreted

(from (2-58)) as a radiative conductivity, although this is only strictly meaningful if the boundary effects can be ignored. The typical penetration depth for the boundary effects is p^{-1}, which is proportional to the geometric mean of the absorption length $(\rho\kappa_A)^{-1}$ and $(\rho\kappa_T)^{-1}$, which we might call an effective extinction length. The rate of energy exchange between radiative and conductive modes of transport is dF/dx, given by equation (2-53). Thus p^{-1} may also be understood as the typical interaction depth for the two types of heat flow.

We can substitute (2-59) into (2-52) to give an explicit expression for U(x), and similarly we can substitute for dt/dx in (2-1) to obtain an expression for F(x). The constant C_1 is eliminated in favour of H using (2-58) and we eliminate C_0 in favour of t(0) by evaluating (2-59) at x=0:

$$C_0 = t(0) - C_2 - C_3 e^{-pL} . \qquad (2\text{-}60)$$

Next (2-57) is used to express U(0) as

$$U(0) = 4\sigma(T_m^4 + 4T_m^3 t(0)) - 3\rho\kappa_T(K_R+K)[C_2 + C_3 e^{-pL}] . \qquad (2\text{-}61)$$

So finally we are left with expressions U(x), F(x) and t(x) which contain only four unknown parameters, C_2, C_3, H and t(0). The condition $T(0) = T_H$ determines t(0); the other 3 are taken care of by the condition $T(L) = T_C$ and the two

radiative boundary conditions (2-36) and (2-37) which relate U and F at x=0 and at x=L. This 3×3 linear algebraic system is straightforward but tedious to solve. In the common situation of identical boundaries, $\varepsilon_C = \varepsilon_H = \varepsilon$, the solution for the heat flux has the reasonably compact form

$$H = \frac{T_H - T_C}{L} (K_R + K) \left\{ 1 + \frac{K_R}{\frac{\varepsilon}{2-\varepsilon} (K + K_R) \frac{L}{D} + K \frac{pL}{2} \coth \frac{pL}{2}} \right\}^{-1} \tag{2-62}$$

where

$$D = \frac{4}{3\rho K_T} . \tag{2-63}$$

For the general case of boundary surfaces which are not identical, the algebraic expression for H is much more complicated. Appendix I lists a FORTRAN program which solves for the heat flux in the general case.

As the coupling coefficient p goes to zero -- that is, as the absorption goes to zero while the scattering remains constant -- the radiative and conductive heat transfer become uncoupled. Since x coth x → 1 as x → 0, we can rewrite (2-62) in the case of a purely scattering medium as

$$H \simeq \left[\frac{K}{L} + \frac{1}{\frac{L}{K_R} + \left(\frac{2}{\varepsilon} - 1\right) \frac{1}{4\sigma T_m^3}} \right] (T_H - T_C) . \tag{2-64}$$

In this case the total heat flux is the sum of two independent contributions. The conductive part is inversely

proportional to the thickness L, but the radiative part is not. We can think of the radiative heat transfer as being determined by a thermal resistance L/K_R in series with a boundary resistance $(4\sigma T_m^3)^{-1}(\frac{2}{\varepsilon} - 1)$, which is independent of the thickness of the batt, and may be assigned half to each boundary. It is this "boundary" resistance which limits the radiative heat transfer to a finite value when the medium is transparent to thermal radiation. If the emissivity ε of either boundary goes to zero, the 'boundary resistance' becomes infinite and there is no radiative heat transport in equation (2-64). Note that such is not the case if there is absorption as well as scattering, as in (2-62). Although the radiative flux near the reflecting wall is zero, over a distance p^{-1} energy is transfered into the radiation field by thermal emission from the fibres. If the batt is sufficiently thick, the effective total thermal conductivity becomes just $K+K_R$, independent of the value of boundary emissivity ε.

These two effects, the boundary resistance determined by the emissivity of the boundary surfaces, and the rearrangement of energy between radiation and conduction in a region near the walls, are responsible for the well-known "thickness effect" in low-density insulation materials (Shirtliffe, 1980; Hollingsworth, 1980). The total thermal resistance of a stack of insulation batts is observed to be smaller than the sum of the resistances measured

individually, because of the boundary terms in the radiative part of the heat transfer.

2.5 Accuracy of the Model

There are several parts to the question of the accuracy of the model for combined radiative and conductive heat transport which is summarised in equation (2-62). The combining of gas and fibre conductivities into a single parameter K involved approximations which relied on the volume fraction f being small. Later, in combining the conductive and radiative portions of the problem, we assumed that the medium could be treated as homogeneous, essentially by-passing the question of thermal contact between the fibres (which participate in the radiative transport) and the air. The solution of the differential equations was performed by replacing nonlinear terms with approximate linear terms. Finally, the question of the intrinsic accuracy of the diffusion model as a solution of the equation of transfer must be considered.

The accuracy of the formula (2-16) for the conductivity of the mixture of fibres and air has already been considered in Section 2.2. For polyester fibres, the fibre correction to K is about 2 Kf, and ignores terms in f^2. For f between 1% and 5%, the resulting error in K should be less than about 0.5%, and will be much smaller at the lower densities. This, however, includes only the mathematical approximations, and not the possibility that the fibres are not randomly oriented in space. In the

extreme case of the fibres lying flat in the plane of the batting, the fibre correction (again, for polyester) would be reduced from about 2 Kf to about 1.2 Kf, a difference of about 0.8f as a fraction of K. This could be as high as 4% for f = 0.05, although we have chosen an extreme case. It should be safe to assume that (2-16) estimates K to an accuracy of 1% for the real material at f = 0.05, if K_{air}, K_f and f can be determined with sufficient precision.

To investigate the thermal contact between the fibres and the air, we return to the isolated cylinder of radius a inside a concentric boundary cylinder of radius R, and reinstate the ℓn r term in the temperature which was dropped from (2-4). We assume the temperature of the fibre is T_a, and at the boundary surface it is T_R. We let the temperature for a < r < R be given by

$$T(r) = \frac{T_R - T_a}{\ell n \frac{R}{a}} \ell n \frac{r}{a} + T_a \quad . \tag{2-65}$$

The presence of additional terms of the form (2-4) does not affect the argument. The function T in (2-65) is a solution of Laplace's equation, as required. The total heat flowing outwards at the fibre surface, per unit length, is

$$\frac{h}{L} = (2\pi a)\left(- K_{air} \left.\frac{dT}{dr}\right|_{r=a}\right)$$

$$= 2\pi \frac{T_R - T_a}{\ell n \frac{R}{a}} \quad . \tag{2-66}$$

The net heat flowing from the fibres into the air must be balanced by a net flow of radiation into the fibres. Consider a slice of the medium of area A and thickness dx. The net power disappearing from the radiation field into this slice is

$$h = \frac{dF}{dx} \cdot A \cdot dx \tag{2-67}$$

and the net outward transport of heat from all the fibres in the slice, from (2-64), is

$$h = 2\pi K_{air} \frac{T_R - T_a}{\ell n \frac{R}{a}} \cdot \frac{f}{\pi a^2} \cdot A \, dx \, . \tag{2-68}$$

Equating (2-67) and (2-68) leads to

$$T_R - T_a = \frac{a^2 \ \ell n \frac{R}{a}}{2f} \frac{dF}{dx} \, . \tag{2-69}$$

It is reasonable to take R as approximately half the mean distance between fibres, so $\ell n \frac{R}{a} \approx \frac{1}{2} \ell n \, f^{-1}$. We can estimate $\frac{dF}{dx}$ using the solution of the previous section. The scale length for energy exchange between radiative and conductive modes is p^{-1}, where p is given by (2-55). So we write

$$\frac{dF}{dx} = \alpha p F$$

$$\approx \alpha p K_R \frac{\Delta T}{\Delta X}$$

where $\alpha \leq 1$, and $\Delta T/\Delta X$ represents the average temperature gradient in the batting. Finally, (2-69) is rewritten as

$$T_R - T_a \approx \alpha(ap)\left(\frac{1}{4}\ln f^{-1}\right) f^{-1}\left(\frac{K_R}{K_{air}}\right)\frac{a}{\Delta X}\cdot\Delta T \ . \qquad (2\text{-}70)$$

For the polyester materials at normal densities, $a \approx 10\ \mu m$, $p^{-1} \approx 5$ mm, $K_R \approx K_{air}$, and $f \approx 0.01$. Then (2-62) gives

$$\frac{T_R - T_a}{\Delta T} \approx 2 \times 10^{-3}\ \frac{\alpha}{f}\ \frac{a}{\Delta x} \ . \qquad (2\text{-}71)$$

By choosing $\Delta X = a$, $f = 0.01$, we can say that the temperature difference between the fibres and the air half-way between two fibres is less than about 20% of the average temperature difference in the batt over a distance of one fibre radius. Perhaps a more meaningful way to express (2-71) is to take $\Delta x = R$, and write $f \approx a^2/R^2$, so that

$$T_R - T_a \approx 2 \times 10^{-3}\ \frac{\alpha}{\sqrt{f}}\ \frac{R}{\Delta x}\ \Delta T \ . \qquad (2\text{-}72)$$

This means that the temperature difference $T_R - T_a$ is less than about 2% of the average temperature gradient over the same distance R. In general, the factor α will be substantially smaller than unity, so the difference will be smaller. The effect of such a difference between the fibre and its surroundings is in any case not so much to reduce the total heat flux directly as to increase the distance

over which the radiative and conductive parts of the heat flux reach their equilibrium proportions. So the 2% factor applies only to a region near the boundary surfaces, and the error in the total heat flux will be smaller by a factor of about $(pL)^{-1}$, typically about 0.1. The total error in the heat flux H will be of the order of 0.2% and is negligible for the calculations in this work.

The error introduced by linearising the differential equations can also be roughly estimated. We noted in Section 2.4 that for a temperature difference of 20 degrees across a batt at a mean temperature of 300 K, the individual terms in the differential equations never varied by more than 2% from the approximate forms assigned to them. But since the net heat flux depends on the insulation properties integrated through the thickness of the batt, the errors tend to cancel to first order. The approximate parameters are correct at the mean temperature, and so are underestimated in half the material and overestimated in the other half. To put this more clearly, we can formally integrate (2-1) to give

$$H \times L = \int_0^L F \, dx = \int_{T_H}^{T_C} K(T) \, dT \, . \qquad (2\text{-}73)$$

But using (2-30) and (2-31), we can write

$$\int_0^L F \, dx = \int_{T_H}^{T_C} \frac{16\sigma T^3}{3\rho\kappa_T} \, dT - \left[\frac{1}{3\rho\kappa_T \cdot \rho\kappa_A} \frac{dF}{dx}\right]_{x=0}^{L} \, . \qquad (2\text{-}74)$$

The object of this is to show how the heat flux H depends on the assumptions that K, κ_T, κ_A and T^3 can be replaced by their values at the mean temperature T_m. The largest part of H is represented by the two integrals over T, which can be evaluated using the relation

$$\int_a^b f(x)\,dx \approx (b-a)\,f(x_m)\left[1 + \frac{(b-a)^2}{24}\,\frac{f''(x_m)}{f(x_m)}\right] \qquad (2\text{-}75)$$

where $x_m = \frac{1}{2}(b+a)$ and terms of higher order in (b-a) have been ignored. So, ignoring for the moment the term in $\frac{dF}{dx}$ in (2-74), we see that the approximations $T^3 \approx T_m$, $K \approx K(T_m)$, etc., introduce in H errors of about

$$\frac{(T_H-T_C)^2}{24T_m^2} \times \frac{T_m^2}{G}\,\frac{d^2G}{dT^2}\bigg|_{T_m} \approx \frac{(T_M-T_C)^2}{T_m^2}\,\frac{(n-1)(n-2)}{24} \qquad (2\text{-}76)$$

where the function G(T) can represent K(T) or $K_R(T)$. For T_m = 300 K, T_H-T_C = 20°, the error in the radiative part is 0.1%, and in the conductive part, (with $K \propto T^{1/2}$) less than 0.01%.

So far the last term in (2-74) has been ignored. It clearly can be thought of as a boundary term, and using the definition (2-55) of the parameter p, we write it as

$$\Delta H_B \approx \frac{1}{L}\left[\frac{1 + \frac{K_R}{K}}{p^2}\,\frac{dF}{dx}\right]_{x=0}^{L} \qquad (2\text{-}77)$$

Again, setting $K_R \approx K$, $\frac{dF}{dx} = \alpha p/2 \cdot H$, we have

$$\frac{\Delta H_B}{H} \approx \frac{\alpha}{pL} \lesssim 0.1 \qquad (2\text{-}78)$$

where $\alpha \lesssim 1$. The terms in (2-77) do not cancel since dF/dx has opposite signs at the two boundaries. Therefore, replacing all parameters by their mean values in (2-74) will introduce an error of a few percent in this "boundary term" (the error will be linear in $T_H - T_C$). Because of (2-78), however, we can be confident that the total heat flux H will be accurate to several tenths of a percent.

The accuracy of the model depends on the parameters f (the filling factor), $\Delta T/T_m$ ($\Delta T = T_H - T_C$), and $(pL)^{-1}$, which represents an average value of $L/F|dF/dx|$ in the batt. The error in K due to the approximate method of combining the individual comductivities of the air and the fibres is about $f^2 K$. Ignoring the details of the net absorption of radiation by the fibres and the subsequent conduction into the air introduces only a negligible error of the order of $a/(L\sqrt{f})$ where a is the fibre radius. Replacement of T^3, K, and the optical parameters by their values at the mean temperature introduces an error in the total apparent conductivity of the batt which is about $(0.2\ K_R + 0.02\ K)(\Delta T/T_m)^2$, plus a part connected with the behaviour of the solution near the boundaries. This last is more difficult to estimate, but should be of the order of $(\Delta T/T_m)(pL)^{-1}$. All of these together add up to an error of

about 1% or less under the conditions of the thermal measurements in Chapter 4. More significant is the possible error introduced by the assumption of randomly-oriented fibres. The necessary correction to K is about -0.8 fK if the fibres are completely parallel to the plane of the batt, and would be some appreciable fraction of this for more realistic distributions. It is linear in f, and may be of the order of 1% for the denser batts (f ≃ 5%).

The accuracy of the diffusion approximation itself -- that is, the replacement of the complete equation of transfer for a homogeneous material by (2-31), (2-32), and the approximate boundary conditions (2-36) and (2-37) -- has been investigated by a few authors who have compared the model with accurate numerical solutions for various hypothetical materials. Berquam and Seban (1971) compared the two-flux model with the numerical results of Viskanta (1965) for isotropic scattering. For two sets of parameters, they also calculated the results of a "modified two-flux" model, with factors of $1/\sqrt{3}$ introduced in the equations. As explained in Section 2.3, this model is fully equivalent to the diffusion model. All their calculations were for slabs of unit optical depth, thinner by a factor of at least 5 than the batts considered in this work; their calculations thus test the model under more stringent conditions, as the approximations ought to improve for thicker materials. Two results were reported using the

"modified two-flux" model. Both had black boundaries and $K_R(T_H) = 13.3$ K. In the first case, with equal scattering and absorption parameters and $T_C = \frac{1}{2} T_H$, the diffusion model predicted a heat flux smaller than the exact solution by 1.7%. The second case assumed no scattering and $T_C = 0.1\ T_H$, and the diffusion model result was too high by 0.5%. In both cases, the accuracy was much better than the ordinary two-flux model. Note that the temperature differences considered are very large, and the medium is optically thinner than a practical insulation layer.

Schuetz (1982) similarly compared the results of a diffusion-model calculation with exact numerical results, obtained this time from a finite-difference computer program. He used experimentally-determined scattering functions obtained from monochromatic measurements on foam and glass-fibre insulations. The scattering was strongly anisotropic in both cases. Boundary emissivities were $\varepsilon_H = \varepsilon_C = 0.86$, and the thickness L was 38 mm. For the glass fibres, this corresponded to an optical thickness of 27, and for the foam, a thickness of 75. Mean temperature was 298 K and the temperature difference was 24°. As expected for an optically thick batt, the heat flux predicted by the diffusion model was very accurate, within 0.2% of the exact result. These conditions are typical of the more highly compressed polyester battings. The lower-density batts are optically thinner, with a greater

temperature difference per extinction length, but the diffusion model should still give much more accurate results that the 1% or so in the calculations of Berquam and Seban discussed previously.

We should also mention the calculations of Modest and Azad (1980a, 1980b) who considered pure radiative transfer in clouds of spherical particles with or without absorption. They calculated the anisotropic scattering functions from Mie theory, and solved the equation of transfer exactly by expanding the phase function in up to 35 Legendre polynomials. They then approximated the scattering function by a part linear in $\cos\theta$ plus a delta-function at $\theta = 0$ (and in some cases, a second delta-function at $\theta = \pi$). This approximate scattering function was used in a diffusion-model solution (and also in an exact solution, which is possible for linear-anisotropic scattering functions). The resulting heat flux is generally close to the exact solution, particularly for optical depths greater than 4 or 5. It would appear from their graphs that the errors could be as large as 5% in some cases. However, I believe this is due to the procedure of approximating the scattering function. Essentially this involved placing all the scattering for $\mu > \mu_f$ into a delta-function at $\mu = 1$. They do not specify the value of μ_f, but it appears to have been chosen as 0.7-0.9, depending on the shape of the forward-scattering peak. About [illegible] the total scattering

will lie in this peak. Remember that the diffusion model uses the moment S_0-S_1, the integral of the scattering weighted by a factor $(1-\mu)$. So the fractional error (reduction) in S_0-S_1 will be about 0.2 $(1-\mu_f)$, with the numerical factor depending on the shape of the peak. Thus for $\mu_f = 0.8$, we would expect the heat flux to be overpredicted by about 4% (for pure scattering) which is indeed observed in their calculations. The other two calculations mentioned, which solved the diffusion model and the exact equation using the same scattering function for both, give a better picture of the accuracy of this approximation.

Nothing we have said so far bears on the question of how accurate it is to define the frequency-averaged parameters κ_A and κ_T and solve the equations with a single group of frequencies. It is difficult to estimate precisely the error involved. Certainly this one-group approximation becomes exact as the temperature gradient is reduced and the insulation approaches thermal equilibrium. An approximate, and probably optimistic, estimate of the error can be obtained by expanding the blackbody function $B(\nu,T)$ in powers of δT, where $\delta T = \frac{1}{\rho\kappa_T}\frac{dT}{dx}$ is the temperature difference per optical depth. This first term, $\delta T \frac{dB}{dT}$, leads to the frequency-averaged equations (2-31), (2-32). The correction to this is smaller by a factor of $\delta T/T$, which is about 1 or 2%. This is a qualitative

argument at best, but should give a rough idea of the accuracy of the one-group approach. The frequency-dependent effective extinction cross-section which enters into κ_T does not vary too dramatically with frequency, which improves the approximation. The absorption cross-section, however, is rather strongly frequency-dependent, and those effects depending on κ_A (the coupling between radiation and conduction) will probably be less accurately predicted.

Ultimately, the accuracy of this approximation could be tested by solving the differential equations for several frequency groups simultaneously. Until the precision of thermal measurements improves, this would seem to involve an unjustifiable increase in the complexity of the calculations.

CHAPTER 3

SCATTERING FROM CYLINDERS

3.1 Introduction

In order to apply the radiative transfer model described in the previous chapter to a practical insulation material we need the absorption and total scattering cross-sections per unit volume and the first angular moment of the scattering. The peak of the thermal weight function dB/dT is at about 800 cm^{-1} (or a wavelength of about 12.5 μm) at 300°K, and 99% of the weight is at frequencies below 2500 cm^{-1} (wavelengths longer than 4 μm). These wavelengths are comparable to the fibre diameter of 25 μm for Polarguard and Hollofil. It will be necessary to consider the behaviour of the far-infrared radiation as an electromagnetic wave in order to obtain accurate scattering and absorption functions. Furthermore, as we shall see in the next chapter, the refractive index of polyester varies strongly with frequency in this region, and the optical properties of the fibres exhibit correspondingly fine detail in their frequency spectra.

Although the absorption and total scattering cross-sections as functions of frequency may be measured directly for the fibres themselves, measuring the angular part $S(\theta)$ of the scattering in order to obtain the first moment S' has so far required the use of a monochromatic (laser) source to

provide a sufficiently strong signal (Schuetz, 1982). It is easier to measure the complex refractive index of the bulk material for the required frequency range and calculate the scattering and absorption functions for the fibres from electromagnetic theory. This is only practicable because of the uniform size of the fibres and the assumption of a particular (random) distribution of fibre orientations.

In section 3.1 we describe the exact theory of electromagnetic scattering from infinitely long dielectric cylinders at oblique incidence, which is due to J.R. Wait (1955). An alternative method is described by Aronson et al (1979) in which scattering at short wavelengths (thick fibres) is described by ray optics, and scattering at wavelengths much larger than the fibre diameter is given by a simplified wave theory (dielectric needle approximation) with an ad hoc bridging formula used in the intermediate region. However, the ray-optics theory requires consideration of multiple internal reflections in the fibre, and the expressions of Aronson et al. are not much simpler than the formulae of the exact theory. The results are presented in terms of the efficiency functions $q(\phi)$, which represent the scattering cross-section normalized to the fibre geometrical cross-section length × diameter.

Section 3.3 gives expressions for the scattering, absorption, and extinction efficiencies Q (again normalized to the fibre geometrical cross-section) for a collection of

randomly oriented cylinders. The computer programs which calculate the single-fibre cross-section from Wait's solution and perform the integrals over fibre angles are described.

In the final section of this chapter, we present numerical results for the extinction, absorption, and scattering functions for randomly-oriented fibres with various (frequency-independent) refractive indices. These curves show behaviour which is qualitatively similar to published results for perpendicular incidence. We discuss the basic features of these functions and their dependence on refractive index and on the ratio of fibre diameter to wavelength.

3.2 Scattering Functions

The problem of electromagnetic scattering from an infinite circular cylinder at oblique incidence was solved by Wait (1955), generalising the much earlier work of Lord Rayleigh (1918) for the case of perpendicular incidence. Wait's solution is described briefly in the book by van de Hulst (1957) in a chapter devoted primarily to perpendicular incidence. Kerker (1969) presents a much more detailed account of scattering at oblique incidence, together with explicit expressions for the scattering coefficients and numerical results from the work of Kerker et al. (1966). Liou (1972) also presents the solution in full, along with numerical results for thin cylinders of ice. In this section we shall be content to outline briefly the method of solving the scat-

tering problem and present the results for the far-field scattered intensity as a function of direction and polarisation. For more detail the reader is referred to any of the works mentioned above. The paper by Liou is particularly recommended for its completeness and clarity.

Figure 3-1 shows the geometry of the scattering. Cylindrical polar coordinates are defined with the z-direction along the fibre axis, and the incident beam at an angle θ_f to the fibre axis, forming a cone tangent to the incident direction. The scattered intensity varies with angle ϕ measured around the cone with $\phi = 0$ at the incident direction, and falls off as $1/r$, where r is the distance from the fibre axis. The fibre itself thus occupies the region $r < a$.

Also shown in Fig. 3-1 is the direction of the electric field vector for each of two polarisations on the incident and scattered rays. Transverse magnetic (TM) polarisation means that the magnetic vector is perpendicular to the plane containing the fibre and the incident or scattered ray; then the electric vector, shown in Fig. 3-1, has a component along the fibre axis. For transverse electric polarization, the electric vector is perpendicular to this plane, and therefore has no component along the fibre direction. For oblique incidence, the scattered radiation is in general a mixture of both polarisations, even if the incident wave is pure TE or pure TM. In this the problem is more complicated

Fig. 3-1

Geometry of scattering from a long cylinder of radius a. The direction of the electric vector for transverse electric (TE) and transverse magnetic (TM) polarisations is shown.

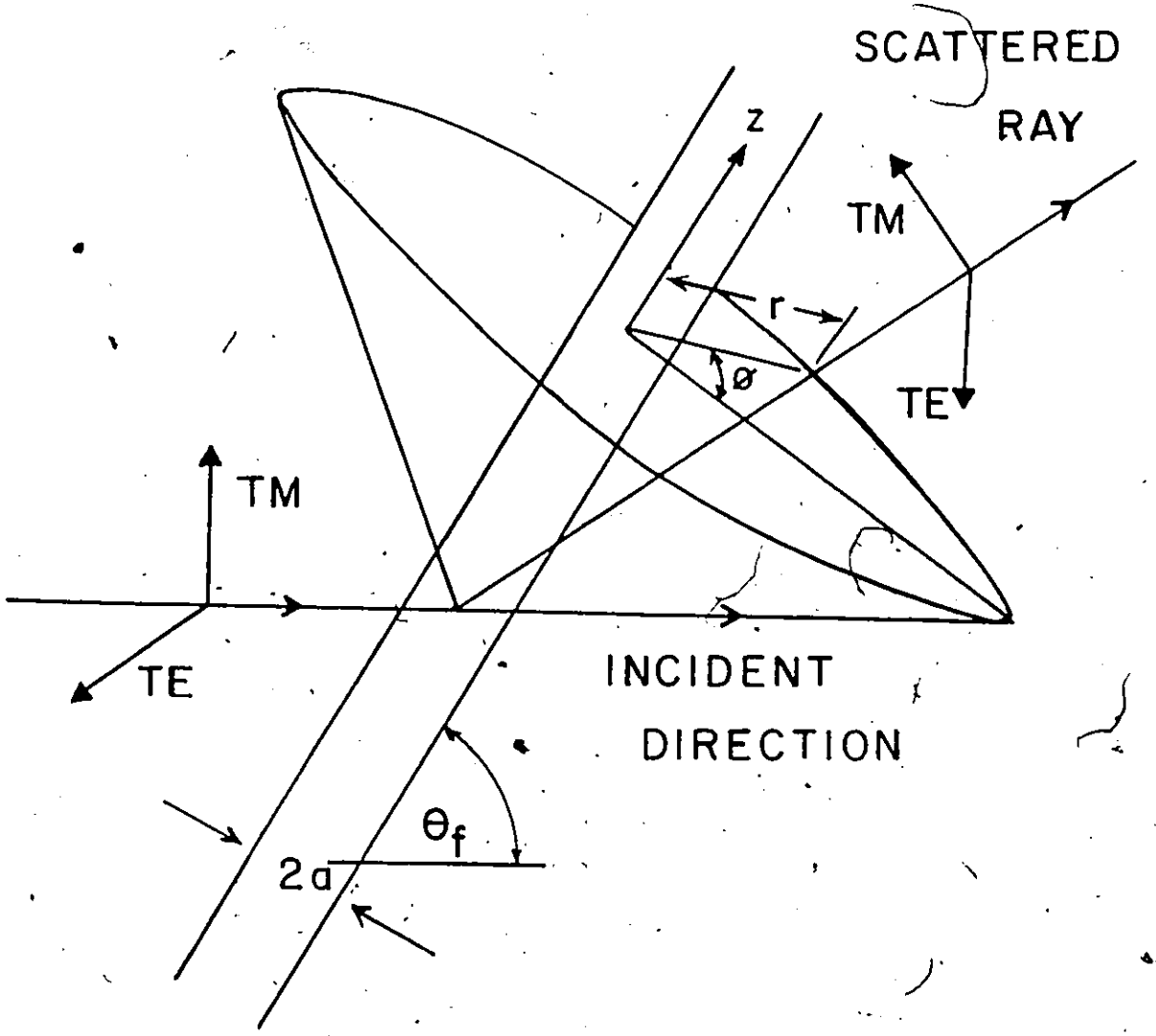
SCATTERED
RAY
z
TM
r
ø
TE
TM
TE
INCIDENT
DIRECTION
θ_f
2a

than in the case of perpendicular incidence. If $\theta_f = 90°$, there is complete reflection symmetry in the scattering plane, and TE (TM) incident radiation can produce only TE (TM) scattered radiation. Similarly, reflection symmetry in the plane of the fibre and incident beam precludes scattering between unlike modes in the forward ($\phi = 0$) direction for any value of θ_f.

What we require then is the function $T(\phi)$, defined by van de Hulst through the relation

$$\frac{u(z,r)}{u_0(z,r=0)} = \left(\frac{2}{\pi kr}\right)^{\frac{1}{2}} T(\phi) e^{-3\pi i/4 - ikr\sin\theta_f} \qquad (3\text{-}1)$$

where u is the amplitude of the scattered radiation, $\omega = 2\pi\nu$ is the angular frequency, $k = 2\pi/\text{wavelength}$ is the usual wavenumber, and the incident radiation has amplitude

$$u_0 = e^{-ik(z\cos\theta_f + r\sin\theta_f\cos\phi) + i\omega t} \qquad (3\text{-}2)$$

There will be four such functions, T_{11}, T_{22}, T_{12}, and T_{21}, where the indices represent the polarisation of the incident (first index) and scattered (second index) radiation, 1 for TM and 2 for TE. Reflection symmetry in the $\phi = 0$ plane requires that $T_{11}(\phi) = T_{11}(-\phi)$, $T_{22}(\phi) = T_{22}(-\phi)$, $T_{12}(\phi) = -T_{12}(\phi)$; and by interchanging incident and scattered directions, $T_{12}(\phi) = -T_{21}(\phi)$. The intensity of the radiation is proportional to the square of the amplitudes in (3-1) and (3-2). It is convenient to divide the scattered intensity by the

incident flux and the fibre diameter 2a, and multiply by the distance r from the fibre axis. The result is a dimensionless scattering efficiency per radian,

$$q(\phi) = \frac{\sin\theta_f}{\pi\alpha} |T(\phi)|^2 \qquad (3\text{-}3)$$

where $\alpha = ka$. This efficiency q is the scattering cross-section per unit angle ϕ divided by the fibre geometrical cross-section, length × diameter. To put it another way, the power scattered between angles ϕ and $\phi+d\phi$ by a section of fibre of length ΔL is given by

$$\Delta P = I_0 q(\phi) \cdot 2a\Delta L \cdot d\phi \qquad (3\text{-}4)$$

where I_0 is the incident flux. Note that $q(\phi)$ is normalized to the total geometrical cross-section, and not to the projected area $2a\Delta L\sin\theta_f$ normal to the incident beam.

The solution of the scattering problem begins with the vector wave equation, which both the electric and magnetic field vectors must satisfy in a uniform medium. It is a standard technique to replace this with a corresponding scalar wave equation,

$$\nabla^2\psi + k^2m^2\psi = 0 \qquad (3\text{-}5)$$

where the time dependence of the potential function ϕ is contained in a factor $e^{i\omega t}$. The complex refractive index is m, and the wave number k is meant to represent the free-space value, ω/c. Stratton (1941) gives a detailed discussion of how such scalar potential functions may be used to con-

struct field vectors which are guaranteed to be solutions of the vector wave equation; two independent solutions are required. As Liou (1972) points out, the solution to (3-3) is a sum of terms of the form

$$\psi_n = Z_n(jr)e^{in\phi}e^{-ihz}e^{i\omega t} \qquad (3\text{-}6)$$

where

$$h = k\cos\theta_f$$

to match the incident wave in (3-2) and

$$j = (m^2k^2-h^2)^{\frac{1}{2}} .$$

Z_n is any solution to Bessel's equation of order n, that is, a linear combination of Bessel functions of the first and second kind. We let m represent the complex refractive index inside the cylinder; outside, we assume $m = 1$, and replace j in (3-6) with

$$\ell = \sqrt{k^2-h^2} = k\sin\theta_f .$$

The solution inside the cylinder must be finite at $r = 0$, so it is constructed exclusively from the Bessel functions of the first kind, $J_n(jr)$. The scattered wave is expressed in terms of Hankel functions of the second kind, defined as

$$H_n^{(2)}(\ell r) = J_n(\ell r) - iY_n(\ell r)$$

where Y_n is the Neumann function, or Bessel function of the

second kind. $H_n^{(2)}$ has the correct behaviour at large r given in (3-1) where J_n and Y_n alone, being purely real, do not. The rather odd-looking factor $e^{-3\pi i/4}$ in (3-1) originates in the asymptotic expansion of the Hankel function.

The final term in the electromagnetic field is the incident plane wave of (3-2), which can be expressed as a series of Bessel functions in the form

$$u_0 = \sum_{n=-\infty}^{\infty} (-i)^n e^{i(\omega t+n\phi-hz)}$$

(see, for example, Stratton, 1941). At the surface of the cylinder, r = a, the tangential components of the vectors E and H must be continuous. This leads to 4 equations, 2 for ϕ components and 2 for z-components. E and H are constructed from a pair of independent potential functions, u and v, representing the two polarisation states. Each potential is expanded in the appropriate functions ψ_n of the form (3-4) for the region inside the cylinder and for the scattered wave outside the cylinder. There are then four sets of expansion coefficients to be determined for each polarisation of the incident wave. The boundary conditions are applied term by term yielding four algebraic equations which can be solved for these coefficients.

The solution for the scattered wave is compared with (3-1) using the asymptotic form for the Hankel function at large argument,

$$H_n^{(2)}(x) \sim \left(\frac{2}{\pi x}\right)^{\frac{1}{2}}(-1)^n e^{-i(x+3\pi/4)}$$

This defines the T-functions of (3-1) in terms of the scattering coefficients. The results for the scattering efficiencies, $q = 1/\pi\alpha|T|^2$ are

$$q_{11}(\phi) = \frac{1}{\pi\alpha}\left|b_{0I} + 2\sum_{n=1}^{\infty} b_{ns}\cos n\phi\right|^2 \qquad (3\text{-}7)$$

$$q_{22}(\phi) = \frac{1}{\pi\alpha}\left|a_{0II} + 2\sum_{n=1}^{\infty} a_{nII}\cos n\phi\right|^2 \qquad (3\text{-}8)$$

$$q_{21}(\phi) = q_{12}(\phi) = \frac{1}{\pi\alpha}\left|2\sum_{n=1}^{\infty} a_{nI}\sin n\phi\right|^2 \qquad (3\text{-}9)$$

Again, the index 1 represents TM polarisation, and 2 represents TE.

Liou gives the most compact expressions for the coefficients, which are reproduced below:

$$b_{nI} = C_n \frac{D_n^2 + A_n(\varepsilon_1)B_n(\varepsilon_2)}{D_n^2 + A_n(\varepsilon_1)A_n(\varepsilon_2)} \qquad (3\text{-}10)$$

$$a_{nII} = C_n \frac{D_n^2 + B_n(\varepsilon_1)A_n(\varepsilon_2)}{D_n^2 + A_n(\varepsilon_1)A_n(\varepsilon_2)} \qquad (3\text{-}11)$$

$$a_{nI} = -b_{nII} = C_n D_n \frac{-A_n(\varepsilon_1) - B_n(\varepsilon_1)}{D_n^2 + A_n(\varepsilon_1)A_n(\varepsilon_2)} \qquad (3\text{-}12)$$

with

$$A_n(\varepsilon_{1,2}) = j \frac{H_n^{(2)'}(\ell a)}{H_n^{(2)}(\ell a)} - \varepsilon_{1,2} \frac{J_n'(ja)}{J_n(ja)}$$

$$B_n(\varepsilon_{1,2}) = j \frac{J_n'(\ell a)}{J_n(\ell a)} - \varepsilon_{1,2} \frac{J_n'(ja)}{J_n(ja)}$$

$$\varepsilon_1 = 1 \quad , \quad \varepsilon_2 = m^2$$

$$C_n = J_n(\ell a)/H_n^{(2)}(\ell a)$$

$$D_n = \text{inh}(\ell^2 - j^2)/(\alpha \ell j) \quad .$$

The primes on the Bessel and Hankel functions indicate a first derivative with respect to the argument. In Wait's (1955) original solution, the a_n's and b_n's were the expansion coefficients of the field vectors directly, rather than of the potential functions. Consequently they are defined somewhat differently than those used here. Our notation follows that of Van de Hulst (1957) and later works.

We note from the expressions (3-7)-(3-9) for the scattering efficiencies that the cross-mode scattering q_{12} is zero in the forward direction, as predicted from the symmetry. Furthermore, at perpendicular incidence the direction cosine $h = k\cos\theta_f$ is zero, and so all the cross-mode coefficients a_{nI} vanish. (The factor D_n in (3-12) is proportional to h.)

From the equations above the a and b coefficients may be calculated from the scattering parameter α (= $2\pi \times$ radius/wavelength), the incident angle θ_f, and the complex refrac-

tive index m for the desired frequency. Each order n requires one evaluation of the n'th order Bessel functions of the first and second kind and their first derivatives with real argument $\ell a = \alpha \sin\theta_f$, and the Bessel function of the first kind and its derivative with complex (if m is complex) argument $ja = \sqrt{m^2 - \cos^2\theta_f}$.

Knowing the scattering amplitude and phase as a function of angle allows calculation of the remaining optical quantities, the extinction and absorption. The loss of energy from the incident wave can be described as the result of interference between the incident wave and the scattered wave close to the incident direction. A widely-used theorem (van de Hulst, 1947) relates the extinction to the imaginary part of the forward-scattering amplitude for a point scatterer (that is, for an object which is small in all dimensions compared to the observation distance). Van de Hulst derives the analogous theorem in his book (1957) for a line scatterer at perpendicular incidence; the argument is essentially unchanged for oblique incidence. The extinction efficiency is

$$q_E = \frac{2}{\alpha} \mathrm{Re}\{T(0)\} \qquad (3\text{-}13)$$

so for TM radiation, we have

$$q_{l,E} = \frac{2}{\alpha} \mathrm{Re}\{b_{0I} + 2 \sum_{i=1}^{\infty} b_{nI}\} \qquad (3\text{-}14)$$

and for TE polarisation,

$$q_{2,E} = \frac{2}{\alpha} \mathrm{Re}\{a_{0II} + 2 \sum_{i=1}^{\infty} a_{nII}\} . \qquad (3\text{-}15)$$

Note that there is no contribution from the cross-mode scattering T_{12} and T_{21}, as these vanish in the forward direction. The efficiency q_E is normalised in the same way as the scattering efficiencies, so the extinction cross-section per unit length for a fibre at any angle to the incoming beam is just $q_E \times$ diameter. For an opaque fibre which is large compared to the wavelength, the efficiency q_E as defined here will be proportional to $\sin\theta_f$.

There are two contributions, scattering and absorption, to the extinction. The total scattering efficiency is obtained by integrating (3-7)-(3-9) over all angles ϕ. Although the total scattering for, say, TM incident radiation can meaningfully be divided into two contributions with different polarisations of the outgoing wave, it is sufficient for our purposes to consider only the total scattered energy for a given incident polarisation. So we write

$$q^0_{1,s} = \frac{2}{\alpha} \{|b_{0I}|^2 + 2 \sum_{n=1}^{\infty} |b_{nI}|^2 + |a_{nII}|^2\} \qquad (3\text{-}16)$$

for TM incident radiation, and similarly (with b_{nI} replaced by a_{nII}) for the total scattering $q^0_{2,s}$ with TE incident polarisation. The absorption cross-section is just the difference of the extinction and the total scattering:

$$q_{l,A} = q_{l,E} - q^{0}_{l,S} \qquad (3\text{-}17)$$

and similarly for the other (TE) mode. Note that for a purely real refractive index, the absorption is zero, and the extinction (3-14) must equal the total scattering (3-15). This relation between the sum of the real parts of the b_{nI}'s and the sum of the squares of both real and imaginary parts of the b_{nI} and a_{nII} coefficients provides a useful check on the computer programs which calculate the coefficients.

We should point out that formulae for "intensity" of scattered radiation given by different authors tend to differ by factors of $\sin\theta_f$ from each other and from the definitions of the efficiencies used here. In part this is due to variations in the definition of intensity, which is used here exclusively to mean the power crossing unit area (in the direction of propagation) per steradian. Kerker (1969) does not define explicitly the intensities I_{ll} etc., but it would appear that they are equal to the radiant energy flux (i.e. the Poynting vector) multiplied by $\sin\theta_f$. In Kerker et al. (1966) the equivalent quantity is termed the radiance and measured in $W/m^2/sr$, although the beam divergence is in one direction only - the power per steradian diverges, or at least is limited by the angular width of the incident beam and the length of the fibre. In Wait's paper (1955), the formulae are given in terms of the field vectors, so there

is no ambiguity; we have already noted that his coefficients contain an extra factor of $\sin\theta$ compared to the definitions used here. Liou (1972) expresses the "intensity", which he defines as the energy flux, in terms of the length R measured along the scattering cone in Fig. 3-1 (the distance of propagation of the waves) but he has apparently replaced $R = r\sin\theta_f$ (instead of the correct $R = r/\sin\theta_f$) at one point, and the expressions he gives for the intensity cannot be reconciled with those of other authors.

The scattering coefficients for a perfectly conducting cylinder (or a fibre coated with a metallic layer thicker than the skin depth) are obtained by letting $m \to \infty$ (Wait 1955; Kerker 1969). The cross-mode coefficients go to zero, as can be seen from (3-12), which has a term proportional to m^2 in the denominator. Kerker gives the remaining coefficients as simply

$$b_n = \frac{J_n(\alpha\sin\theta_f)}{H_n^{(2)}(\alpha\sin\theta_f)} \qquad (3\text{-}18)$$

$$a_n = \frac{J_n'(\alpha\sin\theta_f)}{H_n^{(2)\prime}(\alpha\sin\theta_f)} \qquad (3\text{-}19)$$

The extinction and scattering cross-sections are clearly equal in this case - we have $\mathrm{Re}\{b_n\} = |b_n|^2$ for all n, and similarly for a_n.

Expressions have also been given for the coefficients

a_n and b_n for scattering from a cylinder composed of two concentric layers (a hollow cylinder would be a special case of this) at perpendicular incidence (Kerker, 1969; Kerker and Matijevic 1961). However Samaddar (1970) has shown that this solution cannot be generalised to oblique incidence, and there is no simple solution for arbitrarily-oriented two-layer cylinders.

3.3 Scattering Functions for Fibre Insulations

Practical insulation materials are composed of fibres which are not parallel, and an average over fibre orientations is required. On a large scale the material is homogeneous, and so it is assumed that its optical properties may be approximated by the average properties of a randomly-chosen volume element. The average extinction, absorption, and scattering efficiencies are denoted by Q_E, Q_A, and $Q_A(\theta_S)$ with an additional subscript to indicate polarisation (or two subscripts in the case of scattering functions), following the conventions used in the previous section. The same normalisation is used as for the single-fibre efficiences q, that is, the total absorption (for example) cross-section of a small volume of the medium is Q_A times the geometrical cross-section, length × diameter, of the fibres in that volume element. Included in Q_A is a factor expressing the average projection of the fibres on the incident direction. The scattering efficiency $Q_S(\theta_S)$ is defined as the normalised

cross-section per steradian for scattering at angle θ_s (to the incident direction) into solid angle $d\Omega = \sin\theta_s d\theta_s d\phi_s$. All these efficiency factors are related to the cross-sections per unit volume of Chapter 2 through the factor $2f/\pi a$, which is the fibre diameter × length per unit volume of the insulation material. Therefore, in the notation of Chapter 2, $A = Q_A \cdot (2f/\pi a)$, and $S(\theta_s) = Q_S(\theta_s) \cdot (2f/\pi a)$. The "phase function", which is the angular part of the scattering normalised to the total scattering cross-section is given by

$$p(\theta_s) = Q_S(\theta_s)/Q_S^0 .$$

The absorption and extinction efficiencies for a fibrous material are readily obtained from the single-fibre functions (3-14) and (3-17) by integrating over the assumed distribution of fibre angles. For randomly-oriented fibres,

$$Q_A = \int_0^{\pi/2} q_A(\theta_f)\sin\theta_f d\theta_f \qquad (3\text{-}20)$$

$$Q_E = \int_0^{\pi/2} q_E(\theta_f)\sin\theta_f d\theta_f . \qquad (3\text{-}21)$$

The scattering efficiency $Q_S(\theta_s)$ is derived from the single-fibre functions of $q(\phi)$ of (3-7), (3-8), and (3-9) through the relation

$$\cos\theta_s = \cos^2\theta_f + \sin^2\theta_f\cos\phi \qquad (3\text{-}22)$$

which has been used before. A fibre at angle θ_f contributes to the scattering at all angles $\theta_s < 2\theta_f$. The relationship may be expressed rather awkwardly as

$$Q_S(\theta = \int_0^{2\pi} d\phi \int_0^{\pi/2} d\theta_f \cdot q(\phi)\delta(\theta-\theta_s)\sin\theta_f \qquad (3\text{-}23)$$

where θ_s is a function of ϕ and θ_f. However the numerical computation is straightforward and easy to understand. The range $(0,\pi)$ of θ_s is divided into 64 equal intervals, which are separated by lines of latitude on the scattering sphere. For two angles θ_1 and θ_2 (we drop the s subscript) which are smaller than $2\theta_f$ equation (3-21) gives the corresponding angles ϕ_1 and ϕ_2, restricted to the range $(0,\pi)$ since the intensity in the other half of the cone is a mirror image. Then we simply place all of the scattered power in the range (ϕ_1,ϕ_2) into the interval (θ_1,θ_2), and similarly for the other 63 bins. The integral over fibre angles is performed numerically by a Simpson's rule procedure with 128 steps in θ_f.

The individual contributions to the interval (θ_1,θ_2) can be evaluated exactly as a function of fibre angle. We need to integrate $q(\phi)$ over the range (ϕ_1,ϕ_2). First we expand the squared sum in the definitions (3-7) - (3-9) in terms of the form $\cos n\phi\cos\ell\phi$ or $\sin n\phi\sin\ell\phi$. But

$$\cos n\phi\cos\ell\phi = \frac{1}{2}\cos(n+\ell)\phi + \frac{1}{2}\cos(n-\ell)\phi$$

$$\sin n\phi\sin\ell\phi = \frac{1}{2}\cos(n-\ell)\phi - \frac{1}{2}\cos(n+\ell)\phi$$

so the efficiencies q can be expanded in a Fourier cosine series. Collecting like terms gives

$$q(\phi) = \frac{1}{\rho\alpha}\{\frac{1}{2}\sum_{n=0}^{\infty}|C_n|^2(1 \pm \cos 2n\phi)$$

$$+ \sum_{\ell=1}^{\infty}[\sum_{n=0}^{\infty}\mathrm{Re}(C_n C_{n+\ell}^*) \pm \sum_{n<\frac{1}{2}\ell}\mathrm{Re}(C_n C_{\ell-n}^*)]\cos\ell\phi \quad . \qquad (3\text{-}24)$$

For q_{11} and q_{22}, we pick the + sign, and for the cross-mode scattering q_{12}, the - sign is used. The coefficients C_n represent $2b_{nI}$, $2a_{nII}$, or $2a_{nI}$ according to the polarisation, except for C_0 which is b_{0I} or a_{0II}, without the factor of 2.

In this form, $q(\phi)$ is readily integrated term-by-term between the limits ϕ_1 and ϕ_2, to give the contribution to each of the 64 scattering bins exactly. These contributions are smooth functions of θ_f over the range $\theta_s/2 < \theta_f < \pi/2$, and may be integrated over fibre angles using Simpson's rule. The results are much superior to the more direct procedure of taking a large number of points for both the fibre angle and the angle ϕ, and adding contributions to the scattering bins one at a time. Essentially, this performs both integrals by the trapezoidal rule, and requires a larger number of points for reasonable accuracy.

When the procedure is complete, we have the (appropriately normalised) total power scattered into each of 64 annular regions of width $\Delta\theta = \pi/64$. The solid angle of the

bin between $\theta-\Delta\theta/2$ and $\theta+\Delta\theta/2$ is

$$2\pi[\cos(\theta-\Delta\theta/2)-\cos(\theta+\Delta\theta/2)]$$

or approximately $2\pi\sin\theta$. Therefore we need only divide by $2\pi\sin\theta$ to obtain the function $Q_S(\theta)$. The whole procedure is straightforward, although the bookkeeping is a little complicated. In Appendix 2 the FORTRAN program which calculates $Q_S(\theta)$ is listed. On our Digital LSI-11/23 microcomputer, the calculation of a function $Q_S(\theta)$ for a refractive index $|m| \sim 2$ takes a few minutes, depending on the scattering parameter α ($2\pi a$/wavelength). For $\alpha = 15$, running time is about 8 minutes, and is less for smaller values.

By analogy with (2-24) and (2-29), we define the total scattering efficiency

$$Q_S^0 = 2\pi \int_0^\pi Q_S(\theta)\sin\theta d\theta \qquad (3-25)$$

and the weighted scattering efficiency

$$Q_S' = 2\pi \int_0^\pi Q_S(\theta)(1-\cos\theta)\sin\theta d\theta \; . \qquad (3-26)$$

We also will use the 'transport' efficiency

$$Q_T = Q_A + Q_S' \qquad (3-27)$$

which is averaged over frequency to give κ_T in (2-32).

Q_S^0 and Q_S' are not calculated from the expressions just given, but rather from the single-fibre functions directly. Thus

$$Q_S^0 = \int_0^{\pi/2} q_s^0(\theta_f)\sin\theta_f d\theta_f \quad . \tag{3-28}$$

By using (3-22) to replace the integration over θ_s with an integration over ϕ, we can show that

$$Q'_{1,S} = \frac{2}{\alpha}\int_0^{\pi/2} \{|b_{0I}|^2 + 2\sum_{n=1}^{\infty}(|b_{nI}|^2+|a_{nI}|^2)$$

$$-2\mathrm{Re}(b_{0I}b_{1I}^*)-2\mathrm{Re}\sum_{n=1}^{\infty}(b_{nI}b_{n+1,I}^*+a_{nI}a_{n+1,I}^*)\}\times\sin^3\theta_f d\theta_f \tag{3-29}$$

This expression results from expanding the $q(\phi)$ functions as in (3-24). All the terms in $\cos n\phi$ for $n \neq 0$ then vanish on integration over ϕ. We have shown the result for TM incident radiation; for TE radiation we replace b_{nI} with a_{nII} in (3-29).

Inside an insulation material, the radiation can be assumed to be unpolarised. In what follows we shall deal primarily with efficiency function for unpolarised incident radition, and without regard to polarisation on the scattered wave. These will be represented by Q's without numerical subscripts, and will be obtained by summing over outgoing modes and averaging over incident polarisation.

So, for example, we set

$$Q_A = \frac{1}{2} (Q_{1,A} + Q_{2,A})$$

and

$$Q_s(\theta) = \frac{1}{2} \{Q_{11,S}(\theta)+Q_{22,S}(\theta)+2Q_{12,S}(\theta)\} .$$

Table 3-1 lists several parameters commonly used in the radiative transfer literature with their definitions in terms of the efficiencies Q.

In Appendix 3 the FORTRAN program which calculates the scattering coefficients a_n and b_n is listed. This routine was derived from the expressions given by Kerker (1969) rather than the more concise forms of Liou (1972) which are reproduced in (3-10), (3-11), and (3-12), and is consequently more difficult to follow. Also given is a simpler version which calculates the coefficients for a perfectly-conducting cylinder from (3-18) and (3-19).

Most of the computational labour lies in the calculation of the Bessel functions. Orders from 0 to about 30 or 40 are required for positive real arguments and for complex arguments with absolute values up to about 25. Following the usual practice, we evaluated these functions using the algorithm of Abramowitz and Stegun (1965), in which the Bessel functions of all orders for a single argument are calculated together, using a downward recursion based on the formula

TABLE 3-1

Radiation Parameters Related to Optical Efficiencies

Parameter	Usual Symbol	Corresponding Parameter
Extinction Coefficient (cross-section/unit volume)	β	$\frac{2f}{\pi a} Q_E$
Absorption Coefficient	$\beta-\sigma$	$\frac{2f}{\pi a} Q_A$
Single-scattering albedo	ω_0	$\frac{Q_S^0}{Q_E}$
Phase function	$p(\theta)$	$\frac{Q_S(\theta)}{Q_S^0}$
Anisotropy parameter	$\{\langle\cos\theta\rangle_{\omega_1/\omega_0}\}$	$1-\frac{Q_S'}{Q_S^0}$
Effective or modified extinction coefficient	$\left\{\begin{matrix} K_e^* \\ \beta(1-\omega_0\langle\cos\rangle) \end{matrix}\right\}$	$\frac{2f}{\pi a} Q_T$

$$J_{n-1}(x) = \frac{2n}{x} J_n(x) - J_{n+1}(x) .$$

For sufficiently high orders n (greater than $\sim$ x) the Bessel functions of the first kind increase rapidly with decreasing order, and therefore errors in J_n/J_{n+1} decrease quickly as the recursion is continued. If the process is begun at order n+k, then the error in J_n/J_{n+1} is about J_{n+k}^2/J_n^2 times the error in the starting values. So the starting values J_k and J_{k+1} can be chosen arbitrarily, and will yield a sequence of functions which are accurate except for an overall constant for orders 0 through n, providing k is chosen to be sufficiently large. These functions are normalised using the sum rule

$$J_0 = 2 \sum_{n=1}^{\infty} J_{2n}(x) = 1 .$$

The Neumann functions (Bessel functions of the second kind) $Y_n(x)$ become large at orders $n >> x$, so an upwards recursion is used. The starting values Y_0 and Y_1 are calculated accurately from the sequence $\{J_n\}$ using relations in Abramowitz and Stegun (1965), so no normalisation is required.

On the LST-11/23 computer, the maximum range for floating-point numbers is about 10^{-38} to 10^{+38}. Even when the recursion is begun at very small values of 10^{-36} or so, it is necessary to choose the starting order carefully when the argument x is large to avoid overflow in the recursion

or in the normalisation sum. A routine designed for use on larger machines was found to be unsatisfactory in this respect. Adequate expressions for the starting order n as a function of argument x were derived from the asymptotic expansions of the Bessel functions. The routines were tested along the positive real axis and in a few directions in the complex plane for which tabulated values are available (Abramowitz and Stegun, 1965) and give at least 6-digit accuracy without causing arithmetic overflow for arguments up to 50 in absolute value. (If x is close to a zero of J_n, the accuracy is of course poorer for that particular order n, but the error does not propagate to lower orders.) Appendix 3 also lists these FORTRAN routines for real and complex Bessel functions. The derivatives J_n' and Y_n' are evaluated using the relations

$$J_n'(x) = \frac{n}{x} J_n(x) - J_{n+1}(x)$$

$$J_0'(x) = -J_1(x)$$

(Abramowitz and Stegun, 1965) which also hold for the Neumann functions Y_n.

3.4 Numerical Results for Constant Refractive Index

This section presents numerical results for a collection of randomly-oriented cylinders. It is useful for the time being to deal with a refractive index which is independent of frequency in order to show separately the behaviour which depends on the ratio of fibre size to wavelength, and that which depends explicitly on the refractive index. The functions are qualitatively similar to those published for perpendicular incidence (van de Hulst, 1957; Kerker, 1969; Farone et al., 1963). To provide a scale for interpreting the Q-functions which are shown in this section, the average (over fibre angles) of the factor $\sin\theta_f$ which gives the projection of the fibre areas onto the incident direction is $\pi/4 \approx 0.78$. To put it more clearly, the extinction efficiency calculated purely from geometrical optics for opaque randomly oriented fibres would be $\pi/4$ rather than unity because of the way the efficiencies have been normalised.

Figure 3-2 shows the scattering efficiency as a function of scattering angle. The dashed curve is for $n = 1.85$, $k = 0.033$ where the complex refractive index is

$$m = n - ik \ .$$

These are the values determined for polyester at a frequency of 1000 cm^{-1}. For comparison, results are shown for a much more strongly absorbing material, $n = 1.85$, $k = 0.33$. The

Fig. 3-2

Calculated scattering efficiency Q_S multiplied by $2\pi\sin\theta$ as a function of scattering angle θ, for two values of refractive index and a scattering parameter $\alpha = 7.35$. The calculation is for a collection of randomly oriented cylinders. The dashed curve is for $n = 1.85$, $k = 0.033$, and the solid curve is for $n = 1.85$, $k = 0.33$.

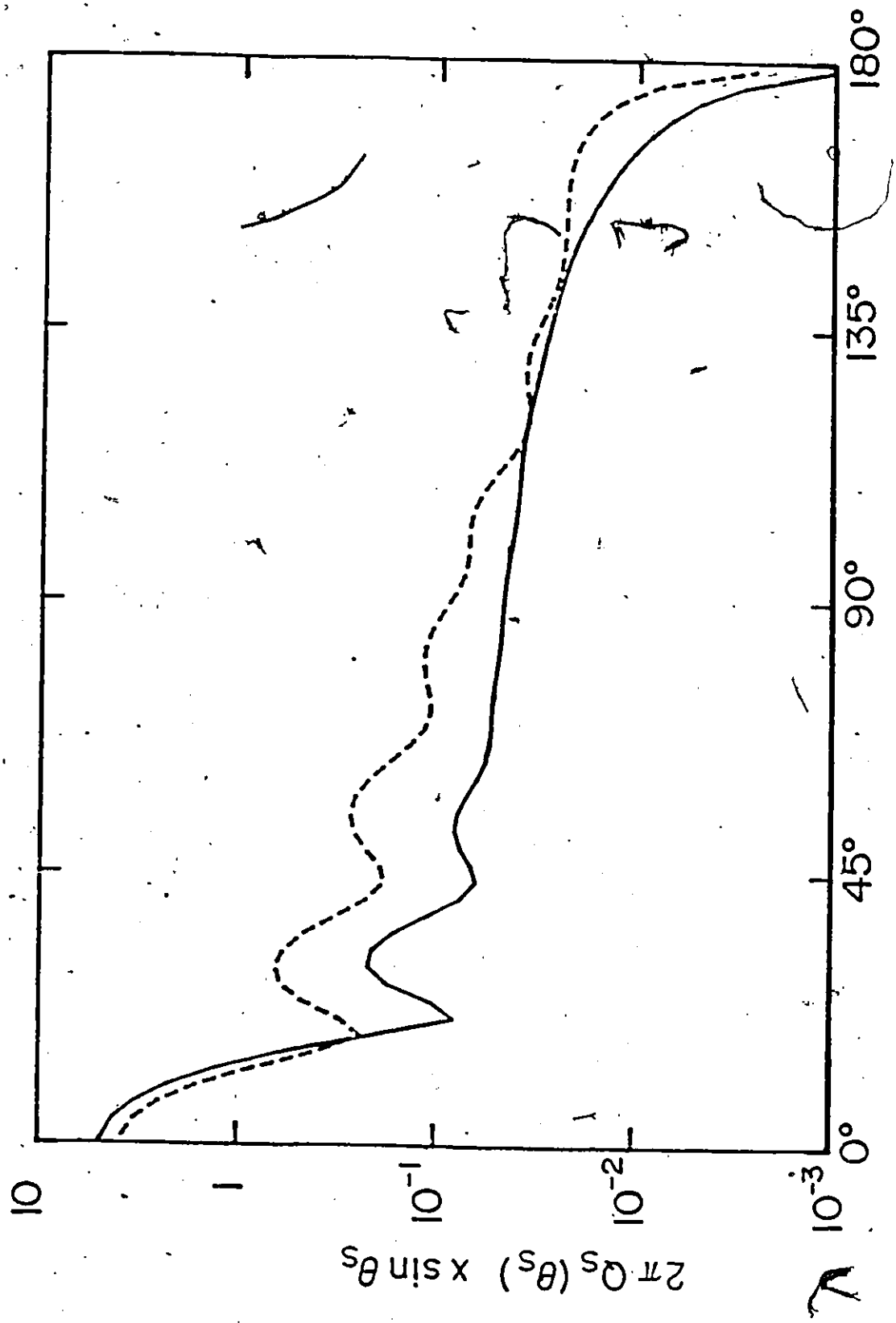
10
1
10^{-1}
10^{-2}
10^{-3}
$2\pi Q_s(\theta_s) \times \sin\theta_s$
0°
45°
90°
135°
180°
SCATTERING ANGLE θ_s

fibre radius is given as 11.7 μm (the value for Polarguard) and the frequency as 1000 cm^{-1}, although any pair of values which give the same value 7.35 for the scattering parameter α would serve equally well.

Note that we have plotted not $Q_s(\theta)$ but $2\pi\sin\theta Q_s(\theta)$. The scattering efficiency per unit solid angle diverges at small scattering angles θ. This results from the process of averaging over fibre directions. Consider again the fibre shown in Fig. (3-1), which lies at angle θ_f to the incident beam. The scattered energy is spread around the edge of a cone centred on the fibre. If we consider a very narrow incident beam and imagine the fibre to be surrounded by a spherical screen, we would see a ring of scattered light projected onto the screen tangent to the spot made by the incident beam. As we now rotate the fibre around the incident direction - keeping θ_f constant - this spot remains fixed. The total power scattered between angles $\pm\Delta\phi$ close to the incident direction is proportional to $2\Delta\phi q(\phi)$. By the time the fibre direction has swept through 360^o in azimuth, this energy has been spread over a solid angle of $\pi(\Delta\phi)^2$, and so the intensity per unit solid angle diverges like $1/\Delta\phi$ as $\Delta\phi \to 0$. This is not true in the general direction θ in which the solid angle $2\pi\sin\theta\Delta\theta$ decreases linearly with $\Delta\theta$. There will be another cusp divergence at the maximum scattering angle $\theta = 2\theta_f$, where the relation (3-22)

between θ and ϕ becomes singular. However, this second singularity changes position as we integrate over polar angles θ_f, and so contributes only a smooth curve to $Q_s(\theta)$. In the forward direction, however, the cross-section per unit solid angle diverges for every angle θ_f, and so the singularity remains in the average over all fibre directions. It is more useful to plot $2\pi\sin\theta Q_s(\theta)$, which gives the normalised cross-section for scattering between angles θ and $\theta+d\theta$, per radian. The total scattering efficiency Q_s^0. is now just the integral over θ of the curves in Fig. (3-2) with no additional solid angle factors.

It is clear that the scattering in Fig. (3-2) is strongly peaked in the forward direction (note the log scale). This forward peak contains about half the total scattered radiation, and changes rather little with the large change in the bulk absorption between the two curves. It can be thought of as the Fraunhofer diffraction which fills in the geometrical shadow of the fibres. The first zero of the diffraction pattern for an opaque cylinder of the same size would occur at 25°. In Fig. (3-3), where the frequency (or equivalently, the radius) has been halved, the first zero would be at about 60°. We see that the pattern is indeed broader, although in both cases the forward peak is narrower than the simple diffraction theory would suggest, presumably because the refracted rays wash out the minimum.

Fig. 3-3

Calculated scattering efficiency $Q_S(\theta)$ times $2\pi\sin\theta$ as a function of scattering angle θ for a scattering parameter $\alpha = 3.87$, and random orientation.

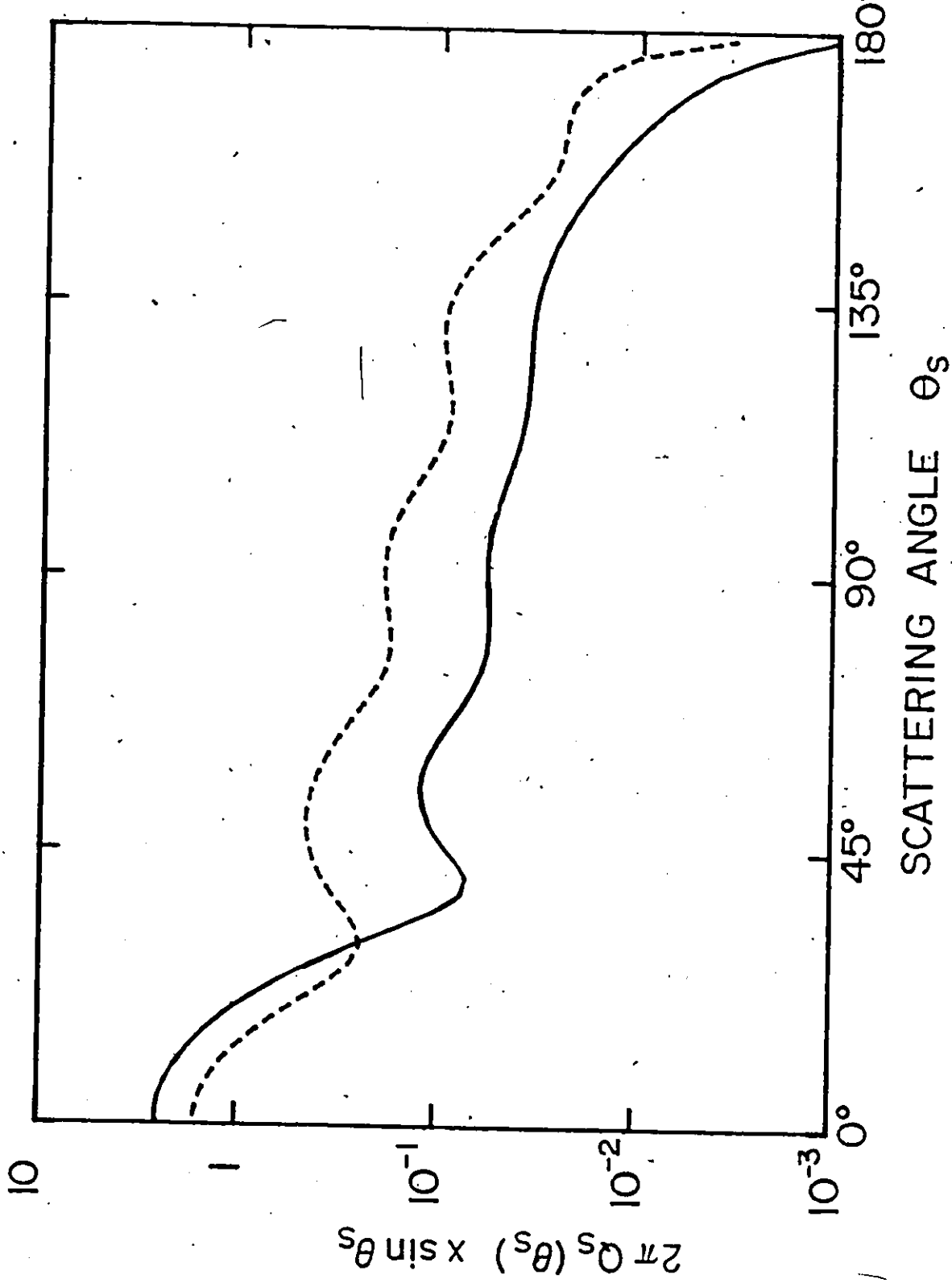
10
1
10^{-1}
10^{-2}
10^{-3}
$2\pi Q_s(\theta_s) \times \sin\theta_s$
0°
45°
90°
135°
180°
SCATTERING ANGLE θ_s

Although the scattering at 500 cm^{-1} in Fig. 3-3 varies more smoothly with angle than the curves in Fig. 3-2, it is clear that scattering is predominately in the forward direction. It is for this reason that radiative-transport models based on isotropic scattering are unsatisfactory for these fibrous materials.

Figures (3-4) and (3-5) show extinction and total scattering efficiencies for the same two refractive indices, $n = 1.85$, $k = 0.033$ and $n = 1.85$, $k = 0.33$ respectively. The horizontal scale is marked in frequency for cylinders of the 23.4-μm diameter of Polarguard fibres. Since the refractive index is independent of wavelength, this is really a scale in scattering parameter α, with $\alpha = 14.7$ corresponding to $\nu = 2000$ cm^{-1}.

The oscillations in both the scattering and the extinction in Fig. (3-4) are typical of cylinders made from weakly-absorbing material. Van de Hulst (1957) shows that this large-scale structure is a function only of the parameter $(m-1)\alpha$ for small k, although the smaller ripples depend more specifically on the refractive index m. Thus the major effect of reducing n is to move the broad peaks in (3-4) to higher frequencies. This slow frequency variation can be calculated by considering the interference between the incident wave and the wave that passes once through the cylinder without reflection at either interface. Such a

Fig. 3-4

Calculated extinction and total scattering efficiencies for randomly oriented fibres of 23.4 μm diameter and constant refractive index 1.85 - 0.033i.

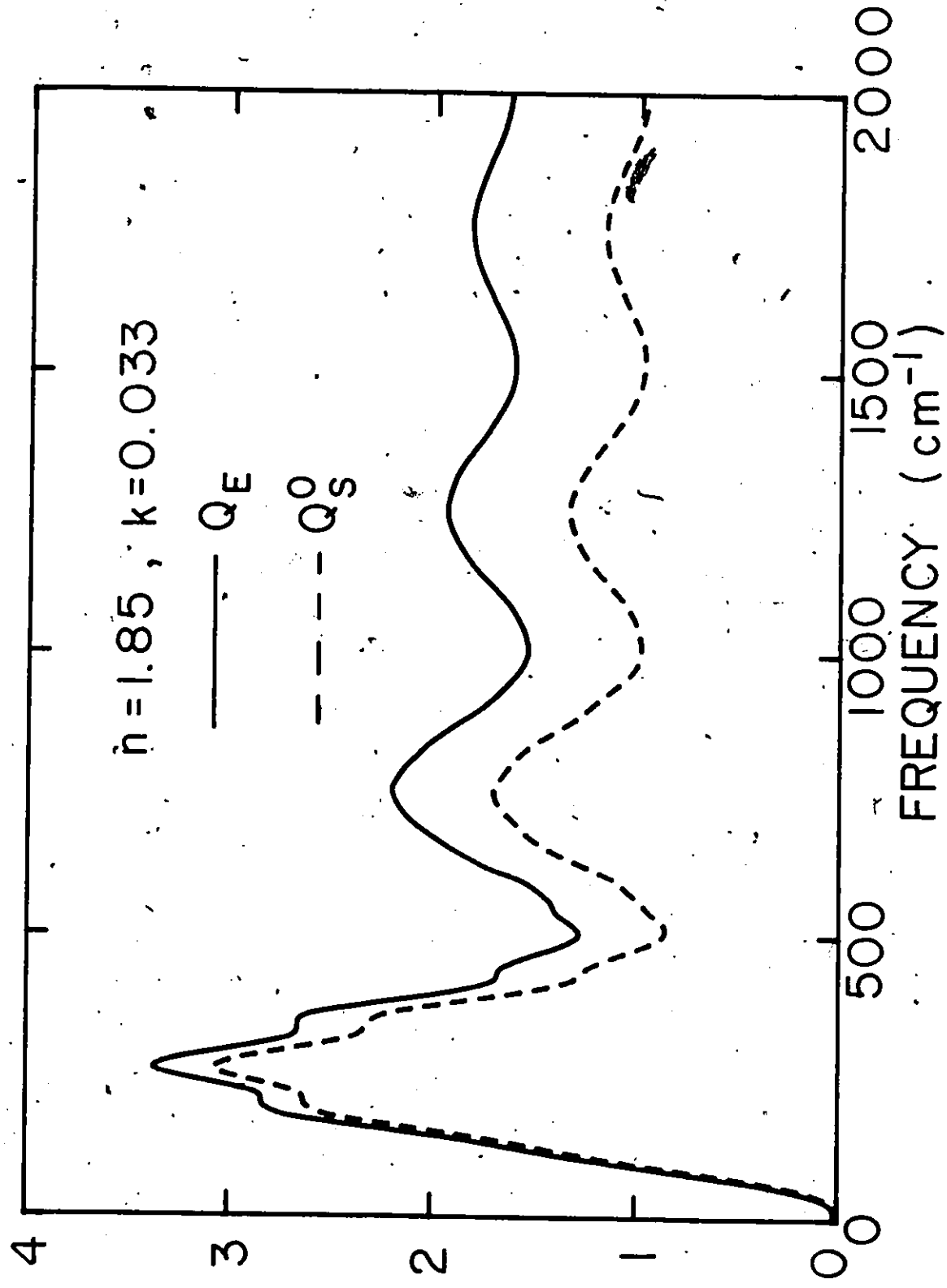
n̂=1.85 , k=0.033
Q_E
Q_S^O
FREQUENCY (cm^{-1})
0
500
1000
1500
2000
0
1
2
3
4

Fig. 3-5

Calculated extinction and total scattering efficiencies for randomly oriented 23.4-μm fibres with a constant refractive index 1.85 - 0.33i.

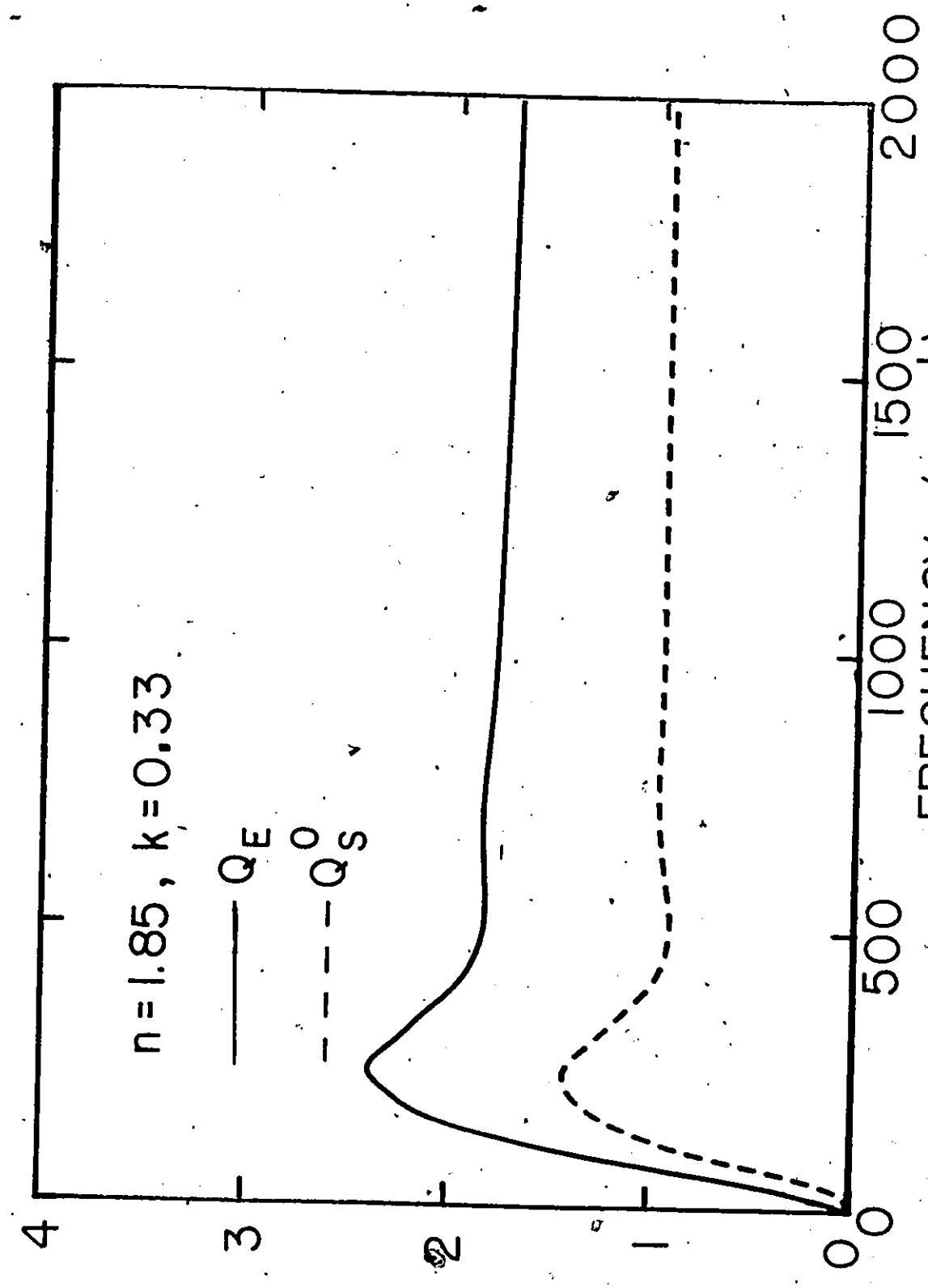
n=1.85, k=0.33
Q_E
Q_S^0
0
500
1000
1500
2000
FREQUENCY (cm^{-1})
0
1
2
3
4

calculation does not indicate where the energy removed from the beam ends up, however.

In Fig. (3-5), where the bulk absorption is much stronger, the structure is largely absent. In both figures, note that the extinction efficiency approaches at high frequencies the value $\pi/2 \approx 1.57$, which we would expect for an opaque object large compared with the wavelength. Van de Hulst (1957) shows that the extinction cross-section in this limit approaches twice the geometrical cross-section.

In Figures 3-6 and 3-7 we see the absorption (solid line) and weighted scattering (dashed curves) efficiencies, which are of more direct interest in the heat transfer problem. The weighted scattering efficiency Q_S' is obtained by multiplying the scattering $Q_S(\theta)$ of Figs. 3-2 and 3-3 by a factor $1-\cos\theta$ which expresses the relative effectiveness of scattering through an angle θ and integrating over scattering angles. As such it represents a 'backscattering' efficiency normalised so that it equals the total scattering efficiency in the case of isotropic scattering, and is correspondingly smaller if the scattering is directed primarily forward. Note the change of scale in going from Fig. 3-4 to Fig. 3-6 or from Fig. 3-5 to Fig. 3-7. In both cases, Q_S' is dramatically smaller than the total scattering efficiency Q_S^0, an indication of the degree to which the scattering is directed forward. Also note that although the absorption Q_A is clearly

Fig. 3-6

The efficiencies for 23.4-μm randomly oriented fibres with refractive index 1.85 - 0.033i. Q_A is the absorption efficiency, and Q_S' is the scattering efficiency weighted with a factor $1-\cos\theta$.

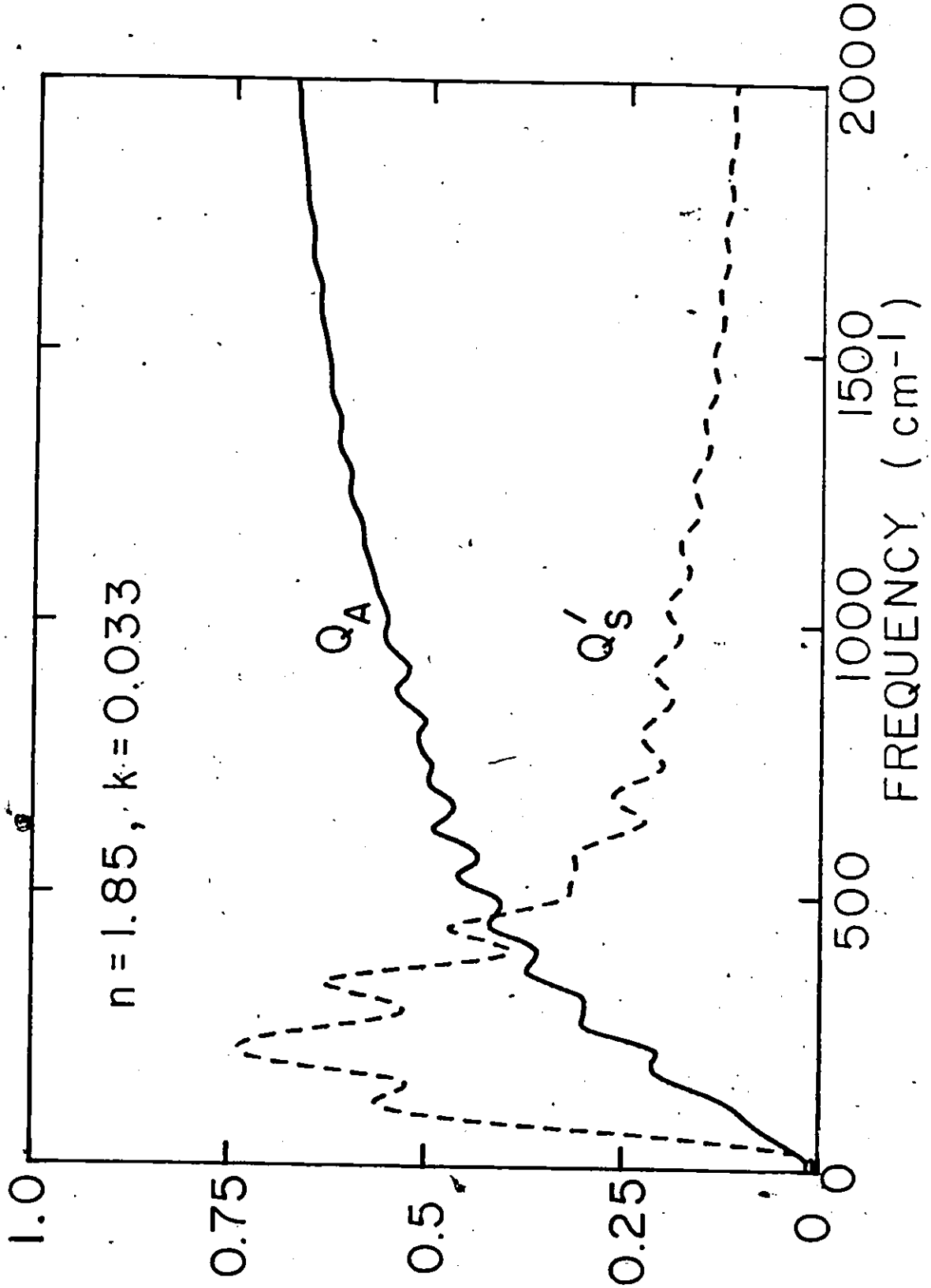
n=1.85, k=0.033
Q_A
Q'_S
1.0
0.75
0.5
0.25
0
0
500
1000
1500
2000
FREQUENCY (cm-1)

Fig. 3-7

Absorption and weighted scattering efficiencies for randomly oriented fibres 23.4 μm in diameter with refractive index 1.85 - 0.33i.

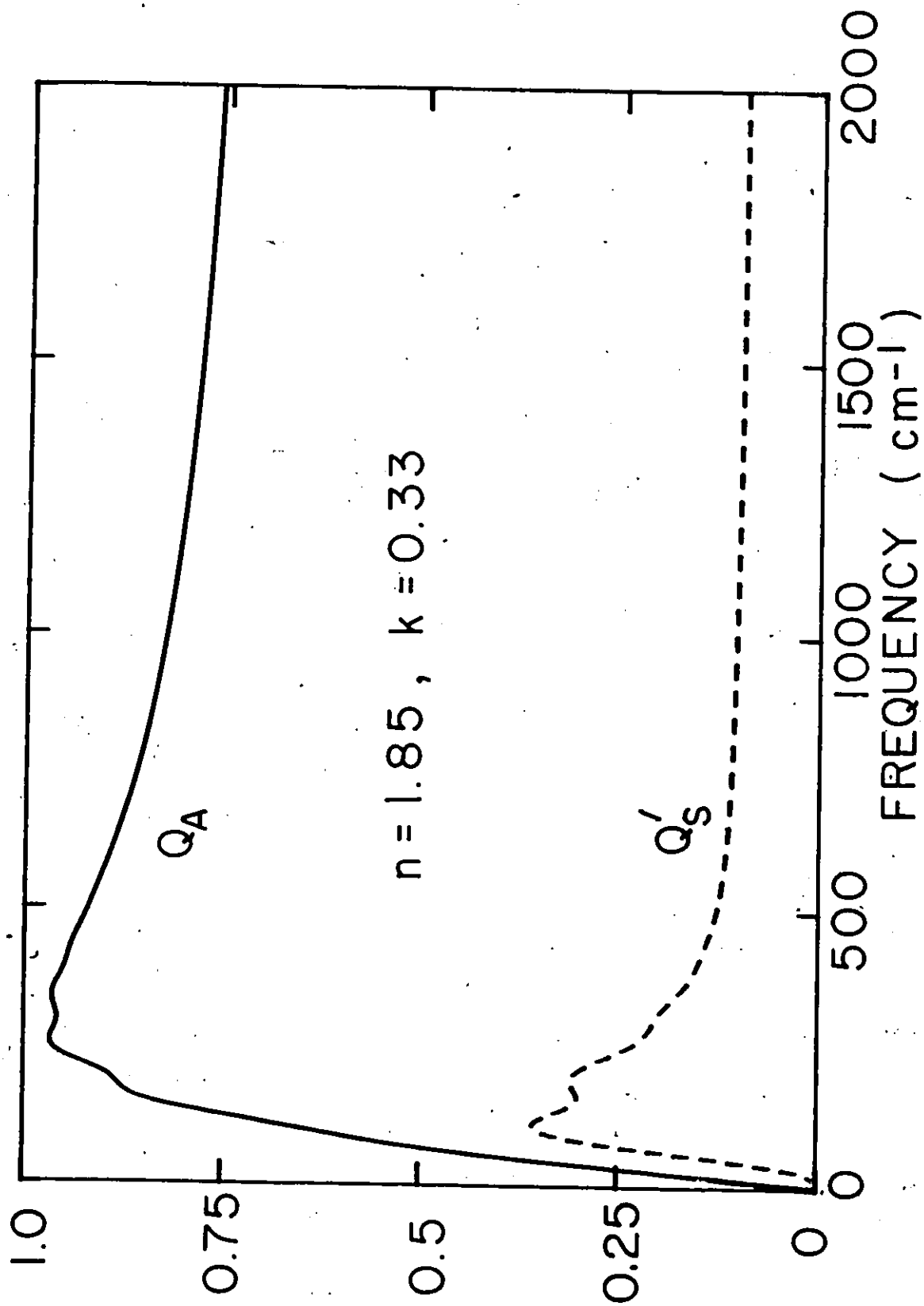
1.0
0.75
0.5
0.25
0
0
500
1000
1500
2000
FREQUENCY (cm-1)
Q_A
Q'_S
n=1.85, k=0.33

stronger in Fig. 3-7 than in Fig. 3-6, the difference is much smaller than the tenfold increase in the bulk absorption coefficient. From geometrical optics, we would expect the absorption efficiency to saturate at 0.78 for a collection of black fibres. At a value of k = 0.33 the extinction is already about equally divided between scattering and absorption.

Finally, Fig. 3-8 shows the 'transport' efficiencies Q_T for the two refractive indices n = 1.85, k = 0.033 (dashed curve) and n = 1.85, k = 0.33 (solid curve). These are simply the sum of the two curves Q_S' and Q_A in Fig. 3-6 and Fig. 3-7. Recall from the previous chapter that the 'radiative conductivity' K_R is inversely proportional to the thermal average K_T of Q_T over frequencies. For reasonably thick batts and reasonably black boundary walls, the radiative part of the heat flux is approximately proportional to K_R. Therefore Q_T, as shown in Fig. 3-8, gives a good measure of the thermal behaviour of the insulation.

Most striking is the similar magnitude of the two curves, considering the large difference in the absorption cross-sections and weighted scattering cross-sections for the two-materials. An increase in k leads to increased absorption Q_A, but this is surprisingly well compensated by a decrease in the weighted scattering Q_S'. Despite a tenfold increase in the bulk absorption, leading to a change from

Fig. 3-8

Transport efficiency $Q_T = Q_A + Q_S'$, calculated for randomly oriented 23.4 μm fibres for two values of the (constant) refractive index n-ik.

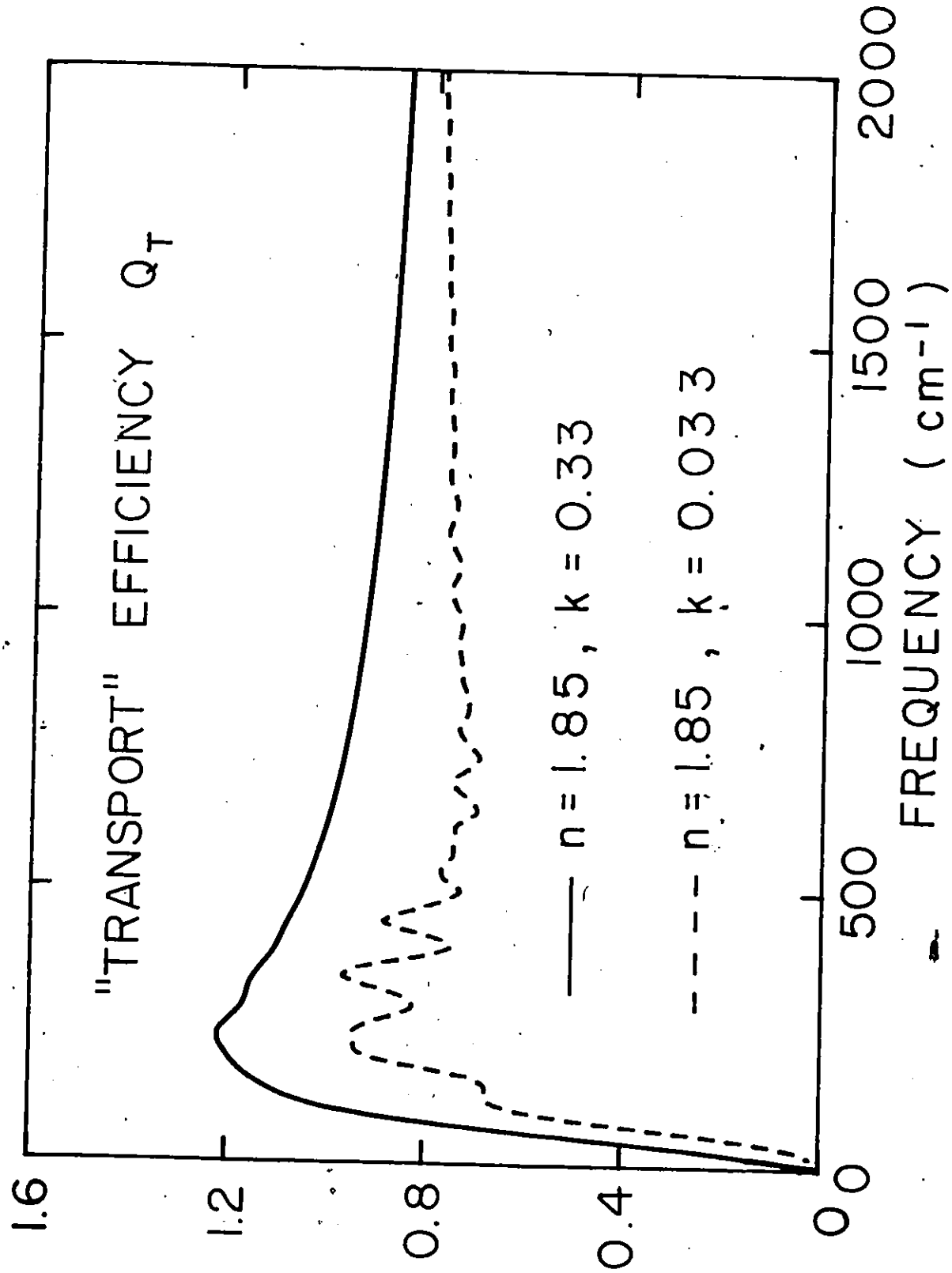
"TRANSPORT" EFFICIENCY Q_T
1.6
1.2
0.8
0.4
0.0
0
500
1000
1500
2000
FREQUENCY (cm^{-1})
n = 1.85 , k = 0.33
n = 1.85 , k = 0.033

moderate absorption to strong absorption in the fibrous material, the overall change in the radiative conductivity appears to be sbout 10%. In practical terms, this means that only rather modest changes in the radiative transfer properties can be effected by choosing different materials for the fibres - always assuming black walls and thick battings.

CHAPTER 4

MEASUREMENTS AND THEORETICAL RESULTS

4.1 Introduction

In this chapter the optical and thermal measurements are described and the results are compared with calculations using the theory of the previous two chapters. Section 4.2 describes the optical measurements. The infrared complex refractive index for polyester was obtained from transmission measurements on Mylar sheet. Values in the literature for the upper and lower ends of the frequency region of interest compared well with our results. These optical constants were then used together with the theory of scattering from cylinders to predict the optical properties of the polyester insulation materials.

As a check on the procedure so far, the extinction and absorption of samples of Polarguard were measured. The absorption was measured in a non-resonant cavity and compared very well with the calculations. Differences between measured and calculated spectra could be due in part to differences in the mechanical and thermal histories of the Mylar film (used to measure n and k) and the insulation materials. The extinction measurements were less accurate due to difficulties in preparing a sufficiently thin and sufficiently uniform sample, but the prominent features of the spectra

agreed reasonably well in the case of Polarguard. The measured extinction cross-section of Hollofil showed definite differences from the extinction calculated using the solid-fibre theory. Qualitatively the discrepancies agreed with calculated results in the literature for scattering from hollow cylinders at perpendicular incidence.

Thermal measurements by Dr. Brian Farnsworth of DREO are described in section 4.3, and the results compared with calculations for Polarguard and Hollofil using the n and k spectra of Mylar and the measured fibre diameters. The agreement is very good for the Polarguard measurements, with no adjustable parameters. For the Hollofil samples the calculations give thermal resistances about 10% too low, which may be explained by additional scattering from the hole in the fibres.

Section 4.4 presents theoretical results for metallic fibres, for fibres of varying diameter, and for glass fibres, without making any comparisons with experiment. It is shown that there is an optimum fibre size for dielectric materials which maximises the thermal resistance per unit weight if the batting density can be kept constant. For glass fibres this diameter is about 2 μm. For a material with a constant refractive index which approximates polyester, the optimum diameter is about 1.5 μ. A considerable improvement in performance is possible if the average fibre diameter is

reduced (neglecting problems of reduced fibre stiffness). Smaller but significant improvements appear to be possible if the fibres and boundary walls are given a reflective (metallic) coating.

4.2 Optical Measurements

The complex refractive index of the bulk material was determined by Dr. Timusk from far-infrared transmittance measurements. Polyester (polyethylene terephthalate, or PET) is available in thin films of very uniform thickness under the name Mylar. Transmission spectra were obtained for several films ranging from 1.5 μm to 24 μm in thickness in order to cover accurately regions of the spectrum where the absorption was strong and those where it was weak. Such spectra show effects of bulk absorption in the medium (which depends on the imaginary part k of the refractive index), of reflection from both surfaces, and of interference between the various orders of internally reflected waves. The position and amplitude of these interference fringes in frequency space depend both on the complex refractive index and on the film thickness. In addition, the frequency spectra of n and k are related to each other through a Kramers-Kronig relation (Moss, 1959). The transmission spectra contain enough information to determine both the real and the imaginary parts of the refractive index.

The two are calculated alternately in an iterative

Fig. 4-1

Refractive index n for polyester (PET) obtained from transmission measurements on Mylar film.

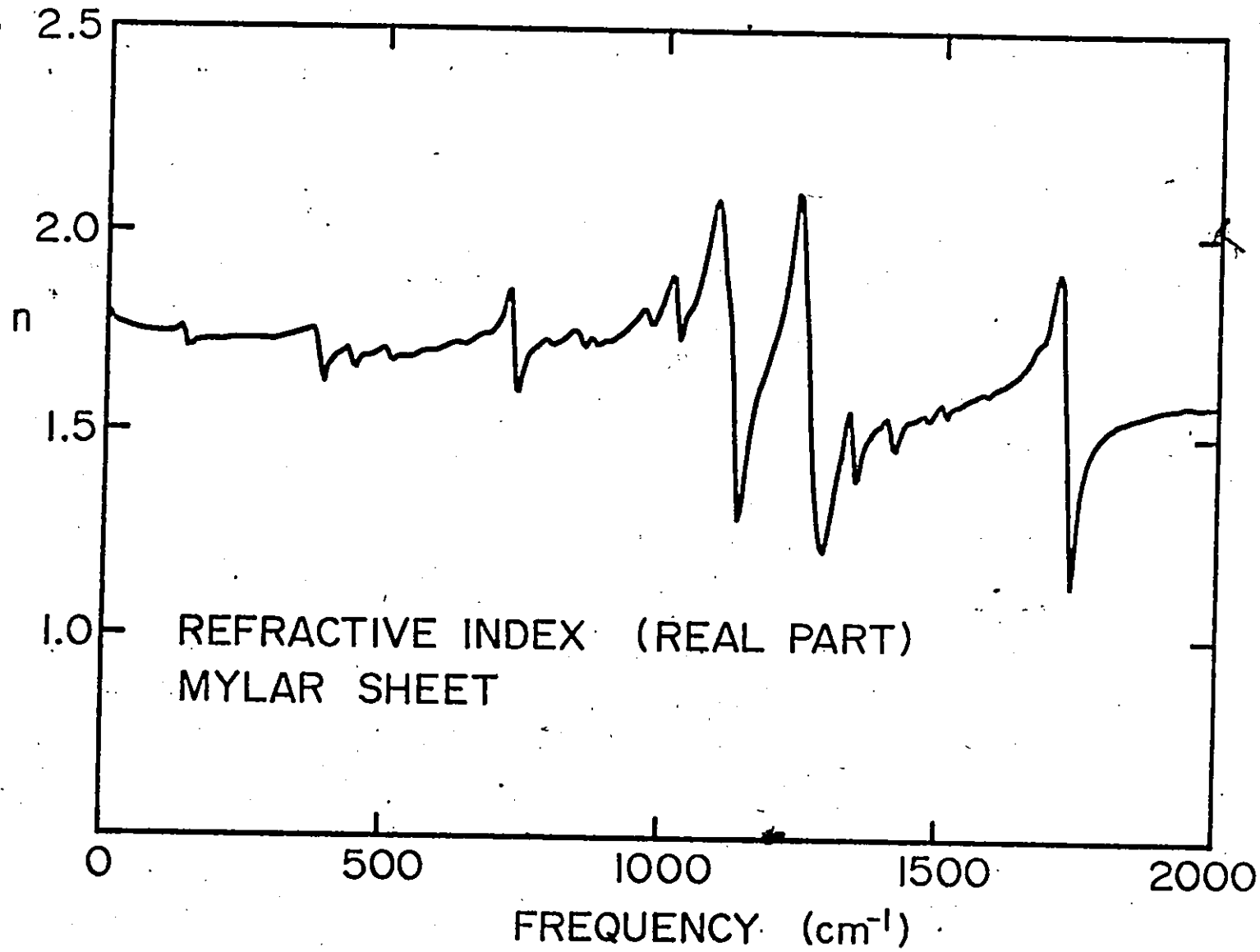
2.5
2.0
1.5
1.0
n
REFRACTIVE INDEX (REAL PART)
MYLAR SHEET
0
500
1000
1500
2000
FREQUENCY (cm⁻¹)

procedure in which the film thickness and the high-frequency index of refraction are adjusted for the best fit. After several iterations the n and k spectra converge. When these final values are used to calculate the original transmittance data as a check, the agreement is better than 1% (or 2% if data from one film thickness is used to predict the transmittance for a different thickness). All measurements were made with unpolarised light. The procedure is described in more detail in McKay et.al. (1984).

Figures 4-1 and 4-2 show the results for n and k at frequencies up to 2000 cm^{-1}. Other workers have obtained results over portions of this range which agree well with those shown here. Loewenstein and Smith (1971) report values for n at 50 cm^{-1} of 1.71 and 1.75 for the two polarisation directions, compared to our value of 1.75. At optical frequencies, we get n = 1.64, which agrees with the values 1.573, 1.541, and 1.645 for the three principal axes of the material obtained by Jarvis et.al. (1980). The relative strength of the absorption lines shown in Fig. 4-2 varies according to the thermal and mechanical history of the sample, which affects the molecular alignment and degree of crystallinity in the material (Koenig and Hannon, 1967). Some differences are expected between the spectra of Fig. 4-1 and Fig. 4-2 and the other published results. There are also likely to be significant differences between the Mylar

Fig. 4-2

Imaginary part k of the refractive index of Fig. 4-1.

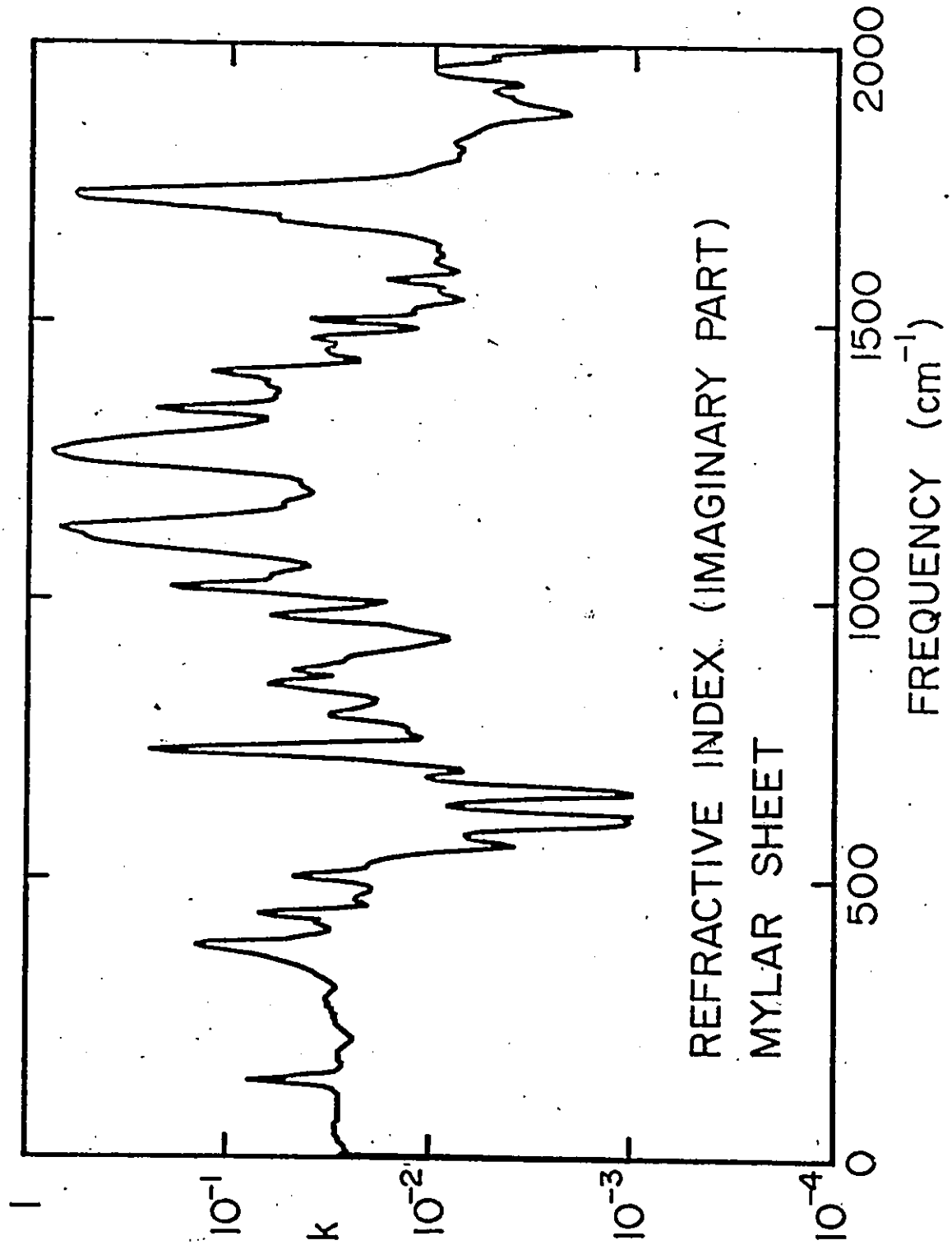
REFRACTIVE INDEX (IMAGINARY PART)
MYLAR SHEET
k
1
10^{-1}
10^{-2}
10^{-3}
10^{-4}
0
500
1000
1500
2000
FREQUENCY (cm^{-1})

values and the true optical constants for the polyester fibres in some frequency regions.

With these n and k values, all the optical properties of the fibre battings were calculated by the methods of Chapter 3. Table 4-1 lists the fibre parameters and the physical properties of polyester which were used for the optical and heat-transfer calculations. The specific gravity can vary from the value listed by 0.7% for moderate variations in the crystallinity of the material (Hefflinger and Knox, 1971). Probably there is a similar uncertainty in the thermal conductivity of PET, but since the fibre contribution is a small part of the heat flow, little error is introduced. The fibre sizes were determined by B. Farnworth by electron microscopy, and have an accuracy of ± 0.5 μm. For the scattering calculations, the Hollofil fibres were treated as solid polyester cylinders. As noted previously, there is no simple solution for electromagnetic scattering from hollow dielectric cylinders, except at perpendicular incidence. For each value of the fibre radius, the efficiencies Q_E, Q_S^0, and Q_S' were calculated at 500 equally-spaced frequency points from 0 to more than 2500 cm^{-1}. Each calculation required about 16 hours on the Digital LSI-11/23 microcomputer.

The absorption cross-section of a Polarguard fibre was measured directly in a non resonant cavity. Llewellyn-

TABLE 4-1

Bulk Properties of Polyester

Density of Polyester (PET) (Hefflinger and Knox, 1971)		1.38×10^3 kg/m^3
Thermal Conductivity of PET (R.C. Steere, 1966)		0.15 W/m-°K
Fibre Radius:	Polarguard	11.7 μm
	Hollofil (outer)	13.2 μm
	Hollofil (inner)	~4.2 μm

(from Farnworth et al. 1979)

$\frac{\text{Length} \times \text{diameter}}{\text{mass}}$:	Polarguard	39.4 m^2/kg
	Hollofil	38.9 m^2/kg

Fig. 4-3

Nonresonant cavity used to measure the infrared absorption cross-section of fibres.

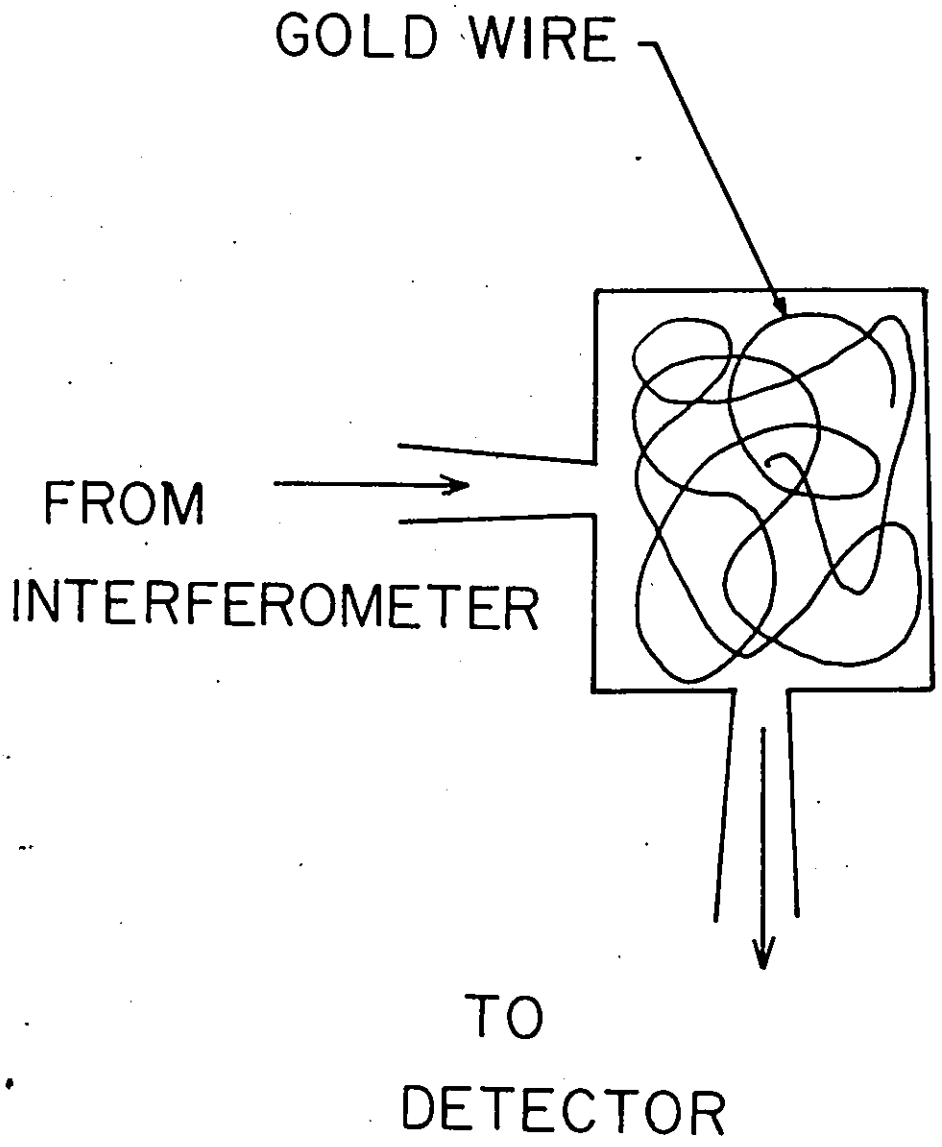
GOLD WIRE
FROM
INTERFEROMETER
TO
DETECTOR

Jones et al. (1980) describe the technique at microwave lengths. For our infrared measurements we used a gold-plated cylindrical cavity 20.0mm in diameter and 19.0 mm deep (Fig. 4-3). Infrared radiation from the Michelson interferometer (modified for Fourier transform spectroscopy) entered through a 3.2 mm hole in one of the circular faces. Another 3.2 mm hole in the curved wall of the cavity led to a pyroelectric detector. The entrance and exit holes were at right angles to each other in order to increase the number of reflections undergone by those rays which reach the detector. It was necessary to place a 21-cm length of 0.75 mm diameter gold wire in the cavity, crumpled so as to fill the volume, in order to improve the pattern of the energy distribution. Ideally, the intensity should be isotropic and uniform throughout the cavity volume.

The absorption cross-section of a small sample placed in the cavity is given by

$$\sigma_a = \sigma_o(F_o/F_a - 1) \qquad (4\text{-}1)$$

where F_o is the measured flux emerging from the empty cavity, and F_a the flux from the cavity with an absorbing sample in it. The effective total cross-section of the cavity walls and the entrance and exit holes is σ_o. To calibrate σ_o we used a sample of known absorption cross-section, a rectangular strip of black polyethylene. This material absorbs all infrared between 400 cm^{-1} and 2000 cm^{-1}, except for a small

reflectance correction. The strip was 40 mm in length, 50 μm thick, and had an average width (measured with a travelling microscope) of 0.375 mm. The total surface area, including both sides and edges, was 34±1 mm^2. For a convex object of arbitrary shape, the geometric cross-section, averaged over viewing angles, is 1/4 the surface area. Since the strip is large compared to the wavelength, we ignored diffraction effects, and set the absorption cross-section of the polyethylene equal to 1/4 its total surface area.

First there was a correction for reflection at the surface. Using the value n = 1.5 for polyethylene, the Fresnel equations for the reflectance (Jackson, 1975) were averaged over polarisations and incident angles. The result was that 9% of the energy would be reflected, and the absorption cross-section was reduced accordingly. Spectra of the polyethylene strip and of the empty cavity were measured, and the factor (F_o/F_a-1) of Eq. (4-1) was averaged over the region 500 cm^{-1} - 1500 cm^{-1} where the noise was lowest. This gave a cavity cross-section σ_c = 20 mm^2, with an uncertainty of 5%. After the contribution of the entrance and exit holes is subtracted, this implies an average loss at the gold walls and wire surface of 2.8%, which seems reasonable in light of the value of 1.7% in this wavelength range indicated by Bennett and Bennett (1966) for freshly-evaporated gold films prepared under 'standard vacuum conditions'.

With this calibration of the cavity completed, the absorption of a 40-cm long Polarguard fibre was measured. The results are shown in Fig. 4-4, plotted as absorption efficiency Q_A. Also shown (solid curve) is the result of the theoretical calculation using the complex refractive index measured on Mylar sheet along with the fibre parameters in Table 4-1. Four separate spectra were averaged to give the experimental curve; the error bars indicate the size of the variation from run to run, due in part to noise (which varies with frequency according to the source spectrum and beamsplitter efficiency) and in part to the nonuniformity of the energy density in the cavity, as the sample was moved between runs. The agreement overall is very good, considering that the two materials were produced by different processes. At some wavelengths, the discrepancies can be assigned to particular microscopic characteristics of the material. The lower absorption for the fibre in the peak at 970 cm^{-1} and in the region 1300 cm^{-1} to 1400 cm^{-1} indicates that the fibre material is less crystalline than the Mylar sheet used for the n and k measurements (Koenig and Hannon, 1967). Jarvis et.al. (1980) show that the peak at 875 cm^{-1} is very dependent on the orientation of the molecules; the fibres may have more randomly-oriented molecules. A limitation on the information which can be derived from Fig. 4-4 comes from the use of a Mylar beamsplitter. The

Fig. 4-4

Calculated (solid curve) and measured (dotted curve) absorption efficiency of Polarguard.

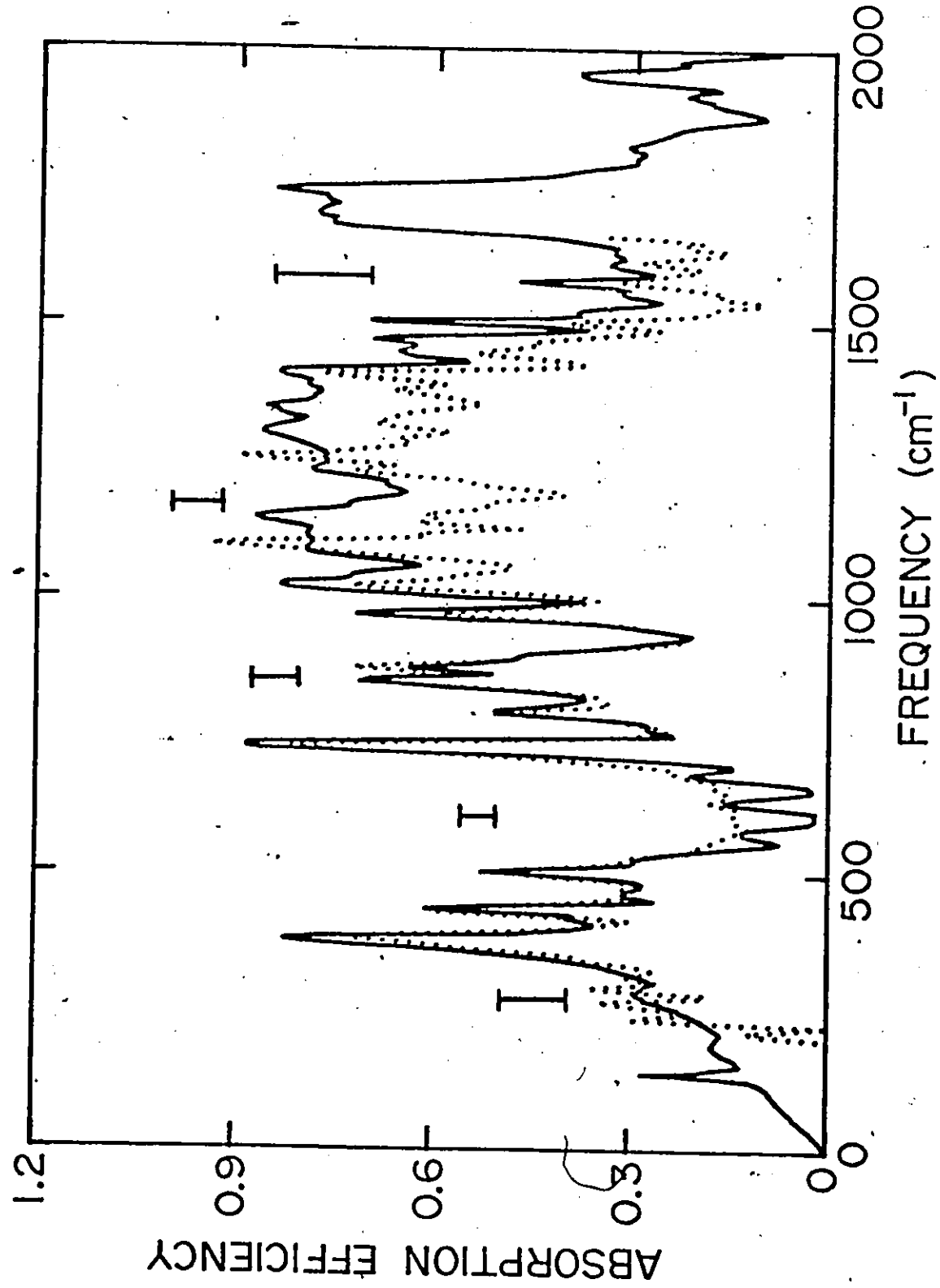
ABSORPTION EFFICIENCY
1.2
0.9
0.6
0.3
0
0
500
1000
1500
2000
FREQUENCY (cm⁻¹)

efficiency of this beamsplitter can decrease abruptly (with a consequent increase in noise) at the absorption lines which are of most interest.

The extinction cross-section of thin samples was measured by Dr. Timusk using the arrangement described in McKay et al. (1984). A small amount of the batting material was spread as uniformly as possible over a 20-mm aperture and placed in front of the beam emerging from the interferometer. A pair of curved mirrors focussed the undeflected radiation onto the detector. Sample densities ranged from 5 to 20 g/m^2 (a monolayer of fibres has density 25 g/m^2, Table 4-1). At such low densities it is difficult to maintain a uniform thickness across the opening, and the accuracy of the measurements is only ±20% because of this. Thicker samples, however, would allow multiple scattering. The extinction coefficient α_E (cross-section per unit volume) times the sample thickness d was calculated from

$$\alpha_E d = - \ln \frac{I}{I_0} \qquad (4\text{-}2)$$

where I is the measured intensity of the beam with the sample in place, I_0 with no sample. Dividing $\alpha_E d$ by the sample mass per unit area gives the cross-section per kilogram κ_E, and dividing again by the geometrical cross-section per unit mass of a single fibre (about 40 m^2/kg, Table 4-1) gives the efficiency Q_E:

$$Q_E = \alpha_E d \times (M/A)^{-1} \times \left(\frac{2}{\pi a \rho_f}\right)^{-1} \qquad (4\text{-}3)$$

where ρ_f is the density of bulk polyester.

Figure 4-5 shows the results for Polarguard and Figure 4-6 for Hollofil (dotted curves). On both graphs the values calculated from the measured n and k are shown (solid curves) assuming solid fibres with random orientations and radii of 11.7 μm and 13.2 μm respectively. In both cases the agreement is generally good within the ±20% overall accuracy, although the smaller-scale structure in the spectra do not match well. The reduced amplitude of the large peak at 300 cm^{-1} is probably due to sample inhomogeneity; excess transmission through the "thin spots" in the sample has a stronger effect when the extinction is high. At higher frequencies peaks will be washed out because of the variation (±5%) in radius from fibre to fibre. There will also be an unavoidable difference between the calculated extinction, in which all scattered rays are considered tobe removed from the beam, and the measured extinction, for which radiation scattered sufficiently close to the forward direction will still strike the detector. For the geometry used in these measurements, the acceptance angle of the detector was about 2°; from Figs.3-2 and 3-3, we see that this may include 5% - 10% of the scattered radiation. Possibly this is the explanation for the missing peak between 700 - 900 cm^{-1}.

Fig. 4-5

Calculated (solid curve) and measured extinction efficiency for Polarguard.

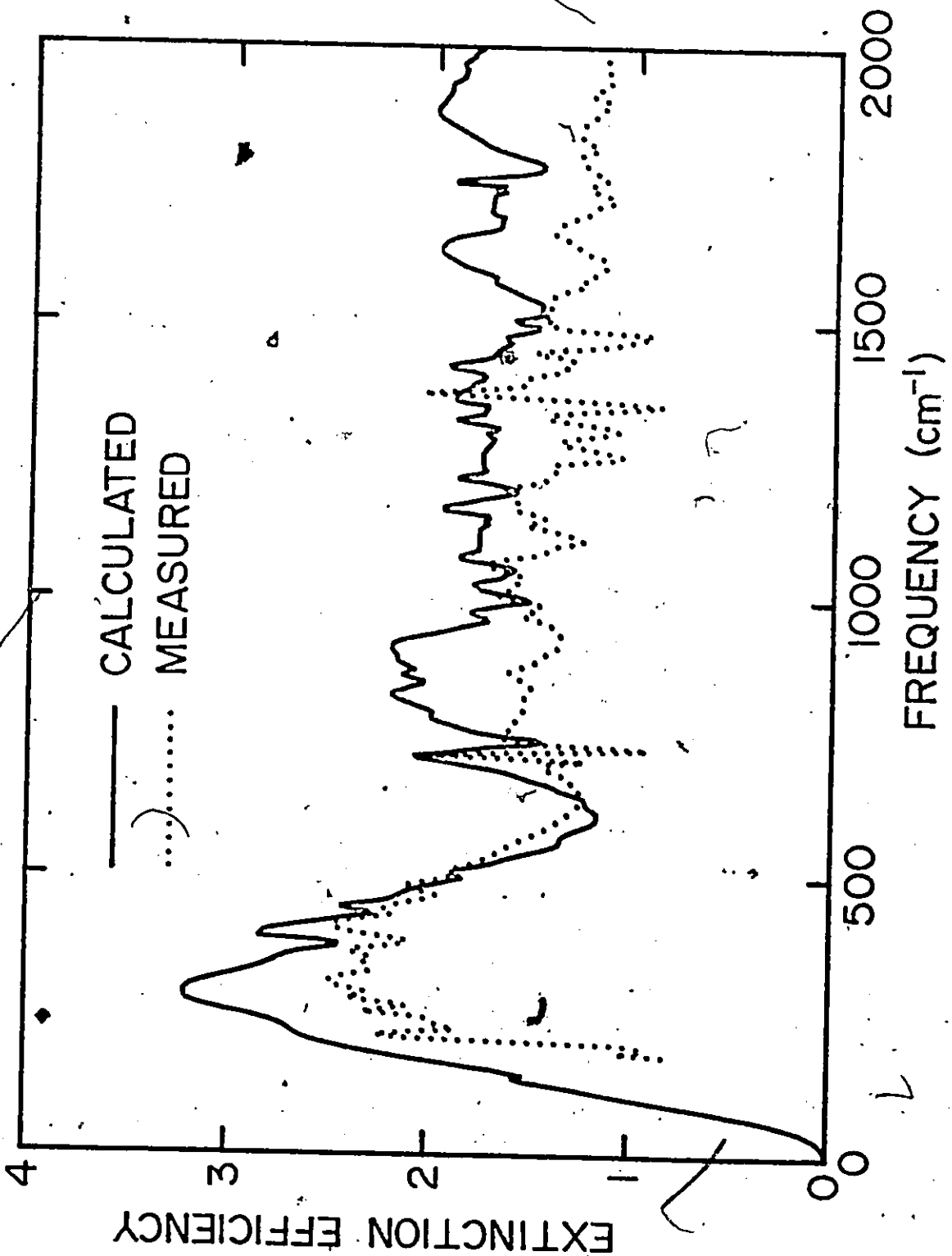
EXTINCTION EFFICIENCY
0
1
2
3
4
500
1000
1500
2000
FREQUENCY (cm⁻¹)
CALCULATED
MEASURED

Fig. 4-6

Extinction efficiency for Hollofil. The dotted curve is the result of direct measurements. The calculated curve ignores the hole in the centre of the fibres.

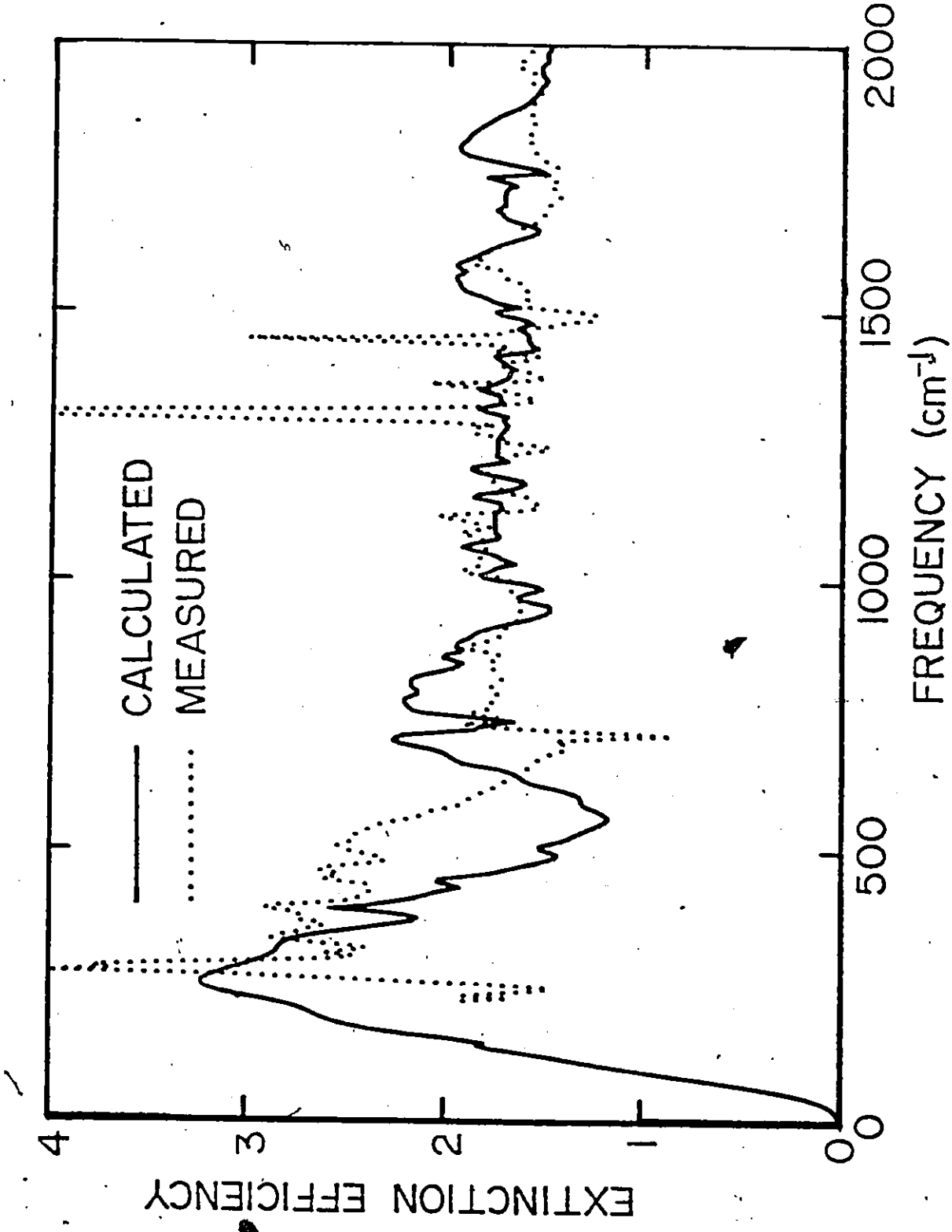
EXTINCTION EFFICIENCY
0
1
2
3
4
0
500
1000
1500
2000
FREQUENCY (cm⁻¹)
CALCULATED
MEASURED

In Fig. 4.6 the noise level is higher, but the match between theory and experiment is excellent at high frequencies. The broadening of the large peak at 200 - 700 cm^{-1} is due to the hole in the fibre, an effect seen clearly in published results for hollow cylinders at perpendicular incidence (Kerker, 1969; Evans et al. 1964). Overall it would appear that the effect of the hole is not very large, but there is considerable uncertainty in these measurements.

Figures 4-7 and 4-8 show more of the calculated optical functions. The efficiency Q_T, that is, the sum of the absorption and "backscattering" efficiency, is shown in Fig. 4-7 (solid curve) for 11.7-μm radius fibres, along with the thermal weight function dB/dT evaluated at 300°K. This weight function indicates the relative contribution of each frequency to the radiative transport. More than 96% of the integral of dB/dT lies below 2000 cm^{-1}. Figure 4-8 shows Q_T (dashed curve) and the absorption efficiency Q_A (solid curve) for polyester fibres with a radius of 13.2 μm. The curves are almost identical with those for the smaller fibres shown in Fig. 4-7 and Fig. 4-4.

In Fig. 4-8 the backscattering and absorption partially complement each other so that Q_T is a smoother function of frequency than either of its components. In the region 500 - 700 cm^{-1} where the absorption is low, the scattering is relatively large; between 1000 and 1400 cm^{-1}, the ab-

Fig. 4-7

The transport efficiency Q_T (sum of absorption and weighted scattering efficiencies) calculated for Polarguard. Also shown is the thermal weight function dB/dT at a temperature of 300°K.

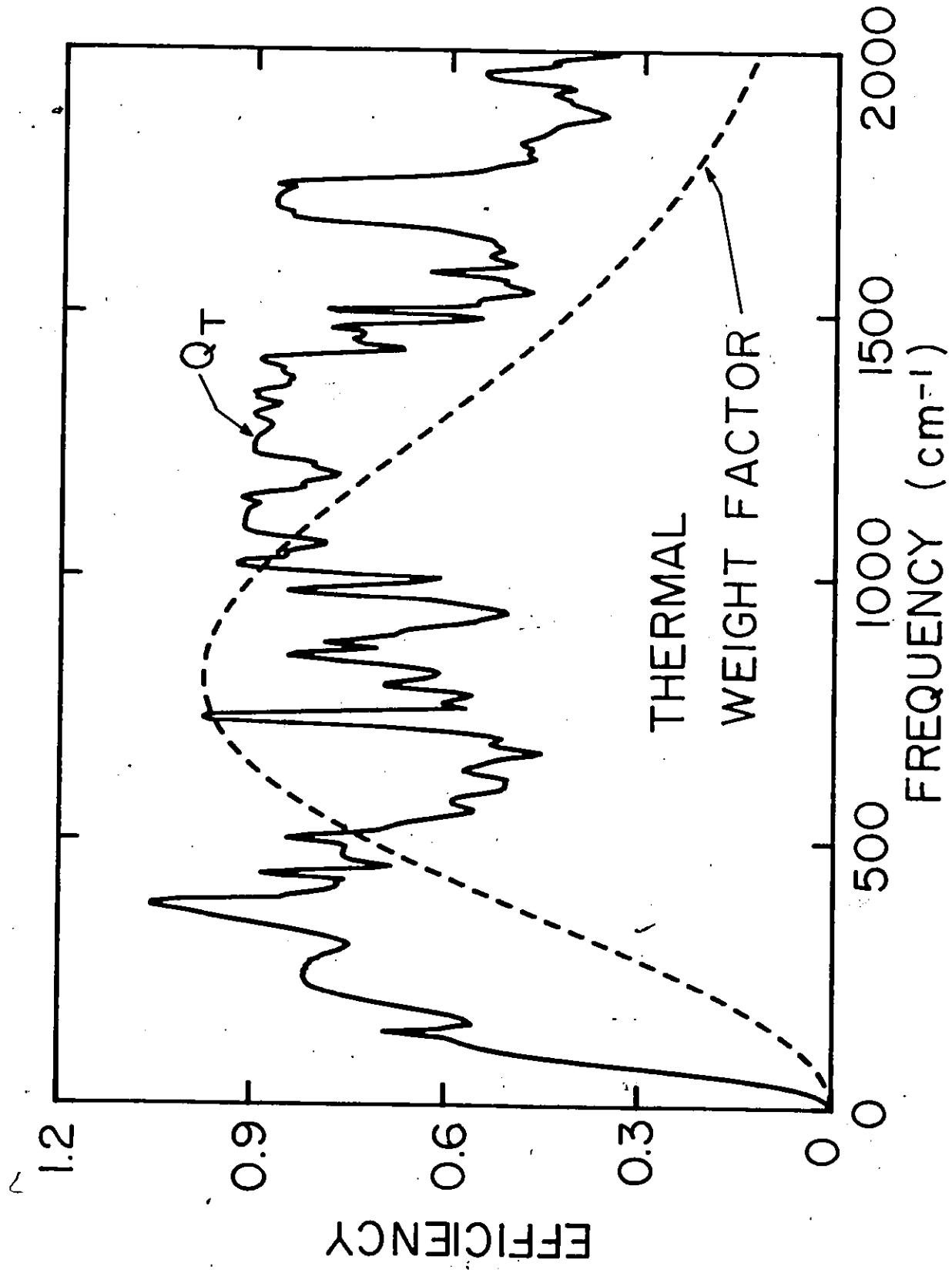
EFFICIENCY
1.2
0.9
0.6
0.3
0
0
500
1000
1500
2000
FREQUENCY (cm⁻¹)
THERMAL
WEIGHT FACTOR
Q_T

Fig. 4-8

Transport efficiency Q_T and absorption efficiency Q_A calculated for randomly-oriented polyester fibres with a diameter of 26.4 μm. This represents Hollofil, if the hole in the fibres is ignored.

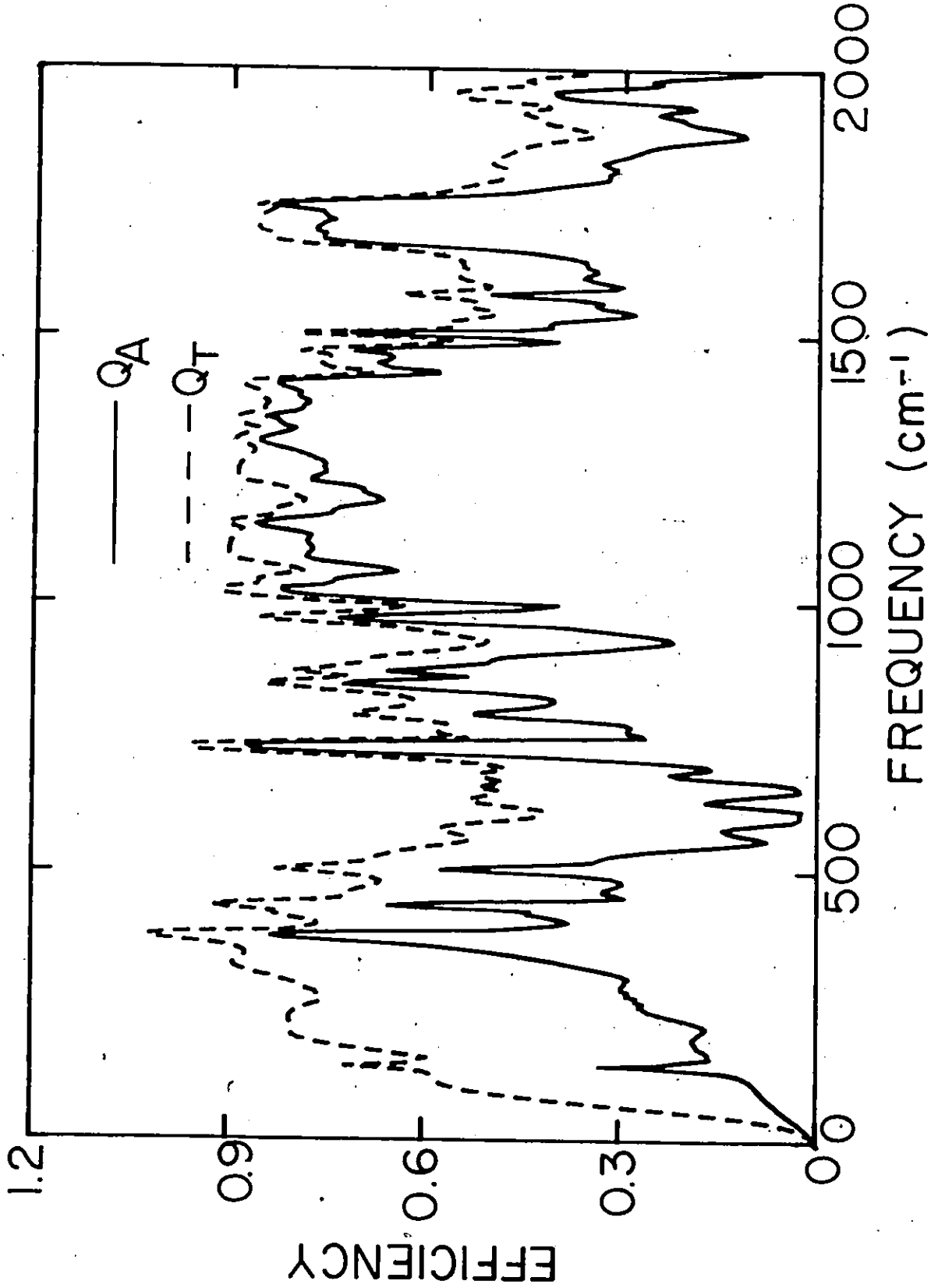
EFFICIENCY
1.2
0.9
0.6
0.3
0
0
500
1000
1500
2000
FREQUENCY (cm⁻¹)
Q_A
Q_T

sorption is strong and the backscattering is very weak. At some frequencies Q_T is larger than the geometrical-optics limit of 0.78 for opaque fibres which absorb and scatter isotropically. The thermal average of Q_T is smaller, about 0.675. Note that Q_T is about half (or less) as large as the extinction Q_E; in a radiative-transfer model based on isotropic scattering, Q_E would replace Q_T. An early attempt on our part to use such a model together with the measured extinction cross-section led to very poor agreement with the measured heat transfer, for reasons that are clear on comparing these two spectra.

4.3 Thermal measurements

The parameters K_A and K_T are obtained by averaging Q_T and Q_A over frequencies with the thermal weight function dB/dT shown in Fig. 4-8, according to (2-32) and (2-33). A factor $2/(\pi a \rho_f)$ is required in going from the efficiency Q to the cross-section per unit mass κ. For hollow fibres, there is a correction to ρ_f to account for the material removed. Table 4-2 shows κ_A and κ_T for Polarguard and Hollofil at a temperature of 30°C. Several parameters which characterise the heat transport are calculated at a nominal batting density of 10 kg/m^3 and listed in the same table. The optical parameters κ_A and κ_T are nearly equal for the two materials, a consequence of their having almost the same surface area/unit mass; the average efficiencies themselves

TABLE 4-2

Calculated Infrared Parameters of Polarguard and Hollofil

	Absorption x-section κ_A (m^2/kg)	'Transport' x-section κ_T (m^2/kg)	Radiative Conductivity' K_R (W/m-K)	Air+fibre Conductivity' K (W/m-K)	Diffusion Length D (mm)	'Coupling' Length p^{-1} (mm)
Polarguard	18.7	26.6	0.0316	0.0268	5.0	1.75
Hollofil	19.0	26.0	0.0324	0.0267	5.1	1.75

Temperature is 30°C, batting density 10.0 kg/m^3.

Thermal conductivity of air was taken to be 0.02627 W/m-K by interpolation from values listed in CRC Handbook of Chemistry and Physics (Weast, 1982)

change very slowly with radius for this size of fibre. Of course, we have not included the effect of the hole on the scattering; we have assumed that it serves only to reduce the weight and the thermal conductivity of the fibres.

At the nominal density of 10 kg/m^3, a little lower than the average uncompressed density of both materials, the radiative conductivity is 20% larger than the total air plus fibre conductivity K. K_R is inversely proportional to density, and at ρ = 12 kg/m^3 or so, the radiative and conductive contributions are equal. Note that K is only slightly different from K_{air}, so that only 2% of the conductive heat flow is carried by the fibres. This contribution is of course proportional to the density.

Two typical length scales for the heat transfer, D and p^{-1} defined by (2-63) and (2-55) respectively, are given in the last two columns. D is equal to 4/3 $(\rho\kappa_T)^{-1}$, and is the effective optical depth or diffusion length for the thermal radiation in the sense that, for black boundaries and in the absence of conduction, the thermal resistance of a batt is proportional to (1+L/D). Here L is the thickness of the batt, so L/D is the "optical" thickness, and the extra 1 is the boundary contribution. Each layer of thickness D is equivalent to adding another opaque sheet between the walls. At a density of 10 kg/m^3, D is about 5 mm. Since $D \propto \rho^{-1}$, we can restate this by saying that one diffusion

length corresponds to a layer of surface density 50 g/m^2. The other length scale, p^{-1}, is the length scale for energy transfer between the radiative and conductive modes. At 10 kg/m^3, p^{-1} is less than 2 mm, which means that the proportions of the total heat flux carried in each mode quickly reach their limiting values (i.e. the values appropriate to an optically thick batt) as we move away from the boundaries. Unlike the other parameters, p^{-1} is only approximately proportional to ρ^{-1}; it also contains a factor $(1+K_R/K)^{-1/2}$, which increases slowly with increasing density.

Two sets of thermal measurements are available to compare with the predictions of the theory. Both were made by Brian Farnworth of DREO using heat-flow meter apparatus. The machine consists of two large parallel plates with blackened surfaces which are maintained at different uniform temperatures. Between the plates is the sample under test, and in series with it (against one of the plates) is the heat-flow meter itself. This is a slab of material (e.g. cork) whose thermal resistance is known, equipped with thermocouples on both surfaces to measure the temperature difference across it. Therefore the heat flow through the meter can be calculated, and the geometry is such that the same heat must flow through the sample under test. From the heat flux and the temperature difference across the sample, its thermal resistance is calculated. The accuracy of such measurements

is limited by the precision of the thermocouples, by the uniformity of the temperature in the directions parallel to the sample surface, and by the calibration of the heat-flow meter.

Table 4-3 lists values for the experimental and theoretical thermal resistance of 5 Polarguard and 3 Hollofil samples. The experimental values were taken from Farnworth et.al. (1979) and were obtained using an apparatus calibrated from measurements on air gaps of varying thickness. The density is roughly the same for all samples, with thickness varying by about a factor of 2. Values of L/D range from 3 - 6 for the Polarguard measurements, and 4 - 8 for Hollofil. Theoretical values were calculated from Eq. (2-62) using the optical functions obtained from measurements on Mylar sheet. No measurements on the fibrous materials themselves, except for the fibre radius, went into the calculation, and no adjustable parameters are used. The results are in excellent agreement (within the experimental uncertainty of 2 - 4%) for all five Polarguard samples. For two of the three Hollofil samples, the theoretical resistances are about 10% too low, while the third agrees within the experimental uncertainty. The largest source of error in the calculations is the uncertainty in the fibre radius (or inner and outer radii for the hollow fibres). An error of ±0.5 μm on each radius measurement gives an uncertainty of ±4% in K_A, K_T and K_R for Polarguard, and ±7% for Hollofil (because 2 measurements

TABLE 4-3

Measured and Calculated Thermal Resistances of Fibre Batts

Sample	Mass/area kg/m^2	Thickness mm	Density kg/m^3	Thermal Resistance Measured m^2-K/W	Thermal Resistance Calculated m^2-K/W
Polarguard					
1	0.220	20.2	10.9	0.40 ±.02	0.39
2	0.295	25.0	11.8	0.485±.01	0.49
3	0.155	12.4	12.5	0.27 ±.01	0.26
4	0.255	24.2	10.5	0.46 ±.01	0.45
5	0.270	26.3	10.3	0.48 ±.01	0.49
Hollofil					
1	0.185	12.2	15.2	0.28 ±.01	0.27
2	0.260	22.0	11.8	0.49 ±.02	0.43
3	0.350	27.4	12.8	0.60 ±.02	0.55

Mean temperature 30°; wall emissivities $\varepsilon_H = \varepsilon_C = 0.92$

Measurements from Farnworth et al. (1979)

are needed). Since the radiative transfer accounts for about half the heat flow, the error in the thermal resistance will be about half these values. The remaining discrepancy in the Hollofil measurements may indicate extra scattering from the central hole, which has 30% of the surface area of the fibre. As noted in the previous section, there was increased extinction observed in measurements on Hollofil as compared to that calculated for solid fibres. The absorption, however, is probably reduced somewhat, and the net effect is difficult to guess. Calculations for hollow fibres at perpendicular incidence using the Mylar n and k would probably provide a useful, though not exact, estimate of the effect of the hole on κ_A and κ_T.

On the other hand, it should be noted that the discrepancy between the theoretical and experimental results for the three Hollofil samples has no regular behavior as a function of sample density or thickness, and is probably due in part to somewhat larger experimental uncertainty than quoted in Table 4-3.

A second set of thermal measurements was made on Polarguard by Dr. Farnworth using a new apparatus calibrated with the aid of standard samples (high-density glass fibreboard) supplied by the National Research Council. The apparatus and measurement techniques are described in McKay et al. (1984). Figs. 4-9 and 4-10 show the results and the theoretical predictions. A set of measurements at constant

thickness (50 mm) and temperature (31.3°C) was made by compressing 1 to 5 layers of 270 g/m^2 (8 oz/sq. yd) Polarguard between the plates. These measurements are shown in Fig. 4-9. The horizontal axis shows $(\text{density})^{-1}$, and the vertical axis is the effective conductivity K_{eff}, defined as the heat flow per unit area divided by the average temperature gradient. The horizontal error bars represent the uncertainty in the batting density, due primarily to the error in measurement of the area of the batt. There is a 1% error in the vertical direction due to calibration accuracy of the apparatus; this is about the size of the experimental circles at the larger values of K_{eff}, and half that size at the lowest value. The solid curve shows the theoretical calculation. Three of the experimental points lie right on the curve, two are below by about the maximum estimated uncertainty, and only one measurement appears to differ significantly from the theory. It is possible the diffusion model breaks down for the two lightest battings, which have densities of about 6.0 kg/m^3 and 5.5 kg/m^3. At such densities, the diffusion length is about 10 mm, or 1/5 the batt thickness. Therefore 40% of the material is within one diffusion length of a boundary surface, where the assumptions of the diffusion model are less accurate. We should also consider the uncertainty in the fibre radius. A smaller fibre radius would move the theoretical curve downward in Fig.

Fig. 4-9

Effective thermal conductivity of Polarguard batts of various densities. Each point represents a thermal measurement. The solid curve is the theoretical calculation using only the fibre radius and the bulk properties of polyester.

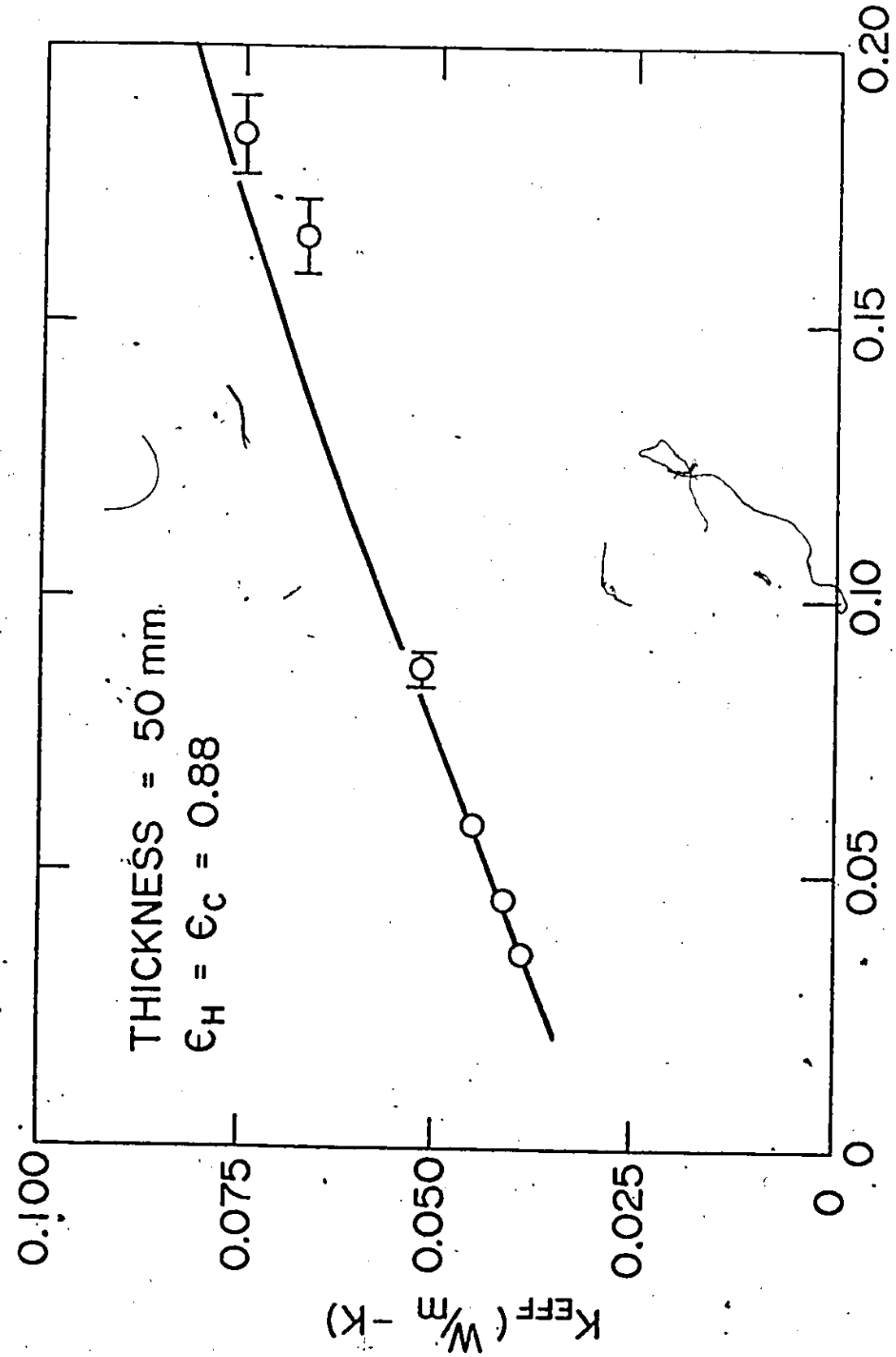
THICKNESS = 50 mm
$\epsilon_H = \epsilon_C = 0.88$
K_{EFF} (W/m -K)
0.100
0.075
0.050
0.025
0
0.05
0.10
0.15
0.20
1/ρ (m³ / kg)

4-9, with points at low density (the right-hand edge of the graph) being more affected, as a larger proportion of the heat transfer is by radiation.

Fig. 4-10 shows measurements at three different temperatures for the same batt. The error bars on the experimental points indicate the calibration uncertainty of the heat-flow meter; the uncertainty in the density is included in the theoretical results, which are shown as the shaded band on the graph. Two points lie below this region by about twice the calibration error bars, while the third agrees well with the prediction. However, the error in the radius measurement has not been included. A 2% error in the fibre diameter (±0.5 μm) would nearly double the width of the shaded region, and comfortably include the experimental points. For measurements with an overall accuracy of a few percent, the simple heat-transfer model appears to be completely adequate.

4.4 Other Materials

Since the heat-transfer model based on the diffusion approximation successfully predicts the thermal resistance within the 5% or so total accuracy of the thermal and density measurements, we can use it to investigate theoretically the effect of changes on fibre size or composition. These are expressed most easily in terms of the effect on the radiative conductivity parameter K_R.

Fig. 4-10

Effective thermal conductivity of Polarguard vs. temperature. The points are thermal measurements, and the shaded region is the range of theoretical values corresponding to densities in the interval 10.9 ± 0.3 kg/m^3.

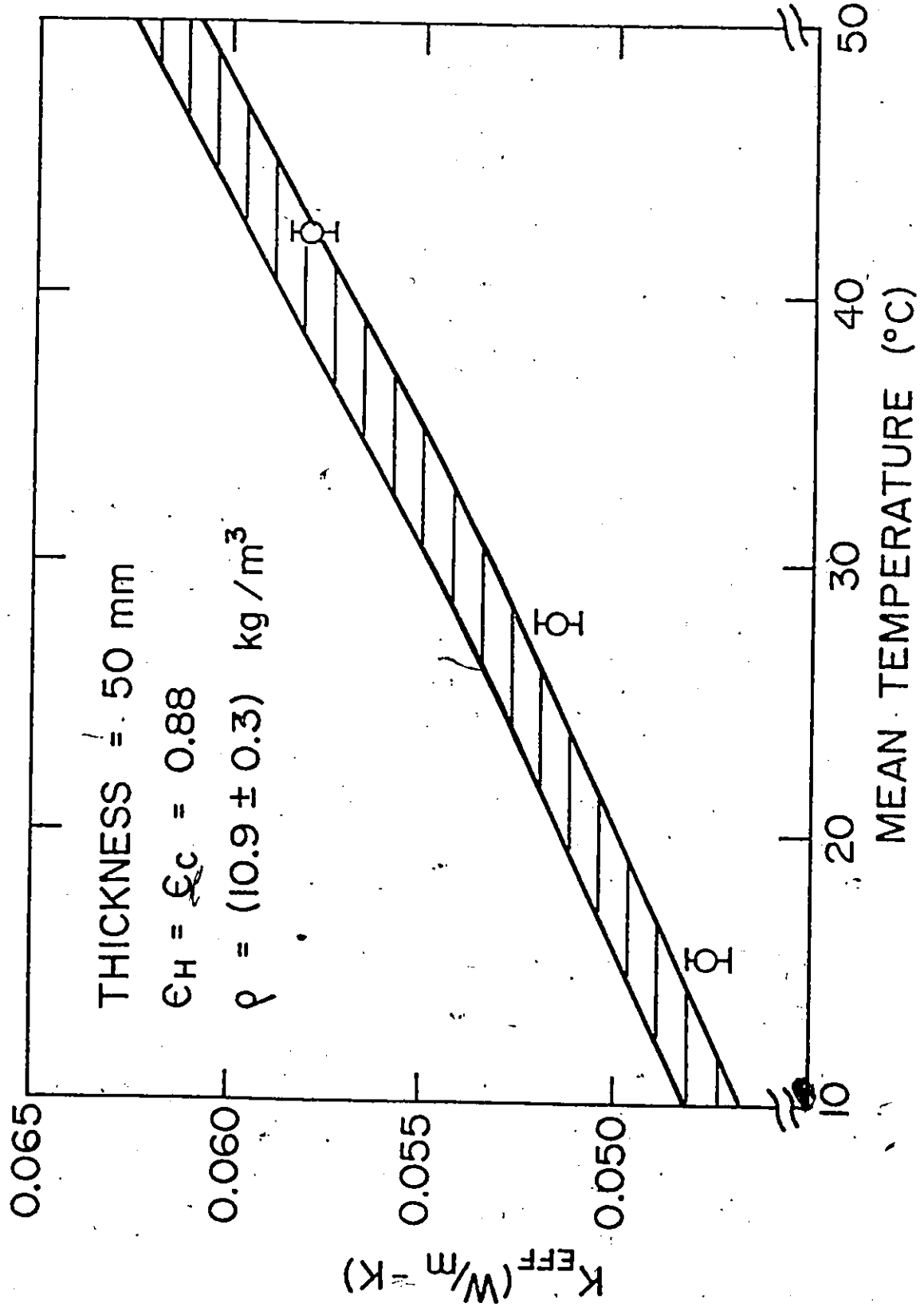
THICKNESS ≒ 50 mm
$\epsilon_H = \epsilon_c = 0.88$
$\rho = (10.9 \pm 0.3)$ kg/m^3
K_{EFF} (W/m-K)
0.065
0.060
0.055
0.050
10
20
30
40
50
MEAN TEMPERATURE (°C)

For a constant (frequency-independent) refractive index, there are two parts to the effect of variations in fibre diameter. The 'radiative conductivity' K_R (equation (2-56) is inversely proportional to the thermally-averaged cross-section per unit volume $\rho\kappa_T$, which is defined in (2-32) as an average over frequency of the absorption plus weighted scattering cross-section per unit volume, $(A+S_0-S_1)$. In chapter 3 this cross-section was expressed as the product of the geometrical cross-section per unit volume $2f/\pi r$ and the 'transport' efficiency Q_T. For large radii (compared to wavelength), the efficiency Q_T approaches a constant, as shown in Fig. 3-8. Therefore the radiative conductivity ought to be proportional to fibre radius for large fibres. As the fibre size is reduced, however, the efficiency itself eventually drops to zero faster than the fibre area/unit volume increases. In Fig. 3-8 this drop in Q_T occurs where the wavelength is roughly 4 times the fibre diameter, the precise value depending somewhat on the refractive index of the material. At very small fibre diameter, the material again becomes transparent and K_R increases. In between there should be an optimum fibre size which provides the maximum thermal insulation per unit weight if the mechanical stiffness of the fibres is not a consideration.

In Fig. 4-11 the variation of K_R with fibre diameter is shown for a material with a constant refractive index

Fig. 4-11

Calculated radiative conductivity parameter K_R for two hypothetical materials as a function of fibre radius. The solid curve is for a material with a constant refractive index $n = 1.7$, $k = 0.02$, and the dashed curve is for perfectly-conducting metallic fibres.

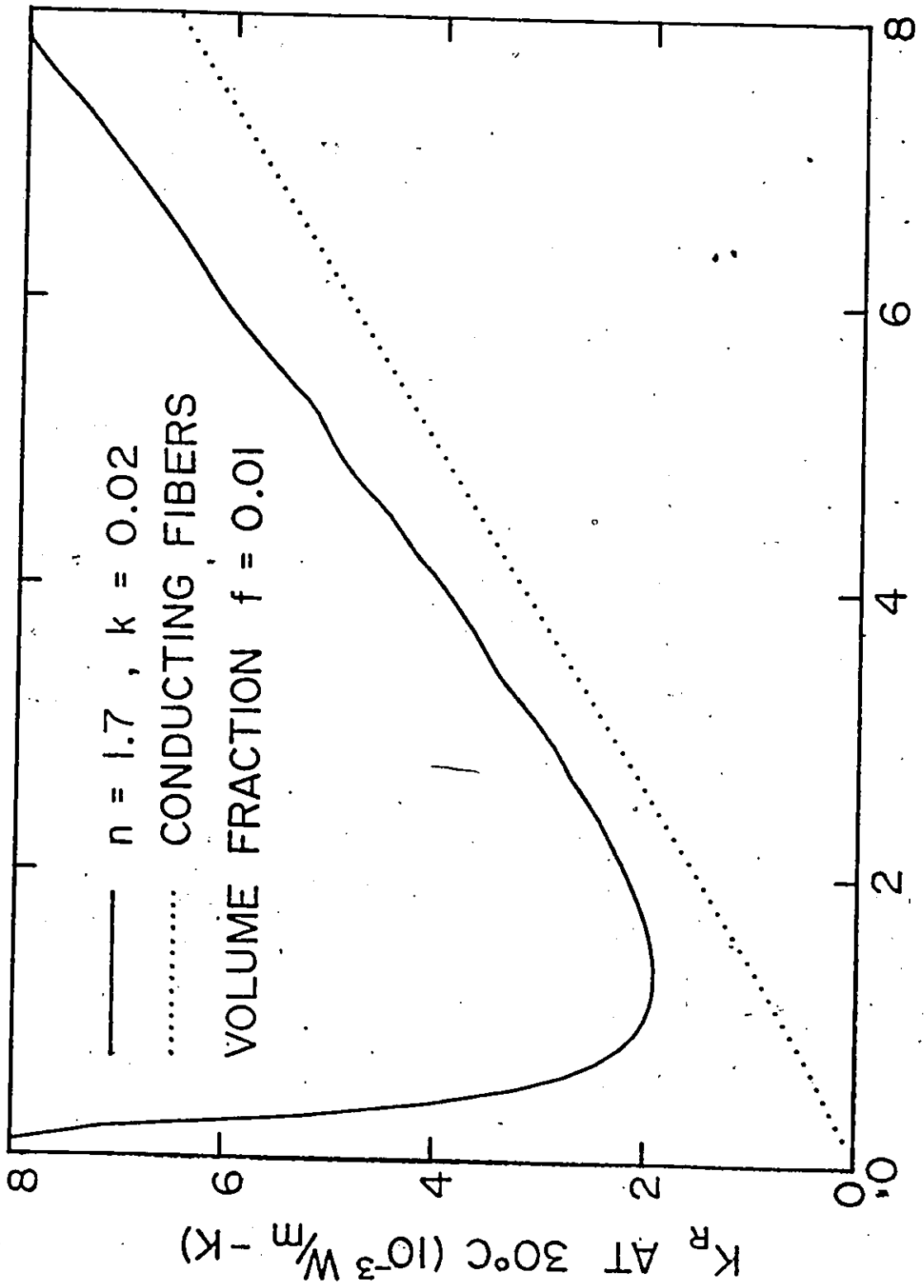
n = 1.7 , k = 0.02
CONDUCTING FIBERS
VOLUME FRACTION f = 0.01
K_R AT 30°C (10^{-3} W/m -K)
FIBER DIAMETER (μm)
0
2
4
6
8

$n = 1.7$, $k = 0.02$. The results shown are for a temperature of 30°C and a constant volume fraction $f = 0.01$, which means that the batting density is held constant.

At large diameters, K_R is approximately proportional to fibre size, with a slope corresponding to $Q_T \approx 0.65$. It has a minimum at about 1.5 μm diameter, and rises steeply below about 1 μm. This suggests that by reducing the fibre diameter, the weight of insulation required for a given level of performance could be increased by a factor of more than 10 (as compared to 25-μm fibres), all else being equal. In practice the reduction in mechanical stiffness of the fibres is a problem, but it is clear that no advantage at all is gained by adding fibres smaller than about 1.5 μm diameter to the batting.

Fig. 4-11 also shows the predicted K_R for a material composed of electrically conducting (infinite conductivity) fibres, which might in practice be represented by fibres with a metallic coating. In this case there is no increase in K_R at small diameter. The reason for this is shown in Fig. 4-12, which gives the total scattering Q_s^0 and the weighted scattering Q_s' (this is equal to Q_T if there is no absorption) for conducting fibres 12 μm in diameter, calculated from (3-18) and (3-19). At low frequencies both efficiencies diverge as $1/\nu$, due to TM scattering from longitudinal currents induced in the fibres. For a real material with a

Fig. 4-12

Total scattering Q_S^0 and weighted scattering Q_S' calculated for metallic fibres 12 μm in diameter.

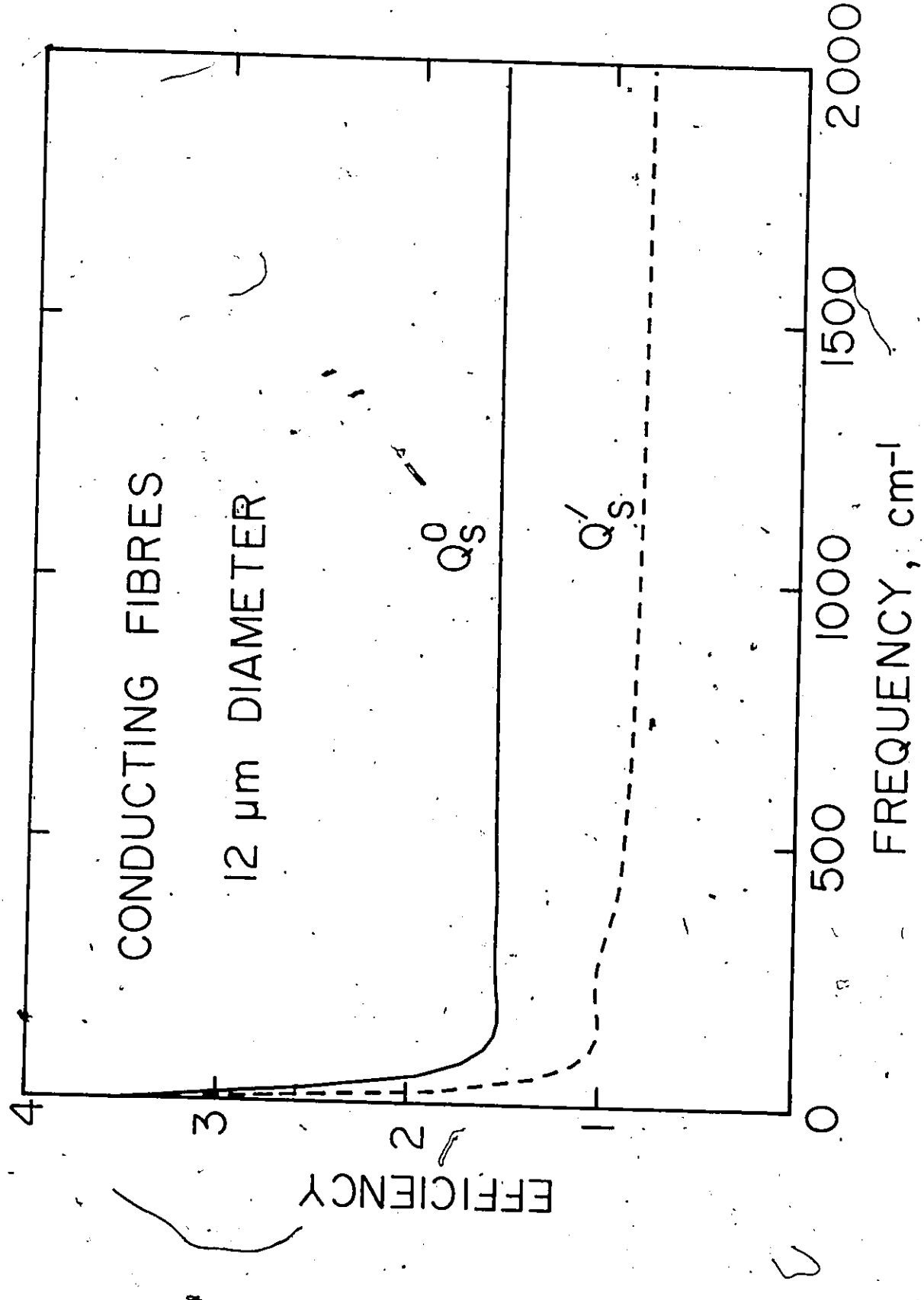
CONDUCTING FIBRES
12 μm DIAMETER
Q_s^0
Q_s'
EFFICIENCY
FREQUENCY, cm-1
0
500
1000
1500
2000
1
2
3
4

finite conductivity and finite fibre length this divergence would be removed. At high frequencies, Q_s' in Fig. 4-12 approaches the value $\pi/4 \approx 0.78$, and the K_R curve in Fig. 4-11 is essentially identical to the straight line generated by assuming a constant value $Q_T = 0.78$. The factor $\pi/4$ is just the average projection of the geometrical cross-section of the fibres onto the z-direction. It is easily shown that the scattering from randomly-oriented large reflecting cylinders (geometrical scattering only) is isotropic, and so $Q_s' = Q_s^0 = \pi/4$. In Fig. 4-12, Q_s^0 has twice this value, the extra scattering being the diffracted wave which fills the shadow behind the fibre (Van de Hulst, 1957). This scattering is close to the forward direction, and does not contribute significantly to Q_T. The 20% increase in Q_T, and consequent 20% reduction in K_R for conducting fibres as compared with dielectric fibres in Fig. 4-11 (for 23.4-μm fibres, K_R is reduced 16% from the value calculated for Polarguard) corresponds to about a 20% reduction in the radiative component of heat transport in reasonably thick batts with black boundary surfaces. A much greater reduction could result if reflective surfaces are used and the insulation is not too thick. Because the absorption cross-section is small, the coupling length p^{-1} (equation (2-55)) is long. In principle, the absorption of the metallic fibres could be calculated from the infrared optical parameters for

metals such as aluminum given by Bennett and Bennett (1966), but since n and k are ~ 50, the scattering coefficients would need to be calculated for high orders (higher than n = 100) which would require excessive computer time, and the Bessel function subroutines would have to be rewritten. In any case the results would not apply very well to real (i.e. somewhat dirty) surfaces. Values reported by Bennett and Bennett for reflectance of plane metallic surfaces suggest that 4% or so absorption is probably a reasonable estimate for Al-coated fibres, within a factor of 2. Very approximately, this would result in a five-fold increase in p^{-1} over the values for Polarguard shown in Table 4-2. Thus the interaction length for energy transfer between radiative and conductive modes would be about 8 mm for Al-coated Polarguard fibres at a density of 10.0 kg/m^3. At best, then, the reduction in radiative thermal transport due to coating the fibres and boundary walls with a reflecting material would be similar to the effect of adding 16% more material (because K_R is reduced 16%) plus an extra 150 g/m^2 (for the increased "boundary resistance" due to the reflective walls) providing the material is several optical depths thick. This is a substantial improvement, but by no means as dramatic as the effects of a large reduction in fibre radius.

In Fig. 4-13 we show Q_A and Q_T for randomly-oriented glass fibres of 6 μm radius (an approximate value for some

Fig. 4-13

Absorption and 'transport' efficiency Q_A and Q_T calculated for randomly oriented glass fibres of 12 µm diameter.

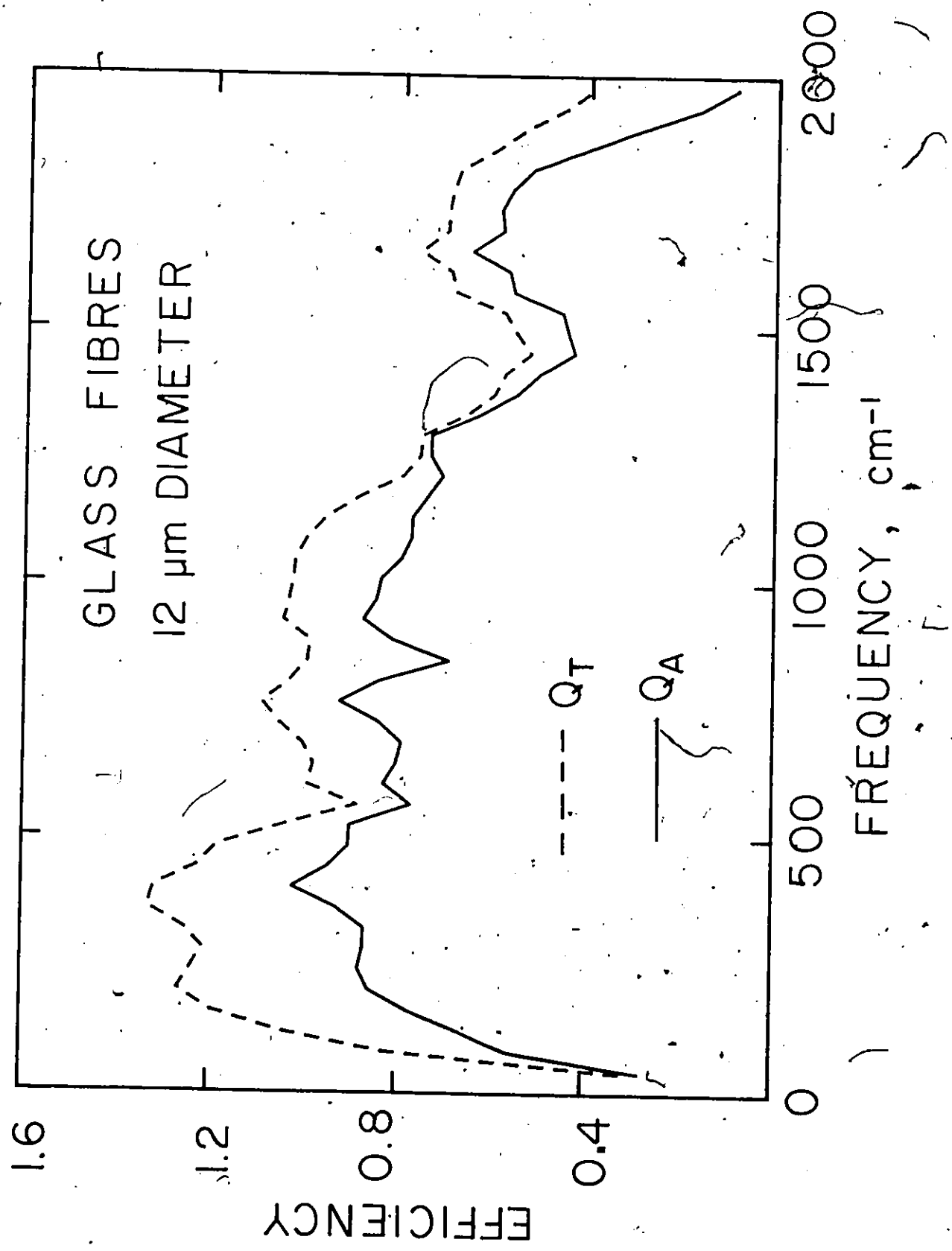
GLASS FIBRES
12 μm DIAMETER
Q_T
Q_A
EFFICIENCY
1.6
1.2
0.8
0.4
0
500
1000
1500
2000
FREQUENCY, cm⁻¹

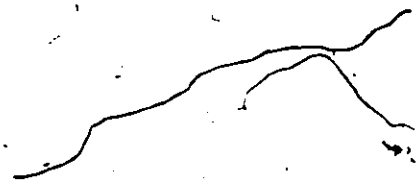

Fig. 4-14

Calculated radiative conductivity parameter K_R for glass fibres as a function of fibre diameter. The temperature is 300° C and the fibre volume fraction is f = 0.01.

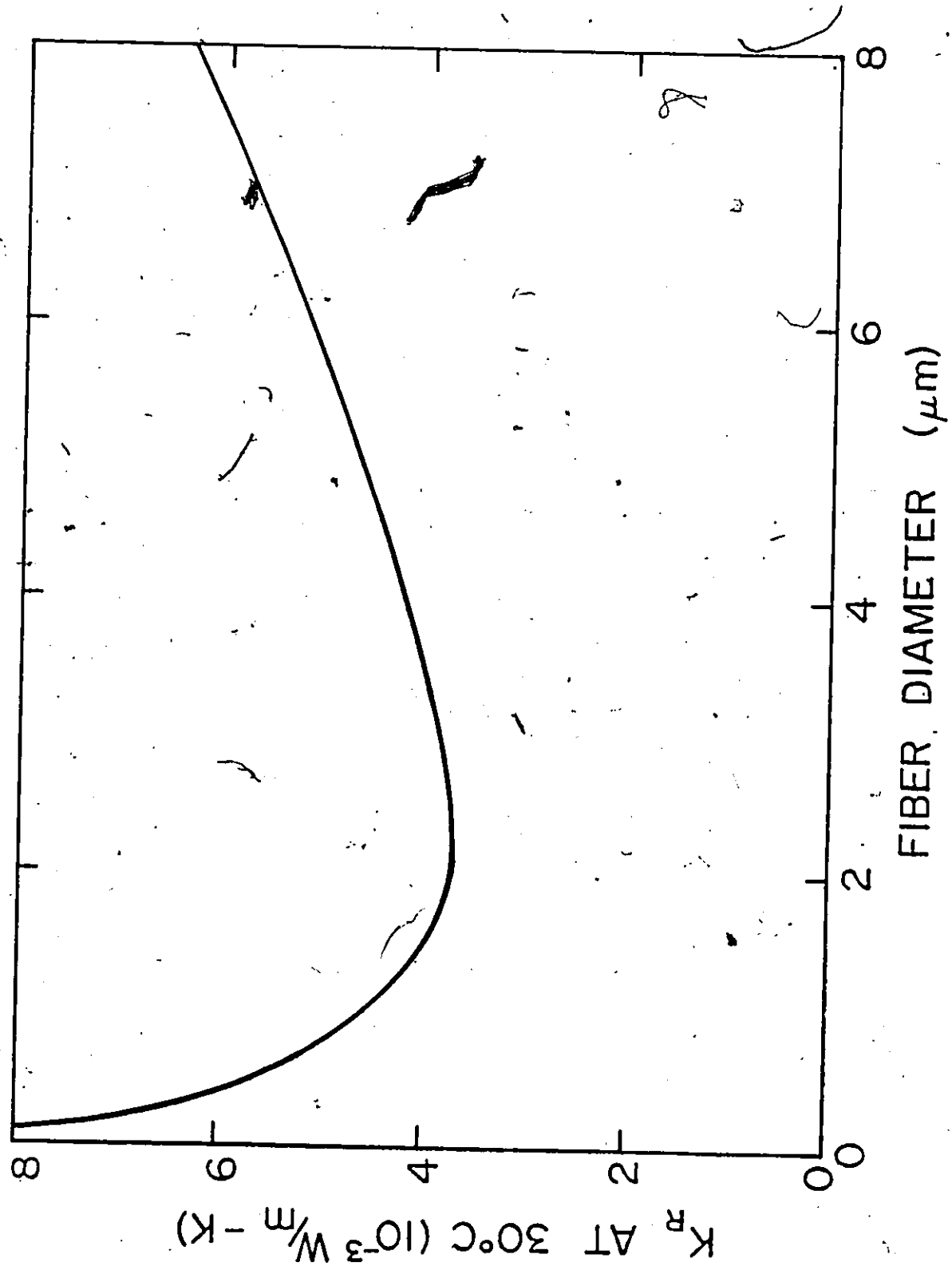
FIBER DIAMETER (μm)
0
2
4
6
8
K_R AT 30°C (10^{-3} W/m - K)
0
2
4
6
8

commercial low-density building insulation). The calculations used the n and k values for ordinary glass measured by Hsien and Su (1979). It is clear that absorption is the most important part (about 80%) of Q_T. In the absence of direct measurements of optical properties, it had often been assumed that scattering and not absorption was the dominant factor in radiative thermal transport in glass-fibre insulation (e.g. Shirtliffe, 1980). The predicted variation of K_R with fibre radius is shown in Fig. 4-14 for a nominal filling factor $f = 0.01$. We see behaviour similar to that shown in Fig. 4-11 for the dielectric fibres, although the minimum value of K_R is not as low in the case of glass fibres, and it occurs for fibre diameters of about 2 μm (at 30°C).

Similar calculations for glass fibre board (fibres randomly arranged in a plane) by Fricke et al. (1983) show very good agreement with thermal measurements on evacuated fibre insulation (Reiss and Ziegenbein, 1983). In ordinary building insulation the fibres are not of uniform diameter and the radiative portion of the heat transport is a smaller part of the total (~ 20%) than for Polarguard and Hollofil, so we have not made quantitative comparisons with thermal measurements for these materials.

CHAPTER 5

CONCLUSION

We have presented calculations of the infrared optical properties of polyester fibre insulation materials based on the properties of the bulk material from which the fibres are made. Comparison between the calculated absorption and extinction coefficients and direct measurements show reasonably good agreement over the frequency range 100 - 2000 cm^{-1}. Some discrepancies are noted for the material Hollofil, which is actually a collection of hollow tubes. The measured extinction cross-section shows behaviour similar to that reported in the literature for hollow cylinders at perpendicular incidence. The absorption cross-section of Polarguard shows some differences from the calculated cross-section which may be related to differences in the microscopic structure of the material in the fibre and the Mylar films from which the refractive index was obtained.

Both the scattering and absorption cross-sections were found to be reasonably large and strongly frequency-dependent. In addition the scattering was highly anisotropic, being strongly peaked in the forward direction. A diffusion model which could accomodate absorption and anisotropic scattering was used to model radiative heat transfer in the insulation. It was found that the combination of absorption and scattering

which was required as a parameter in the model varied much less dramatically with frequency than either the absorption or the scattering separately, which helped to justify replacing the frequency-dependent integrodifferential equations with frequency-averaged "grey" differential equations. The heat transport calculated from the model agreed very well with direct measurements of thermal resistance as a function of density and temperature for the polyester materials. Differences of about 10% in the case of Hollofil may again be related to the presence of the hole in the centre of the fibre.

The calculated thermal resistances were derived from the bulk properties of polyester and used no adjustable parameters. The close agreement with experiment should establish the adequacy of the diffusion, or P-1, approximation for thermal transport calculations in practical insulation materials. At the same time, it shows that models based on pure absorption, pure scattering, or isotropic scattering will not be accurate if correct optical parameters are used. Nor will the two-flux model give correct results for reasonably thick materials, although this depends on exactly how the model equations and parameters are defined, as explained in Chapter 2. At the same time, a qualitative discussion of the dependence of the heat transfer on the properties of the medium indicates that all these models can represent a wide

range of measurements if the parameter is fitted to thermal measurements rather than derived from specific optical properties.

Results for the "radiative conductivity" of two materials as a function of radius were presented in the last section of Chapter 4. For dielectric fibres there is a minimum in the radiative conductivity for a fibre size of one or two microns, depending on refractive index. The true optimum size would also include considerations of the mechanical stiffness of the fibres, but calculations of the type presented here are clearly useful for optimising insulation properties. It is shown that modest improvements could be obtained by giving the fibres a metallic coating, particularly if the boundaries were also reflective. A complete calculation of the heat transfer would depend critically on the reflectance of the metal surfaces. It should be possible to measure this using the nonresonant cavity, but a sample with surface area of a few cm^2 would be required. A rough estimate suggests an improvement of about 50% for a 270 g/m^2 batt with the characteristics of Polarguard, and less for thicker slabs.

There are several approximations in the solution which could be eliminated if more accuracy is needed. The simplest improvement is to replace the approximate analytic solution of the nonlinear radiation and conduction equations

with an exact numerical solution. This would certainly be desirable if the temperature difference across the material were much larger. Next in difficulty is an improvement in the treatment of the angular variation of the radiative intensity, particularly near the boundaries. Methods which rely on an expansion of the scattering function in Legendre polynomials should probable be avoided, or at least approached with care, as the phase function for randomly-oriented fibres has a divergence at $\theta = 0$. It may be possible to formulate the problem in terms of an expansion of the smoother quantity $2\pi\sin\theta Q_s(\theta)$ in appropriate functions. Most difficult to improve on is the approximation that the material is grey. Pomraning (1973) discusses methods of formulating the problem with several frequency groups. Unless this question is tackled, it is probably not very useful to put a great deal of effort into improving the other steps in the calculation.

REFERENCES

Abramowitz, M. and Stegun, I (1965), Handbook of Mathematical Functions, Dover, NY.

Aronson, J.R., Emslie, A.G., Ruccia, F.E., Smallman, C.R., Smith, E.M. and Strong, R.F. (1979), Applied Optics 18, 2622.

Bankvall, C. (1973) J. Test. and Eval. 1, 235.

Bennett, H.E. and Bennett, J.R. (1966), in Optical Properties and Electronic Structure of Metals and Alloys, edited by F. Abelès, North-Holland, Amsterdam.

Bergquam, J. and Seban, R. (1971), J. Heat Transfer 93, 236.

Bhattacharyya, R.K. (1980) in Thermal Insulation Performance, (ASTM STP 718) edited by D.L. McElroy and R.P. Tye, ASTM, Philadelphia, pp. 272-286.

Cabannes, F., Maurau, J-C, Hyrien, M. and Klarsfled, S.M. (1979), High Temperatures -High Pressures 11, 429.

R. Caps, A. Trunzer, D. Büttuer, J. Fricke and H. Reiss (1983) Presented at the 18th International Thermal Conductivity Conference, Rapid City, S. Dakota (to be published).

Chandrasekhar, S. (1960), Radiative Transfer, Dover, New York.

Davis, L. and Birkebak, R. (1973), J. Appl. Phys. 44, 4585.

Davis, L. and Birkebak, R. (1974), Biophys. J. 14, 249.

Evans, L., Chen, J., and Churchill, S. (1964), J. Opt. Soc. Am. 54, 1004.

Farnworth, B. (1983), Text. Res. J. 53, 717.

Farnworth, B., Crow, R. and Dewar, M. (1979), DREO Report #818, Defence Research Establishment, Ottawa.

Farone, W., Kerker, M. and Matijević, E. (1963) in Electromagnetic Scattering, edited by M. Kerker, McMillan, New York.

Hager, N. and Steere, R. (1967), J. Appl. Phys. 38, 4663.

Hefflinger, C. and Knox, K. (1971) in The Science and Technology of Polymer Films, edited by O.J. Sweeting, Wiley, New York, Vol. II, p. 599.

Hollingsworth, M. (1980) in Thermal Insulation Performance (ASTM STP 718) edited by D.L. McElroy and R.P. Tye, ASTM, Philadelphia, p. 255.

Hsien, C. and Su, K. (1979), Solar Energy 22, 37.

Jackson, J. (1975) Classical Electtrodynamics, 2nd. ed., Wiley, New York.

Kerker, M. (1969) The Scattering of Light and Other Electromagnetic Radiation, Academic Press, New York.

Kerker, M., Cooke, D., Farone, W., and Jacobsen, R. (1966) J. Opt. Soc. Am. 56, 487.

Kerker, M. and Matijević, E. (1961), J. Opt. Soc. Am. 51, 506.

Koenig, J. and Hannon, M. (1967), J. Macromol. Sci. (Phys.) B1, 119.

Larkin, B. and Churchill, S. (1959), A.I.Ch.E. Journal 5, 467.

Liou, K-N. (1972) Appl. Optics 11, 667.

Llewellyn-Jones, D., Knight, R., Moffat, P. and Gebbie, H. (1980) IEE Proc. A. 127, 535.

McKay, N., Timusk, T. and Farnworth, B. (1983), presented at the 18th International Thermal Conductivity Conference, Rapid City, South Dakota (to be published).

McKay, N., Timusk, T. and Farnworth, B. (1984), J. Appl. Phys. 55, 4064.

Modest, M. and Azad, F. (1980a), J. Heat Transfer 102, 92.

Modest, M. and Azad, F. (1980b), J. Quant. Spectrosc. Radiat. Transfer 23, 117.

Moss, T.S., (1959), Optical Properties of Superconductors, Butterworths, London.

Pomraning, G. (1973), The Equations of Radiation Hydrodynamics, Pergamon Press, Toronto.

Lord Rayleigh (1918), Phil. Mag. 36, 365.

Reiss, H. and Ziegenbein, B. (1983), presented at the 18th International Thermal Conductivity Conference, Rapid City, South Dakota (to be published).

Samaddar, S.N. (170), Nuovo Cimento 66B, 33.

Shuetz, M. (1982), M.Sc. Thesis, M.I.T., Cambridge, Mass.

Shirtliffe, C. (1980) in Thermal Insulation Performance, eds. D.L. McElroy and R.P. Tye, ASTM, Philadelphia.

Shokair, I. and Pomraning, G. (1981), J. Quant. Spectros. Radiat. Transfer 25, 325.

Steere, R.C. (1966), J. Appl. Phys. 37, 3338.

Stratton, J. (1941), Electromagnetic Theory, McGraw Hill, New York.

Van de Hulst, H.C. (1949), Physica 15, 740.

Van de Hulst, H.C. (1957), Light Scattering by Small Particles, Wiley, New York.

Verschoor, J. and Greebler, P. (1952), Trans. ASME 74, 961.

Viskanta, R. (1965), J. Heat Transfer 87, 143.

Wait, J.R. (1955), Can. J. Phys. 33, 189.

Yuen, W. and Tien, C. (1980), J. Heat Transfer 102, 86.

Yuen, W. and Wong, L. (1980), J. Heat Transfer 102, 303.

APPENDIX 1

HEAT-FLOW PROGRAM

```
C
C                    Subroutine HEAT
C
C
C       Returns total heat flux in watts/square meter, given
C     batt density, fibre bulk density, thermal conductivity of air
C     and polyester, transport and absorption mean opacities,
C     thickness, Celsius temperatures at the boundaries, and
C     emissivities at the boundaries. All parameters are in MKS.
C
C     Inputs :
C            RHOB     - density (kg/m3) of batting
C            RHOF     - density of bulk fibre material
C            KAIR     - Thermal conductivity of air
C            KPOLY    - conductivity of fibre material
C            KAPT     - transport mean opacity, kappa-T
C            KAPA     - mean absorption kappa-A
C            Z        - thickness of batt
C            TC,TH    - Celsius temperatures at walls
C            EPC,EPH  - emissivities of walls
C
C     Outputs:
C            H        - heat flux in W/sq m
C            /PHEAT/  - common block containing the following
C                       output parameters:
C            P        - "interaction" coefficient p
C            ALPH0    - these are the coefficients of the solution
C            ALPH1    - for the temperature T(x), called C0 - C3
C            ALPH2    - in the text.
C            ALPH3    -   T = a0 +a1x +a2 exp(-x)+ a3 exp(Z-x)
C            KCON     - conductivity of air + fibres
C            KRAD     - "radiative conductivity" :
C
C
      SUBROUTINE HEAT(RHOB,RHOF,KAIR,KPOLY,KAPT,KAPA,Z,TC,TH,
     +  EPC,EPH,H)
      REAL KAIR,KPOLY,KAPT,KAPA,KCON,KRAD
      COMMON/PHEAT/P,ALPH0,ALPH1,ALPH2,ALPH3,KCON,KRAD
      DATA SIGMA/5.6696E-8/
      TKC=TC+273.15
      TKH=TH+273.15
      T0=.5*(TKC+TKH)
      DELT=TKH-TKC
C
      GAMF=RHOB*(KPOLY+5.*KAIR)/(RHOF*3.*(KPOLY+KAIR))
      KCON=(1.-GAMF)*KAIR+GAMF*KPOLY
```

```
C
C  This is the conductive part for air + randomly-oriented fibres
C
      KRAD=16.*SIGMA*TO**3/(3.*RHOB*KAPT)
      P=SQRT(16.*SIGMA*RHOB*KAPA*TO**3/KCON+3.*RHOB**2*KAPA*KAPT)
      C=1.5*RHOB*KAPT
      A=EPC/(2.-EPC)
      DC=A*2.*SIGMA*(TKC**4-TO**4)
      EC=C*A
      A=EPH/(2.-EPH)
      DH=A*2.*SIGMA*(TKH**4-TO**4)
      EH=C*A
      XPZ=EXP(-P*Z)
      R1=1./Z
      IF(P.GT.1.E-15) R1=P/(1.-XPZ)
      C3=DH+.5*DELT*KCON*(EH+R1*(1.+XPZ))
      C4=DC-.5*DELT*KCON*(EC+R1*(1.+XPZ))
      A3=KRAD*EH+KCON*(EH+P*(1.-XPZ)/(1.+XPZ))
      A4=KRAD*EC+KCON*(EC+P*(1.-XPZ)/(1.+XPZ))
      B3=-(KRAD+2.*R1*Z*KCON*XPZ/(1.+XPZ))
      B4=KRAD+EC*Z*(KRAD+KCON)+R1*Z*KCON*(1.+XPZ**2)/(1.+XPZ)
C
      DET=A3*B4-A4*B3
      ALPH0=(C3*B4-C4*B3)/DET
      ALPH1=(C4*A3-C3*A4)/DET
C
      ALPH2=0.
      ALPH3=0.
      IF(P.LE.1.E-15) GO TO 1
      ALPH2=.5*DELT/(1.-XPZ)-ALPH0/(1.+XPZ)+ALPH1*Z/(1./XPZ-XPZ)
      ALPH3=-(.5*DELT/(1.-XPZ)+ALPH0/(1.+XPZ)+Z*ALPH1/(1.-XPZ**2))
C
1     H=-ALPH1*(KRAD+KCON)
      ALPH0=ALPH0+TO-273.15    ! Gives starting point in Celsius
      RETURN
      END
```

APPENDIX 2

PROGRAMS FOR RANDOMLY ORIENTED FIBRES

```
C
C                          Program FIBRE
C
C       This is the program that calculates the extinction
C     and total scattering cross-sections, the (1-cos theta)
C     weighted scattering, and the differential cross-section as a
C     function of angle for 64 scattering angles. The normalisation
C     is arranged so that the total scattering is just the sum of
C     the values for individual angles (do not divide by 64 or
C     multiply by sin theta).
C
C     Inputs : the program calls a routine SFIBR which fills the
C              COMMON block /SPAR/ with the following parameters:
C
C     KFMIN  - first frequency point to use.
C     KFMAX  - last   "       "    "  "
C     AZERO  - scattering parameter alpha (2pi x radius/wavelength)
C              at first frequency point
C     DA     - increment in alpha between successive frequencies
C     EN, CAY - real arrays containing refractive index n-ik at
C              512 equally-spaced frequencies.
C
C
C     Outputs: When the program is finished, the array SAVG contains
C              the efficiencies for extinction, total scattering, and
C              (1 - cos theta)-weighted scattering for each of up to
C              511 points (the 512th frequency may not be used).
C              The array SCAT contains the differential scattering
C              efficiency times (64/pi)x(2pi sin theta) for each of
C              64equally-spaced scattering angles pi/128, 3pi/128,
C              ..., 127pi/128.
C
C
      COMPLEX RFRAC
      VIRTUAL DSPH(64,64),SAVG(3,511),SCAT(64,511)
      COMMON/SPAR/KFMIN,KFMAX,AZERO,DA,EN(512),CAY(512)
      COMMON/ASVBL/K12
      DIMENSION FCOEF(82)
      DATA PI/3.1415926535/
      DTHET=PI/256.
      CALL SFIBR        ! Fills /SPAR/ and opens output file (12)
      CALL SFILL        ! Initialisation for FILL
      FCTR=DTHET/1.5    ! The Simpson's rule factor h/3; DTHET=pi/256
      JMAX=5
            DO 1 KF=KFMIN,KFMAX      ! Set output arrays to zero
            SAVG(1,KF)=0.
            SAVG(2,KF)=0.
```

```
            SAVG(3,KF)=0.
                    DO 1 N=1,64
1                   SCAT(N,KF)=0.
C
C   Now the real calculations begin. The outer loop runs through
C   fibre angles, and the inner loop through frequencies.
C
        DO 20 I=1,128
        MXBIN=1+(I-1)/2          ! Max bin # of scattered radiation
        THETA=FLOAT(I)*DTHET
        SNTH=SIN(THETA)
        FACT=FCTR*SNTH           ! For the total scattering integral
        IF(MOD(I,2).EQ.1) FACT=2.*FACT  ! Double weight on even pts
        IF(I.EQ.128) FACT=.5*FACT       ! Half weight for endpoint
        FACT2=FACT*SNTH**2       ! for the (1-cos) weighted average
        FACT3=FACT/PI            ! To normalise the bins: *2 for other
C                       half of integral; /2pi from defn. in INTNS
C
        CALL FILL(THETA,0,JMAX,DSPH)     ! Fills DSPH
        JMAX=0                   ! will be highest JMAX required by INTNS
C
        DO 18 KF=KFMIN,KFMAX
        RFRAC=CMPLX(EN(KF),-AMAX1(CAY(KF),0.))
        ALPHA=AZERO+FLOAT(KF-1)*DA
        CALL INTNS(ALPHA,THETA,RFRAC,32,JNEW,XTNCN,FCOEF)
        JNEW=MIN0(JNEW,63)               ! These statements check
        IMAX=MAX0(IMAX,JNEW)             ! to see if more
        IF(JNEW.LE.JMAX) GO TO 9         ! coefficients are
        JMIN=JMAX+1                      ! needed, and update
        JMAX=JNEW                        ! JMAX and DSPH if
        CALL FILL(THETA,JMIN,JMAX,DSPH)  ! required.
C
9       SAVG(1,KF)=SAVG(1,KF)+XTNCN*FACT
        SAVG(2,KF)=SAVG(2,KF)+FCOEF(1)*FACT
        SAVG(3,KF)=SAVG(3,KF)+(FCOEF(1)-.5*FCOEF(2))*FACT2
C The integral of 1 is 2pi, and of cos(phi)**2 is pi
C
                DO 11 KBIN=1,MXBIN
                XSCAT=0.
                        DO 10 J=1,JNEW
                        XSCAT=XSCAT+FCOEF(J)*DSPH(J,KBIN)
10                      CONTINUE
11                      SCAT(KBIN,KF)=SCAT(KBIN,KF)+XSCAT*FACT3
        IF(MOD(KF,5).EQ.1) TYPE 200,I,KF,JNEW
18      CONTINUE
20      CONTINUE
C
C       Now the arrays are ready for output.
C
        DO 30 KR=KFMIN,KFMAX             !Rewrite output file
```

```
      KF=KR
30    WRITE(12'KF) (SAVG(N,KF),N=1,3),(SCAT(N,KF),N=1,64)
C
      CLOSE(UNIT=12)
      STOP ' Finished at last.'
200   FORMAT('+  Angle #',I4,' of 128, frequency #',I4,I6,
     + ' coefficients')
      END
C
C     ********************************************************
C
C                     Subroutine FILL
C
C           This subroutine fills the array DSPH with the values
C     of delta(sin kphi) for each interval of scattering angle and
C     all values of k up to KMAX, for the fibre angle specified.
C
      SUBROUTINE FILL(THETA,KMIN,KMAX,DSPH)
      VIRTUAL DSPH(64,64)      ! (KMAX, number of bins)
      COMMON/SBINS/SNB(64),CKI(64)     ! Filled by SFILL
      DIMENSION SKOLD(64),PHI(64)
      DATA PI,DTHET/3.1415926536,2.4543692606E-2/
C
      K1=KMIN
      IF(K1.GT.0) GO TO 2
      IMX=INT(THETA/DTHET-.00
      IMAX=IMX+1
      IF(IMX.LE.0) GO TO 6
      SINV=1./SIN(THETA)
      OLDPH=0.
            DO 1 I=1,IMX
            SHPH=SINV*SNB(I)
            PHNEW=2.*ATAN(SHPH/SQRT(1.-SHPH**2))
            PHI(I)=PHNEW
            DSPH(1,I)=PHNEW-OLDPH
1           OLDPH=PHNEW
      DSPH(1,IMAX)=PI-OLDPH
      K1=1
2     IF(IMAX.LE.1) RETURN
      DO 3 K=K1+1,KMAX+1
3     SKOLD(K)=0.
            DO 4 I=1,IMX
            PH=PHI(I)
                  DO 4 K=K1+1,KMAX+1
                  SKPH=SIN(PH*FLOAT(K-1))
                  DSPH(K,I)=(SKPH-SKOLD(K))*CKI(K)
                  SKOLD(K)=SKPH
4                 CONTINUE
            DO 5 K=K1+1,KMAX+1
            DSPH(K,IMAX)=-SKOLD(K)*CKI(K)
```

```
5               CONTINUE
        RETURN
6       DSPH(1,1)=PI            ! All scattering is into first bin
                DO 7 K=2,64
7               DSPH(K,1)=0.
        RETURN
        END

C ***********************************************************
C
C                       Subroutine SFILL
C
C               Fills constant arrays for FILL.
C
        SUBROUTINE SFILL
        COMMON/SBINS/SNB(64),CKI(64)
        DATA PI,DTHET/3.14159265536,2.4543692606E-2/
C
        CKINV=1.
              DO 1 K=1,64
              CKI(K)=CKINV
              CK=FLOAT(K)
              SNB(K)=SIN(CK*DTHET)
   1          CKINV=1./CK
        RETURN
        END
```

APPENDIX 3

SCATTERING COEFFICIENT AND BESSEL FUNCTION PROGRAMS

```
C                    Subroutine SYL
C
C  Returns complex scattering coefficients AN1,AN2,BN1 for a cylinder
C  of complex refractive index M ,with axis at angle THET to the
C  incident direction.
C
C       ALFA     - 2*pi*radius/wavelength.
C       NMAX     - highest order desired (first coefficient has
C                  order 0 ).
C       NUM      - highest order calculated. NUM is at least 2
C                  unless NMAX is smaller. Coefficients of higher
C                  order are estimated to be small by a factor of
C                  1E-8 and are set to 0.
C
C  AN1, etc. must have length at least (2,NMAX+1).
C  If ALFA*sin(THET)<1E-10, routine gives NUM=0 and fills arrays
C  with zeroes.
C
C
      SUBROUTINE SYL(ALFA,THET,M,NMAX,NUM,AN1,AN2,BN1)
      DIMENSION BJ(75),WY(50)
      COMPLEX AN1(1),AN2(1),BN1(1),CJ(75)
      COMPLEX M,MINV,AJ,HP,H1,RANK,JN,JN1,JNP,DELTA,GAM
      COMPLEX C1,C2,C3,C4,C5,C6,D1,D2,D3,CINV
      STIR(DEL,TWOEN)=(TWOEN/3.14/DEL)**(1./TWOEN)*TWOEN/2.718
C     APPROXIMATE ARGUMENT TO GIVE DELTA=DEL
      BETA=SIN(THET)
      AL=ALFA*BETA
      IF(AL.GE.1.E-10) GO TO 10
      NUM=0
      GO TO 6
   10 AJ=M*M-COS(THET)**2
      GAM=CSQRT(AJ)
      AJ=ALFA*GAM
      NUM=NMAX
      IF(NUM.LE.2) GO TO 2
      DO 1  I=2,NMAX
      TWOEN=FLOAT(2*I-2)
      NUM=I
      IF(AL.LE.STIR(1.E8,TWOEN)) GO TO 2
    1 CONTINUE
    2 CALL NEUMR(AL,NUM,NY,BJ,WY)
      IF(NY.LT.NUM) NUM=NY
      CALL BESSC(AJ,NUM,CJ)
```

```
      HANK=CMPLX(-BJ(2),WY(2))
      JN=-CJ(2)
      MINV=1./M
      B1=BETA/ALFA
      C1=B1*GAM**4*MINV
      C2=BETA**2*MINV*GAM**4
      C3=B1**2*(M**3-MINV*COS(THET)**2)
      C4=(BETA*GAM)**3
      C5=BETA**4*M*GAM**2
      C6=2.*COS(THET)/3.1415927/ALFA**2*(M-MINV)*GAM**2
        DO 5 N=0,NUM
        I=N+1
        EN=FLOAT(N)
        H1=HANK
        JN1=JN
        HANK=CMPLX(BJ(I),-WY(I))
        JN=CJ(I)
        HP=H1-HANK*(EN/AL)
        JNP=JN1-JN*EN*CINV(AJ)
        BJL=REAL(HANK)
        BJLP=REAL(HP)
        BJL1=REAL(H1)
        D1=JN*JN
        D2=JN*JNP
        D3=JNP*JNP
        DELTA=D1*(2.*EN*C1*HANK*H1-C2*H1*H1-C3*(EN*HANK)**2)
     +  +C4*D2*(M+MINV)*HANK*HP-D3*C5*HANK*HANK
        DELTA=CINV(DELTA)
        AN1(I)=EN*D1*C6*DELTA
        D1=D1*(EN*C1*(BJL*H1+BJL1*HANK)-C2*H1*BJL1-C3*EN*EN*HANK*BJL)
     +  -D3*C5*HANK*BJL
        AN2(I)=(D1+D2*C4*(M*HANK*BJLP+MINV*HP*BJL))*DELTA
        BN1(I)=(D1+D2*C4*(MINV*HANK*BJLP+M*HP*BJL))*DELTA
    5   CONTINUE
    6 IF(NUM.EQ.NMAX) RETURN
      N1=NUM+2
      N2=NMAX+1
      DO 7 I=N1,N2
      AN1(I)=CMPLX(0.,0.)
      AN2(I)=CMPLX(0.,0.)
    7 BN1(I)=CMPLX(0.,0.)
      RETURN
      END
C
C
C*************************************************************************
C
C
C   SYL (alternate)
C         Alternative version of SYL to calculate scattering
```

```
C       coefficients
C       for perfectly-conducting infinite cylinders. .
C
        SUBROUTINE SYL(ALPHA,THETA,M,NMAX,NUM,AN1,AN2,BN1)
        COMPLEX M,AN1(1),AN2(1),BN1(1)
        COMPLEX HANK,HANKP,CINV
        DIMENSION BJ(50),Y(50)
                DO 1 N=1,NMAX+1
                AN1(N)=(0.,0.)
                AN2(N)=(0.,0.)
1               BN1(N)=(0.,0.)
        X=ALPHA*SIN(THETA)
        XINV=1./X
        CALL NEUMR(X,NMAX,NUM,BJ,Y)
        YTOP=1.E38*AMIN1(1.5,ABS(X)/FLOAT(NUM)) ! Limit of Y
        BJ1=-BJ(2)                              !in YP calc.
        Y1=-Y(2)
                DO 2 N=1,NUM+1
                BJ2=BJ(N)
                Y2=Y(N)
                ENX=FLOAT(N-1)*XINV
                BJP=BJ1-ENX*BJ2
                BN1(N)=CMPLX(BJ2,0.)*CINV(CMPLX(BJ2,-Y2))
                BJ1=BJ2
                IF(ABS(Y2).GT.YTOP) GO TO 2     ! (to avoid overflow)
                YP=Y1-ENX*Y2
                AN2(N)=CMPLX(BJP,0.)*CINV(CMPLX(BJP,-YP))
2               Y1=Y2
        RETURN
        END
C
C  ********************************************************************
C
C               Subroutine BESSC
C
C     Routine to generate integer-order Bessel functions of the
C     first kind for complex arguments.
C
C     Usage: CALL BESSC(Z,NMAX,BJ)
C
C       Z    - complex variable containing argument
C       NMAX - maximum order desired
C       BJ   - complex array of length at least NMAX+1 complex
C              variable swhich on output contains the NMAX+1 complex
C              values of the Bessel functions of order 0 through NMAX
C
C           The method is essentially that of Abramowitz and Stegun,
C       described in their "Handbook of Mathematical Functions". It
C       uses a downward recursion with arbitrary starting values. The
C       functions are normalised using a sum rule.
```

```
C
C       The routine has been tested, but not exhaustively. Error
C     is largely due to roundoff, and is higher if the argument is
C     large and the order small, which means that the recursion has
C     been carried through many oscillations of the function.
C     Nevertheless, accuracy is generally 6 digits or better for
C     arguments up to 50, except near zeroes of the functions. It
C     is possible that this does not hold for all directions in the
C     complex plane.
C
C          Use BESSR (below) to calculate Bessel functions of real
C     arguments. NEUMR is used to calculate simultaneously Bessel
C     functions of the first and second kinds, for real arguments.
C     (Bessel functions of the second kind are called Neumann
C     functions).
C
      SUBROUTINE BESSC(Z,NMAX,BJ)
      COMPLEX Z,ZINV,BJ(1),SUM,ZA,ZB,ZC,CINV
      IF(NMAX.LT.0) STOP'   BESSC: negative order'
      ZAB=CABS(Z)
      NMP=NMAX+1
      IF(ZAB.GT.1.E-5) GO TO 2
      EN=1.                        ! If mod(z)<1E-5 ,the functions
      ZA=(1.,0.)                   ! are approximated by the leading
      ZB=.5*Z                      ! term in the series expansion,
        DO 1 N=1,NMP               ! which is accurate within a factor
        BJ(N)=ZA                   ! of about Z**2.
        ZA=ZA*ZB/EN
    1   EN=EN+1.
      RETURN
C
C     Downward recursion to get Bessel functions
C
    2 CALL STBESR(ZAB,NMAX,NST,NORM)     ! Returns NST and NORM
      IF(NMAX.LE.NST) GO TO 4
        DO 3 N=NST,NMP             ! These functions are less than about
    3   BJ(N)=(0.,0.)              ! 1E-40 in magnitude, and are set to
      NMP=NST-1                    ! zero.
C
C       Set starting values
C
    4 ZINV=2.*CINV(Z)
      EN=FLOAT(NST)
      ZA=(1.E-28,1.E-29)           ! Starting values for the recursion
      ZB=(0.,0.)                   ! are chosen as small as possible
      SUM=ZB                       ! while avoiding underflow when the
C                                  ! functions are normalised.
C     Begin the recursion
C
        DO 5 N=NST,2,-2
```

```
      IF(N.LE.NORM) SUM=SUM+ZA          ! Increment SUM unless ZA
C                                         is small
        DO 5 I=0,1
        ZC=EN*ZINV*ZA-ZB          ! This is the recusion equation
        IF(N-1.LE.NMP) BJ(N-I)=ZC       ! Store the function if the
        ZB=ZA                           ! order is less than NMAX+1
        ZA=ZC
5     EN=EN-1.

      SUM=CINV(SUM+SUM+ZA)              ! The normalisation factor
        DO 6 N=1,NMP
6     BJ(N)=BJ(N)*SUM                   ! Normalise the functions
      RETURN
      END
C
C*************************************************************
C
C               Subroutine BESSR
C
C     Routine to generate integer-order Bessel functions for real
C     arguments.
C     X     - Argument of function
C     NMAX  - Highest order desired
C     BJ    - Array of dimension at least NMAX+1 which contains Bessel
C             functions on output, starting at order 0 in BJ(1).
C
C               The method is the same as used in BESSC above.
C
      SUBROUTINE BESSR(X,NMAX,BJ)
      DIMENSION BJ(1)
      IF(NMAX.LT.0) STOP'   BESSR: NEGATIVE ORDER'
      NMP=NMAX+1
      IF(ABS(X).GT.1.E-5) GO TO 2
      BJ(1)=1.
      EN=1.
      XEN=.5*X
      HAF=XEN
        DO 1 I=2,NMP
        BJ(I)=XEN
        EN=EN+1.
1     XEN=XEN*HAF/EN
      RETURN
C
C     Get Bessel functions by downward recursion
C
2     CALL STBESR(ABS(X),NMAX,NST,NORM)
      IF(NMAX.LE.NST) GO TO 4
        DO 3 N=NST,NMP
3     BJ(N)=0.
      NMP=NST-1
```

```
    4 XINV=2./X
      EN=FLOAT(NST)
      BJN=1.E-36
      BJP=0.
      SUM=0.
        DO 5 N=NST,2,-2
        IF(N.LE.NORM) SUM=SUM+BJN
          DO 5 I=0,1
          TEM=EN*XINV*BJN-BJP
          IF(N-I.LE.NMP) BJ(N-I)=TEM
          BJP=BJN
          BJN=TEM
    5     EN=EN-1.
      SUMI=1./(SUM+SUM+BJN)
C
C     Normalise
C
        DO 6 N=1,NMP
    6   BJ(N)=BJ(N)*SUMI
      RETURN
      END
C
C ***************************************************************
C
C   NEUMR
C
C     Routine to generate Bessel functions and Neumann functions for
C     real arguments.
C     Usage: CALL NEUMR(X,NMAX,NY,BJ,Y)
C       X    - argument
C       NMAX - maximum order desired
C       NY   - highest order calculated; may be less than NMAX to
C              avoid floating-point overflow. Remainder of arrays
C              set to zero.
C       BJ   - output and work array of length at least NMAX+1 real
C              variables. On output it contains the NMAX+1 values of
C              Bessel functions (of the first kind) of order 0 to NMAX
C       Y    - array of length NMAX+1 which contains the Neumann
C              functions (Bessel functions of the second kind) on
C              output.
C
      SUBROUTINE NEUMR(X,NMAX,NY,BJ,Y)
      DIMENSION BJ(1),Y(1)
      IF(NMAX.LT.0) STOP'    NEUMR: NEGATIVE ORDER'
      IF(X.LE.0.) STOP'    NEUMR: NEGATIVE OR ZERO ARGUMENT'
      NMP=NMAX+1
      XINV=2./X
      IF(X.GT.1.E-5) GO TO 2
      BJ(1)=1.
      EN=1.
```

```
      XEN=.5*X
      HAF=XEN
      NY=1
C
      DO 1 N=2,NMP
      IF(XEN.NE.0.) NY=N
      BJ(N)=XEN
      EN=EN+1.
      XEN=XEN*HAF/EN
1     CONTINUE
C
      SO=BJ(3)
      S1=1.5*BJ(4)
      SUM=1.
      BJN=BJ(1)
      BJP=BJ(2)
      GO TO 8
C
C     Get Bessel functions by recursion
C
2     CALL STBESR(X,NMAX,NST,NORM)
      BJN=1.E-36
      BJP=0.
      SUM=0.
      SO=0.
      S1=0.
      IF(NMAX.LE.NST) GO TO 4
C
      DO 3 N=NST,NMP
      BJ(N)=0.
3     Y(N)=0.
C
      NMP=NST-1
C
4     DO 6 N=NST,2,-2
      IF(N.GT.NORM) GO TO 5
      IF(MOD(N,4).EQ.0) SGN=-1.        ! For n=4,8,12,...
      IF(MOD(N,4).NE.0) SGN=1.         ! For n=2,6,10,...
      SUM=SUM+BJN
      SO=SO+BJN*SGN*2./FLOAT(N)
      S1=S1+BJP*SGN*FLOAT(4*N+4)/FLOAT(N*N)
5           DO 6 I=0,1
            TEM=FLOAT(N-I)*XINV*BJN-BJP
            IF(N-I.LE.NMP) BJ(N-I)=TEM
            BJP=BJN
6           BJN=TEM
C
      SUMI=1./(2.*SUM+BJN)
      DO 7 N=1,NMP
      BJ(N)=BJ(N)*SUMI
```

```
      IF(BJ(N).NE.0.) NY=N
7     CONTINUE
C
C     Get the zero- and first-order Neumann functions to start
C     the recursion.
C
8       TEM=ALOG(X)-.115931517
        Y(1)=.6366197724*SUMI*(TEM*BJN+2.*SO)
        Y(2)=.6366197724*SUMI*((TEM-1.)*BJP-BJN/X+S1)
C
C     Get the remaining Neumann functions by recursion
C
        IF(NY.LT.3) GO TO 10
        DO 9 N=3,NY
9       Y(N)=FLOAT(N-2)*XINV*Y(N-1)-Y(N-2)
C
10      IF(NY.GE.NMP) GO TO 12
        DO 11 N=NY+1,NMP
11      Y(N)=0.
12      NY=NY-1
        RETURN
        END
C
C ***************************************************************
C
C   STBESR.
C     Routine to get the starting value of N for BESSR, designed to
C     avoid overflow in the recursion. Also generates the order NORM
C     to which the normalisation sums must be carried.
C
C       X       = The modulus or absolute value of the argument
C       NMAX    = The maximum order of Bessel function desired
C       NST     = on output, starting order for the recursion
C       NORM    = on output, maximum order for the normalisation sum
C
C          NST is calculated to give at least 6 digits of accuracy in
C       the highest-order Bessel function calculated. If NMAX and X
C       are such that J(NMAX) will be smaller than the smallest
C       floating-point number (10**-38 or so) NST may be less than
C       NMAX, and the calling program must set the corresponding
C       J-functions to zero.
C          NORM is set so that functions of higher order will
C       contribute less than 10**-8 to the normalisation sum.
C
C             The method uses asymptotic expansions of J for real
C       arguments along with Stirling's approximation of the
C       factorial.
C
C
      SUBROUTINE STBESR(X,NMAX,NST,NORM)
```

```
C
      IF(X.GT.2.) GO TO 1
      NORM=6+INT(6.*X)
      GO TO 2
    1 NORM=15+INT(1.5*X)          ! Empirical formula
    2 NORM=NORM+MOD(NORM,2)       ! Ensure NORM is even
C
      EN=FLOAT(MAXO(NMAX,2))
      TST=ALOG(X*1.3591409/EN)
      TSTN=TST*EN
      IF(TSTN.LT.-10.) GO TO 3
C
C   J(NMAX) is larger than 1E-5.
C
      NST=NORM
      RETURN
    3 IF(TSTN.LT.-100) GO TO 4
C
C   Get NST by requiring J(NST)/J(NMAX) to be less than 1E-5
C
      NST=INT(12./(1.-TST))+NMAX+1
      NST=NST+MOD(NST,2)
      NST=MAXO(NST,NORM)
      RETURN
C
C   J(NMAX) is smaller than 1E-44. Find (by Newton-Raphson) NST
C    such that J(NST) is between 1E-44 and 1E-56 or so.
C
    4   DO 5 K=1,5
        NST=NMAX+INT((100.+TSTN)/(1.-TST))
        EN=FLOAT(NST)
        TST=ALOG(X*1.3591409/EN)
        TSTN=TST*EN
        IF(TSTN.GT.-120..AND.TSTN.LT.-90.) GO TO 6
    5   CONTINUE
    6 NST=NST+MOD(NST,2)
      NORM=MIN0(NST,NORM)
      RETURN
      END
C
C*********************************************************************
C
C   CINV
C       Routine to get the inverse of a complex number while avoiding
C    overflow from an intermediate calculation of the modulus-squared.
C    On exit, CINV contains the value 1/Z.
C
C ***** WARNING: CINV must be declared complex in a COMPLEX CINV *****
C *****          statement in the calling program.               *****
C
```

```
      COMPLEX FUNCTION CINV(Z)
      X=REAL(Z)
      Y=AIMAG(Z)
      IF(ABS(X).LT.ABS(Y)) GO TO 1
      R=Y/X
      W=1./(X+Y*R)
      CINV=CMPLX(W,-R*W)
      RETURN
    1 R=X/Y
      W=1./(X*R+Y)
      CINV=CMPLX(R*W,-W)
      RETURN
      END
```